ESTÉVEZ, JOSEPH EVANS, Ph.D. Fundamental Properties of Thermoset Resin with Boron Nitride Nanotube Reinforcement for Radiation Shielding Applications. (2014) Directed by Dr. James Ryan and Dr. Ajit Kelkar. 120 pp

Boron nitride nanotubes (BNNT's), like carbon nanotubes (CNT's), have properties beneficial for application in various fields of science including materials, electronics, and medicine. B^{10} has one of the largest neutron capture cross sections of any isotope and presents an opportunity to incorporate radiation shielding in composite materials by infusing the matrix with BNNT's. However, due to the challenges in synthesizing quality BNNT's, little research has been done to further the technology. The aim of this research is to: 1) Create theoretical models to substantiate that there are no detrimental effects on the fundamental properties, such as: modulus, strength and glass transition temperature. 2) Acquire structural information on the BNNT's and the resin system infused with BNNT's and 3) Generate experimental data which will verify the computational models. Structural information has been obtained on the BNNT's and nanocomposites by analytical and microscopic techniques. Calculations of the fundamental mechanical material properties of BNNT's are performed utilizing molecular dynamics simulations via Material Studio by Accelrys Inc. After the full characterization of the BNNT's, BNNT's have been dispersed into the Epon862/W thermoset resin system. Glass transition temperature is predicted by simulating

the annealing process and monitoring the density of the material at various temperatures. Also, interfacial information between the BNNT's and resin system has been described to provide a foundation for engineers who work on the fabrication of nanocomposites. Experimentally determined glass transition temperature data, from differential scanning calorimetry (DSC), confirms the accuracy of the computational models. Also, models in which the BNNT's undergo hydrogenation have been performed to understand the effects of hydrogenation on the properties of the BNNT's and the nanocomposite. Previous studies have demonstrated that CNT's have improved the mechanical and thermal properties of nanocomposites. This research has demonstrated that BNNT's will have advantageous effects on the fundamental properties of composites while incorporating radiation shielding.

FUNDAMENTAL PROPERITES OF THERMOSET RESIN WITH BORON NITRIDE NANOTUBE REINFORCEMENT FOR RADIATION SHIELDING APPLICATIONS

by

Joseph Evans Estévez

A Dissertation Submitted to
the Faculty of The Graduate School at
The University of North Carolina at Greensboro
in Partial Fulfillment
of the Requirement for the Degree
Doctor of Philosophy

Greensboro
2014

Approved by

_____
Committee Chair

APPROVAL PAGE

This dissertation written by Joseph Evans Estévez has been approved by the following committee of the Faculty of The Graduate School at The University of North Carolina at Greensboro.

Committee Chair _____

Committee Members _____

_____

_____

_____

_____
Date of Acceptance by Committee

_____
Date of Final Oral Examination

TABLE OF CONTENTS

Page

LIST OF TABLES

Page

LIST OF FIGURES

Page

LIST OF ABBREVIATIONS

BNNT	Boron Nitride Nanotube
CNT	Carbon Nanotube
MWBNNT	Multiple Walled Boron Nitride Nanotube
DGEBF	Diglycidyl Ether of Bisphenol F - epoxy resin
EPON 862	Liquid epoxy resin manufactured from epichlorohydrin and Bisphenol-F
W	Diethyl-toluenediamine - curing agent
DETDA	Diethyl-toluenediamine
DFT	Density Functional Theory
T_g	Glass transition temperature
MD	Molecular Dynamics simulations
GGA	Generalized Gradient Approximation
SEM	Scanning Electron Microscope
LDA	Local Density Approximation
B3LYP	Becke, 3 parameter, Lee-Yang-Par
NPT	Constant number of particles, constant pressure, and constant temperature
NVT	Constant number of particles, constant volume, and constant temperature

CHAPTER I

INTRODUCTION

Motivation

Space Radiation has become one of the major factors in successful long duration space exploration. Exposure to space radiation must not exceed three percent lifetime excess risk of cancer mortality and is limited to a maximum of 25 roentgen equivalents in mammals (rem) in any 30 day period, 50 rem within a year and 100-400 rem for the duration of a career depending on gender [1]. Space radiation will also affect materials and electronics. Hazards to materials include degradation of properties, such as, modulus, strength or glass transition temperature. Electronics may experience single event effects, gate rupture, burnout of field effect transistors and noise. Currently aluminum is the major component in most space structures due to its lightweight and good structural properties. However, aluminum is ineffective at blocking space radiation. This has led scientists and engineers to find a radiation shielding solution that will effectively mitigate the hazards to astronauts, materials and electronics while in space [1]. Space radiations is composed of two types of radiation, ionizing and non-ionizing radiation. Non-ionizing radiation is radiation that does not have a sufficient amount of energy to ionize the matter with which it interacts.

Ionizing radiation is categorized into three specific types: 1.) Galactic Cosmic Rays (GCRs), 2.) Solar Particle Events (SPEs) and 3.) Trapped Radiation in the Van Allen Belts. GCRs are particles that originate outside our solar system and are made up of heavy ions.SPEs are particles that are produced by solar events from the sun, such as solar flares [1]. Neutron radiation is produced by the interaction of GCRs and SPEs with matter. Researchers began to look for materials that would be good at fragmenting larger particles to smaller less harmful particles and capturing neutrons, which can pass through material much more efficiently than charged particles. The new radiation shielding material must be lightweight, structurally strong and effective at blocking all three types of ionizing radiation. The first and simplest solution was to use hydrogen [1]. It is good at fragmenting large ions, such as, GCRs, can effectively block or slow down most neutron radiation and is lightweight [1, 2]. However, hydrogen is not a structural material. Then researchers began to look at polymers which contain large amounts of hydrogen. Again, these materials are not structural materials and would require large amounts of material to achieve the structural properties needed. Then researchers began to look at composite materials, which contained good structural properties and use polymers that contained large amounts of hydrogen.

Composites are made up of two parts, the matrix and the reinforcement. The matrix is typically a hydrogen containing polymer which acts as a network to hold together the fiber reinforcement. The fiber reinforcement gives the mechanical strength to a composite. The ratio of fiber reinforcement to matrix is known as the fiber volume ratio. The fiber volume ratio is used to predict the mechanical properties of a composite.

A higher fiber volume ratio will lead to a mechanically stronger composite and a lower fiber volume ratio will lead to a weaker composite. In order to achieve the structural strength required, most composites must contain high fiber volume ratios. This minimizes the amount of polymer matrix or radiation shielding material. Thus, traditional methods of making composites strong and lightweight did not provide sufficient radiation shielding capability.

When nanotechnology is incorporated into a polymer matrix composite, the resulting three component material is known as a nanocomposite. The three-phase composite is made up of the fiber reinforcement, resin matrix, and nanofiller. Nanofillers are typically nanoparticles, nanotubes, or nanofibers and alter the properties of the original composite. For example, nanomaterials have been shown to alter the Young's Modulus, thermal conductivity, thermal resistivity, and conductance [3-8]. Typically the fabrication and introduction to these nanofillers begins by infusing the resin. Other techniques involve putting sheets of nanofibers between sheets of fiber reinforcement, carbon fibers. One nanomaterial that attracted much attention in the composite materials community was carbon nanotubes (CNT). They are lightweight and one of the strongest materials in existence. It was hypothesized that if researchers could add CNTs to the resin of a composite, they could effectively enhance the mechanical properties of the resin and therefore enhances the mechanical properties of the overall composite. After some time, researchers found ways to infuse resins with CNTs and alter the properties of composites [7]. Unfortunately, CNTs are not good for radiation shielding applications. After the discovery of CNTs, researchers had begun to look at alternate combinations of

elements to see if it was possible for other materials to construct hexagonal geometries like what was seen in CNTs. There were many theorized combinations of materials predicted to form nanotubes and the one that was of most interest to the radiation shielding community was Boron Nitride Nanotubes (BNNTs). BNNTs are a good radiation shielding material because the boron 10 isotope has one of the largest neutron capture cross sections, nitrogen has a better neutron capture cross section than carbon and BNNTs have similar predicted mechanical properties to CNTs [9]. Also, BNNTs are good at adsorbing hydrogen because of the asymmetric charge distribution created between the boron-nitrogen bonds. Unfortunately, BNNTs are difficult to synthesize and there have not been many computational studies on the material. Hence, more work characterizing the material and synthesizing high purity BNNTs is a cornerstone in incorporating these nanotubes into nanocomposites for radiation shielding.

Scope and Objectives

The Diglycidyl Ether of Bisphenol F (EPON 862) and curing agent Diethylmethylbenzenediamine (DETDA "W") resin system has been thoroughly studied and is useful in many industries, such as, marine, automotive and aerospace. Recently, there have been studies to infuse this resin system with nanofillers, such as, CNTs and Tetraethyl orthosilicate (TEOS) nanofibers. There have been no studies infusing this resin system with BNNTs. Thus, to successfully create three-phase radiation shielding composites for space application the objectives will be:

- Computational Model Predicting the Young's Modulus of BNNT
- Computational Model Predicting the Effect of Hydrogen on the Young's Modulus of BNNTs
- Computational Model Predicting the Young's Modulus of the Epon 862/W resin system
- Computational Model Predicting the Young's Modulus of the Epon 862/W resin system and BNNT.
- Computational Model Predicting the Glass Transition Temperature (Tg) of the Epon 862/W resin system
- Computational Model Predicting the Tg of the Epon 862/W resin system with BNNTs
- Experimentally develop an optimized method of infusing the resin system with BNNTs
- Fabricate two phase composites consisting of the resin system and BNNT nanofillers at varying percentages using the optimized method
- Analysis of the Young's Modulus and Tg of the fabricated panels and comparing with Computational Models

Literature Review

Boron Nitride Nanotubes

Boron Nitride Nanotubes (BNNTs) were first theoretically predicted in 1994 by Cohen and fabricated shortly thereafter in 1995 via arc discharge by Chopra et al [10,

11]. BNNTs are similar in structure to Carbon Nanotubes (CNTs) but the carbon atoms are replaced with alternating boron and nitrogen atoms, with almost identical lattice parameters, bond angles, and bond spacing [12]. Techniques used to synthesize CNTs in many cases, were adapted to synthesize BNNTs. New synthesis conditions and parameters had to be implemented in order to successfully synthesize BNNTs. Boron Nitride (BN) is a binary compound that is made up of group III and V elements but closely resembles the bonding and structural orientation of CNTs. Its close resemblance to this carbon system is due to the properties, polymorphism similarities and structure of BN. The BN bond possesses a local dipole moment that is due to the difference in electronegativity between the Boron and Nitrogen atoms. This gives the covalent bond between Boron and Nitrogen a significant ionic component. The chirality of BNNT's is determined in the same way you would determine the chirality for CNTs, the chiral vector R. The equation for the chiral vector is as shown:

$$R = na_1 + ma_2$$

The way a sheet of hexagonal BN is wrapped is determined by the integer indices (n, m) in the chiral vector equation. The indices (n,m) determine the number of unit vectors in two directions on the hexagonal BN lattice. BNNTs can take on three conformations; armchair, zigzag and chiral. The indices determine the conformation of the nanotubes. Armchair nanotubes are when indices n=m and zig zag nanotubes are when m=0. Any other variation of n and m are chiral tubes of (n,m) [12]. BNNTs are isoelectronic, having a band gap of 5.0 to 6.0 eV and is independent of chirality [13-15]. This makes

BNNTs a good insulating material and also distinguishes itself as unique when compared to CNTs, which have metallic or semiconducting properties [11, 13, 16]. Since, BNNTs have a band gap that is independent of chirality, all tube chiralities emit in the violet to ultraviolet range. Also, due to the independence of chirality, BNNTs have one strong Raman active phonon mode at 1370 cm^{-1} [11, 17]. The structural similarities of BNNTs and CNTs lead researchers to believe that these two structures have similar mechanical properties. BNNTs and CNTs have superb mechanical properties but BNNTs have a slightly lower predicted Young's Modulus when compared to CNTs, of 0.7 to 0.9 GPa. There are some distinct differences between CNTs and BNNTs. The most obvious difference between CNTs and BNNTs is the color of the material; CNTs are black while BNNTs are white [11]. This indicates various differences in their optical properties, such as adsorption peaks, excited states, etc [18-21]. Also, BNNTs exhibit better thermal and chemical stability [11, 22, 23]. This makes the applications for both CNTs and BNNTs case specific. They are good structural materials and can be used as nanofillers to enhance the mechanical properties of composites [16, 24-26]. Also, BNNTs are predicted to be a good radiation shielding material due to the large neutron capture cross section of B^{10}, although B^{10} has only a 20% isotopic abundance [27]. The biggest difference in application of the two nanotubes is whether or not you need a insulating or conducting/semiconducting material [11].

Synthesis Methods for Boron Nitride Nanotubes

BNNT synthesis has presented a challenge to the research community. Many similar, well-studied techniques commonly used to fabricate CNTs were investigated at

first. It was quickly discovered that many parameters such as growth temperature, precursor gases, catalyst, environment and growth mechanisms were different. BNNTs were synthesized using: arc-discharge, laser ablation, balling milling, chemical vapor deposition (CVD) and template synthesis. The most common methods include arc-discharge, CVD and laser ablation [28].

Arc-discharge was the first technique to yield BNNTs. They were generated between a tungsten rod packed with BN material and a cooled copper electrode. Primarily, multi-walled BNNTs were generated with the first attempt with diameters ranging from 1-3nm. It was theorized that the metal electrodes fragmented into particles during the process and acted as the catalyst or nucleation sites for BNNT growth [29]. Researchers tried to improve the synthesis method by using two HfB_2 electrodes and were successful in producing single-walled and dual-walled BNNTs [30]. The major challenge was that pure BN could not be used as electrodes because of the insulating nature of the material. Conductive Boron compounds, such as, ZrB_2 and YB_6 were commonly used in a nitrogen environment [31-33]. This technique was low yield because of the lack of control in growing only pure BNNTs structures as opposed to other BN species. However, the BNNTs synthesized were highly crystalline due to the high synthesis temperature of 3000K. Also, this technique became fruitful because it proved that boron could act as its own catalyst in the synthesis process.

Laser Ablation was first used to grow BNNTs by Goldberg et al in 1996. Laser ablation is a technique in which a laser is used to vaporize a solid target creating a plume of the material and then the plume interacts with molecules in the vacuum systemor

substrate to form different types of structures, usually in the nanometer range. In the case of Goldberg et al, a Cubic Boron target was heated to 5000K using a CO2 laser. This resulted in synthesis of multi-walled BNNTs in the melted portion of the target [34]. They experimented with different boron targets and found that hexagonal BN would yield multi-walled and single-walled BNNTs [10]. Catalysts are not needed to act as nucleation sites for the growth of BNNTs when using laser ablation. However, using Ni or Co catalysts resulted in longer tubes and a higher concentration of single-walled BNNTs [35]. Highly crystalline BNNTs are formed with the laser ablation process, but many other BN nanomaterials, such as, onions, flakes and cones are formed degrading the yield and purity. There is a recent technique that is similar to laser ablation in many aspects that has been found to be the best technique for producing highly crystalline and high purity of BNNTs called the Pressure Vapor Condenser (PVC) method. This technique was developed in 2012 by the National Aeronautics and Space Administration (NASA) and will be discussed in detail later on.

Ball milling is another technique developed to synthesize BNNTs. Chen et al was the first to synthesize BNNTs via this method in 1999 [36]. Hexagonal BN powder was first ball milled and then annealed at 1300 degrees Celsius, yielding bamboo-like nanostructures. The powder before annealing is highly disordered amorphous nanostructures. No catalysts were needed because the iron of the chamber was satisfactory to promote nucleation and growth. This process yields a small quantity of BNNTs because the nanotubes are mixed with a lot of amorphous species. Also, the qualities of the BNNTs are low because of the poor crystallinity or bamboo-like structure.

After annealing, more crystallized, ordered structures are generated. The mechanical properties of the bamboo-like BNNTs are poor and cannot be used as structural fillers within composites. There were some attempts to improve the quality of the BNNT structures by introducing NH_3 as a reactantgas during the process and optimizing the annealing method [37]. These improvements lead to a higher yield of BNNTs with a significant reduction in diameter of the tubes, less than 10 nm. Even with the improvements to the process the yield was still significantly lower than other methods and the BNNTs were mixed with a large number of amorphous species. Ball milling is a cheap and simple setup for creating bamboo-like BNNTs but the purity must be improved if this is to become a viable method of fabrication for this particular method of making BNNTs.

Templated growth has become popular in fabricating aligned or semi aligned nanostructures, such as, nanowires or nanotubes. There are two current template syntheses methods used for the growth of BNNTs: CNT substitution reaction and use of a porous alumina filter membrane [38-41]. The CNT substitution reaction proved the most effective at growing BNNTs, but majority of nanotubes were contaminated with carbon. B_2O_3 is reacted with CNTs in a NH_3 or nitrogen environment to produce the boron carbon nitride (BCN) nanotubes. Post-processing, such as, oxidation was implemented to remove extra carbon, but carbon within the nanotubes lattice is not easily removed and carbon doped BNNTs remained the final product. Researchers also found, they could improve the yield of BNNTs by adding a metal oxide. The main advantage of this method is that it allows the tailoring of the BNNTs morphology by selectively choosing

the CNT template. The BNNTs will maintain and adopt the morphology of the template CNTs. Thus, allowing the ability to form specific BNNT structures or chiralities, such as, BNNT ropes [42, 43]. The porous alumina template method decomposed Trichloroborazine at 700-950 degrees Celsius to fill the alumina pores with BN material [44]. The synthesized BNNTs had an average diameter of 280 nm and were found to be polycrystalline in nature. Templated synthesis methods struggle in generating high crystallinity and high purity BNNT material.

CVD is one of the most widely used and well known techniques used for synthesizing nanomaterials. It is a chemical synthesis method in which a chamber is flooded with a precursor gas or gases and the precursor gas interacts with the substrate within the CVD chamber to create various types of solid materials. There are many forms of CVD in use today. Often times a catalyst is deposited on a substrate to act as nucleation site for the growth of nanotubes [45]. CVD can also be used to create various types of micro/nano films and is often used in the semiconductor industry. Lourie et al was the first group to successfully grow highly crystalline BNNTs utilizing the CVD method in 2000. They used a Borazine precursor and various catalysts, such as, Ni, NiB, and Co to synthesize the first BNNTs [46]. Growth temperatures were in the range of 1000-1100 degrees Celsius, which is common to many CVD growth methods [46-49]. The most promising CVD technique utilizes boron and a metal oxide as the reactants [50]. They based their technique on boron oxide CVD [51]. A deposited film of MgO/Al_2O_3 catalytic film is deposited onto a substrate using pulse laser deposition (PLD). Then a combustion boat was filled with Boron powder, MgO, and FeO

precursors with a 4:1:1 molar ratio. The patterned substrate with the catalytic film was placed on top of the combustion boat and placed into a closed-end quartz tube in a horizontal furnace. The furnace was heated to 1200 degrees Celsius and an ammonia flow was started and maintained for 1 hour. The substrate was then cooled and removed from the tube furnace. This technique is based on the Vapor Liquid Solid (VLS) growth mechanism and yielded high purity BNNTS, in milligram quantities [51]. This was the first step in producing a large quantity highly crystalline/high purity BNNTs on a silicon substrate. While one of the more promising techniques, further investigation is required before this method could be used for commercial application.

The most recent and best suited method for commercial application is the Pressure Vapor/Condenser (PVC) method, which was developed by NASA. It was developed in 2009 and was just recently patented in 2012. They claim to make long single and few walled BNNTs with small diameters [52]. A pure boron target is centered in a pressurized chamber full of N_2 gas at 20 times atmospheric pressure. The target is locally heated using a 1kW free electron laser which creates a plume of 4000 degrees Celsius boron vapor. The density difference between the hot boron vapor and room temperature N_2 gas drives the boron plume upward. The upward plume comes in contact with a condenser coil, cooling the boron vapor into droplets. Still being propelled upward, the N_2 gas begins to diffuse into the boron plume and come in contact with the boron droplets which act as nucleation sites. Quickly BNNT fibrils begin to form and interlock. The upward flow of the boron plume aligns the BNNTs using shear stress. The final product is of high crystallinity and purity. By sweeping the condenser coil across the chamber,

NASA was able to increase yield and make this method viable for commercial application. It is also shown that some of the parameters could be changed depending on availability of equipment, such as, heating laser and pressure on chamber. It is also noted that these BNNTs have higher surface area then those generated by CVD or Ball milling [52]. The majority of the BNNTs have 2-5 walls but there are single walled BNNTs as well. All walls are smooth and along the axis of the tubes and easily separated with little mechanical force. BNNTs formed by PVC method grow without catalyst, are naturally aligned and are highly crystalline. The fact that no catalysts are needed to grow the nanotubes eliminates the need to purify the sample of carbon or metals. Also, since the tubes are aligned and have the appearance of cotton fibers, many textile methods are applicable to process the BNNT material into yarns or threads [52]. The PVC method is the most promising method in making BNNTs applicable in electronics, materials, biotechnology and many other fields.

Computational Studies of BNNTs

Since the synthesis of BNNTs has been a challenge, many groups have turned to computational techniques to understand the properties of these nanotubes. Now that we understand what BNNTs are and the syntheses challenges that are faced, we will now look at various computational techniques used currently. Computational science is an interdisciplinary field where mathematical models are constructed to model or simulate specific systems [53]. The capability to execute material simulations over numerous characteristic lengths and time scales has made computational science a useful tool for science and innovation. There are many computational techniques used today and are

application specific [53]. Depending on the order of detail you enter a different regime of computational simulation and length scale. The range of length scales is as follows: Electronic/Atomistic (10^{-12}-10^{-9}m), Atomistic/Microscopic (10^{-9}-10^{-6}m), Microscopic/Mesoscopic (10^{-8}-10^{0}m), Mesoscopic/Macroscopic (10^{-6}-10^{2}m) [53]. Of course the smallest length scale is the most computationally intensive and cannot be used to simulate long periods of times. Each length scale provides different boundary conditions and assumptions that govern the interaction within the regime [53].

Ab intio methods and first principles are used at the Electronic/Atomistic length scale and is the most computationally intensive of all the length scales. These methods are often called quantum mechanical computer simulation methods. They function by solving the Schrodinger equations approximately and often times these methods use the Born-Oppenheimer approximation. These methods can give information pertaining to the chemistry of materials, molecular geometry, and quantum mechanical ground and excited states. Also, these quantum mechanical methods are good at giving Nuclear Magnetic Resonance (NMR), Infrared (IR), and Ultra Violet (UV) spectroscopic data. The strategy of this method is to solve the electronic Schrodinger equation in each time step and calculate the effective potential of the nuclei. Once you have calculated the effective potential you can compute the forces on the nuclei and move them according to Newton's Equations of motion. The mass difference between the electrons and the nuclei is so large that the electrons are said to move instantaneously with the nuclei of the atoms. A majority of the methods are based on Density Functional Theory (DFT) and Hartree-Fock (HF) models [54-60]. Software examples using these quantum mechanical

methods include: ACESII, AMPAC, CPMD, GAMESS, QUANTUM ESPRESSO, SIESTA, VASP, CASTEP, GAUSSIAN, Molpro and Material Studios [53].

Semi-empirical methods and atomistic simulation methods are used at the Atomistic/Microscopic length scale. These methods give a wide range of properties from bulk transport properties of solids and liquids to thermodynamic properties. Due to the vast amount of information that can be obtained with these methods, it has gained a lot of attention from all fields of science and engineering. Molecular Dynamics (MD) and Monte Carlo (MC) simulations are the oldest and most commonly used semi-empirical methods. MD and MC were the first computational methods developed and implemented on computers. These methods determine the behavior of the system mainly by their energy and do not take the electrons into account. At this length scale, classical interaction potentials are used to describe the system and additional interactions must be considered to model Coulomb interactions, covalent bonds, bending and torsion on molecules effectively because of its neglect of the quantum mechanical electronic contributions. The Lennard-Jones potential is the most common generic model used in this length scale because of its numerical efficiency and simplicity [61-66]. Available software packages include: CHARMM, DL POLY, GROMACS, NAMD, IMD, XMD and GROMOS [53].

Mesoscale methods such as finite element method are used to define the Microscopic/Mesoscale length scale. This regime is used to find the properties of block-copolymers, soft matter, and biological systems, such as, polymers, colloidal or amphiphiles system [67-80]. These systems are defined by their energy and their

entropy. In this length and time scale, particles are a collection of elementary particles, such as, atoms or molecules that come together to be treated as a classical particles. These methods are often called coarse grain methods and are used to study large systems of atoms for extended periods of time. Also, some of these methods incorporate a hybrid particle/mesh method that is used by engineers in materials design [53].

Continuum methods are used to describe the Mesoscopic/Macroscopic length scale [53]. These models explain the properties of fluids and visco-elastic behavior of solids based on the Navier-Stokes Equation. Typically, these methods are mesh methods, such as the Finite Element Method (FEM). FEM's most prominent feature is its ability to define a continuum in discrete elements. Each discrete element is connected via a topological map called a mesh. Then the FEM interpolation functions are built upon the mesh, which guarantees the compatibility of the interpolation. Often times a mesh must be very fine in order to avoid local distortions or high gradients, which in turn, causes the simulation to be computationally expensive. Typically, these codes are based on a solution of the continuum conservation equations of momentum, energy and mass. Also, they use constitutive equations to understand material response to external loading. This regime is good for technical applications where direct connections to macroscopically measured parameters are investigated, while neglecting microscopic and molecular quantities [53, 81-83]. The most promising and demonstrated computational techniques lay within the Electronic/Atomistic to Atomistic/Microscopic range [84]. These simulations were based on various techniques to extrapolate data, such as, Density Functional Theory (DFT), Møller–Plesset perturbation theory (MP), Density Functional

Tight Binding Model (DFTB), and the Tersoff-Brenner potential. The following are a review of research on BNNTs that utilize the above techniques.

Russian Academy of Science by Enyashin et al used DFTB to accurately predict the effects of bending and twisting on BNNTs and CNTs. Some of the strengths of using DFTB as opposed to the full DFT are, DFTB's can exceed the limits of system size that are constrained in DFT and access longer time scales [85]. However, there is a sacrifice in accuracy due to a large amount of assumptions, especially in the repulsive potential, that allows for larger systems to be simulated as well as being able to simulate for longer periods of time [85]. The study consisted of holding the atoms of a geometry optimized CNT or BNNT and holding the atoms at each end of the two different nanotubes, (5,5) CNT and (17,0) BNNT, and perform a bending and twisting test. Bending of the nanotubes can be defined by two distinct stages for both nanotubes. Stage one, the bonds between the atoms in the nanotubes begin to stretch and contract to accommodate for the bending strain. Stage two, buckling occurs within the nanotubes structure and bonds begin to break. After breaking of the bonds occurs new bonds are formed in the CNT and BNNT. Giving rise to capped nanotubes, which are energetically favorable. However, CNTs have a greater flexibility in creating new bonds and ring formations, such as, tetragons, pentagons and heptagon rings. BNNTs are limited in the bonds that can be created seeing as it is energetically unfavorable for bonds to be created between two Boron or two Nitrogen atoms. Even though both nanotubes undergo the same two stages of deformation, there are still clear differences in the reaction of the nanotubes which can be correlated to the overall structure of the nanotubes. For example, the CNTs

begin to experience buckling at 65-69 degrees of bending as opposed to the BNNTs which don't experience breaking of bonds until 89-92 degrees [86]. Also, the bending of the CNT is shown to be more energetically favorable for angles less than 25 degrees and lower for angles greater than 25 degrees. Thus, covalent bonds between the carbon atoms prove to be more difficult to break in comparison to the B-N ionic-covalent bonds after 25 degrees of deformation [86].

Next, twisting deformation was performed on both the CNT and BNNT nanotubes holding fixed the top and bottom atoms and rotating them around the z-axis of the tube. Distinct characteristics and differences are shown between the CNT and BNNT. CNTs undergo at least five distinct stages, whereas, BNNTs undergo two stages. The CNT's first stage ranges from 0 degrees to ~40-45 degrees which corresponds to only changes in the bond angles and lengths of the covalent bonds. Stage two ranges from 45 degrees to ~110 degrees, where a steeper change in the change of energy is shown as well as the formation of convex and concave zones. The CNT is in a strained state where the deformation energy is at a maximum [86]. The third stage ranges from 110 degrees to ~120 degrees and covalent C-C bonds break and the tube partially restores back to its original atomic structure. After the third stage the tube is defined by two sections, the upper and bottom half of the tube which are similar to the original structure and what is known as the neck, which contains different shaped rings as was seen in the bending deformation. The fourth stage ranges from 130 degrees to 175 degrees where the majority of the deformation occurs near the neck region of the tube. The fifth stage occurs at ~174 degrees where the tube continues to deform until covalent bonds are

broken once again. After stage five a cyclic process continues, where the tube is partially restored and the neck of the tube continues to deform breaking and forming new bonds after reaching the strain state or deformation energy is at a maximum [86]. The first stage of BNNT deformation is what is called "plastic twisting" which occurs between zero and 75 degrees [86]. This means that 75 degrees marks the elastic limit of BNNTs. After 75 degrees, the second stage occurs and a breakdown of the structure begins. No metastable states, such as a neck are formed in the BNNTs and distortion of the entire structure continues to occur and atomic rearrangement is seen in the walls of the tube. These metastable states in CNTs contribute to the ability of Carbon to form sp^3, sp^2 and sp bonds or various C_n polygons, where as the polar nature of the B-N bond prevents such metastable states and restricts the formation of energetically unfavorable B_nN_n polygons, B-B and N-N bonds [86-88]. In conclusion, the DFTB has proven to be a valuable computational technique in determining the deformation mechanisms in CNTs and BNNTs.

A study performed by the Panjab University department of Physics uses the Tersoff-Brenner potential to calculate the elastic modulus of BNNTs. Tersoff-Brenner Potential is a bond order potential, which is a class of empirical potentials that are implemented in MD simulations [89, 90]. An advantage to these types of potentials over molecular mechanics force fields is the ability to describe several different bonding states of an atom with the same parameters [89, 90]. The potential describes bonds with four parameters: bonding environment, number of bonds, bond angle and bond length [89, 90]. Thus, the potential can be written as a simple pair potential depending on distance

between two atoms, but the strength of the bond is modified by the environment of the bond [89, 90]. The Tersoff-Brenner potential was created to describe carbon systems, but with some modifications to the parameters, it should give a relatively accurate result for BNNTs. Of course, the Tersoff-Brenner potential is not as accurate as ab initio approaches but allows for greater computational speed and analysis of larger computational systems. The parameters used by Verma et al, are very close to that of CNTs with some slight modifications for the difference in elements. The simulation is begun by taking a sheet of hexagonal boron nitride and bending/rolling it into different BNNTs. First, the coordinates for the Boron and Nitrogen atoms were generated creating the hexagonal sheet structure. Then energy minimization is performed to relax the tube and to find its optimal geometry. This is performed by shifting the atoms in small steps and calculating the energy of the entire system. If after the shift of the atom yields a lower overall energy then the coordinate is saved or if it yields a higher overall energy the atom is returned to its original position. Similarly, the elastic modulus is calculated by applying stress along the axis of the tube and calculating the energy of the tube as the atom positions begin to accommodate the force applied [91]. The modulus reported by Verma et al, ranged from 0.982 TPa to 1.137 TPa depending on diameter of the tube. This model predicts a correlation to Young's modulus and diameter of the tube which disagrees with previous literature. However, Verma et al did state that the parameters used in this potential were similar to that of CNTs and more adjustments to the parameters, such as, wall thickness could lead to a further reduction of the Young's modulus, which would bring the results in agreement with previous literature [91, 92].

Also, shear modulus was calculated using the Tersoff-Brenner potential and shown to have a dependence on diameter, decreasing with increasing diameter nanotubes. In conclusion, the Tersoff-Brenner potential is a very powerful and effective computational tool, but the user must be careful in choosing the best parameters for their system. Otherwise, computational results become unreliable.

A study performed by Tanskanen et al describes bonding preference of Hydrogen onto BNNTs or CNTs in different lattice planes on armchair or zigzag nanotubes. This study uses a combination of quantum techniques, Møller–Plesset perturbation theory and Density Functional Theory, to perform the optimization of the hydrogenated structures and calculate the electronic properties of the structures. Møller–Plesset perturbation theory is a quantum chemistry ab initio. It is an improvement to the Hartree-Fock method because it uses Rayleigh-Schrodinger perturbation theory to add an electron correlation effect and is usually to the second, third, fourth or fifth order. Of course there are advantages and disadvantages to this method. For example, perturbation theory (PT) calculations do not contain many variations and are difficult to make comparisons with other quantum chemistry techniques. PT in general overestimates correlation energies, and geometry optimization only works well when the structure is near equilibrium. Some advantages to PT include: most ab initio programs can perform them, it is much quicker in most cases than other ab initio methods such as DFT or Hartree-Fock and it is good at calculating relative energies [93, 94]. Tanskanen et al used the second order Møller–Plesset perturbation theory (MP2) to accompany DFT in performing the geometry

optimization for the sheets of Boron Nitride and Carbon. Hydrogenated graphene sheets prefer the (111) lattice plane as opposed to Hydrogenated Boron Nitride which prefers the c-BN or (110) lattice plane. These are said to be strain-free structures but Boron Nitride is nonplanar and bends at a curvature of 1.7nm [95]. By using DFT and MP2 to calculate the relative energies of the Hydrogenated BNNTs and CNTs, it becomes obvious to which is the preferred lattice plane for each structure. The CNTs prefer the (111) lattice plane because the Hydrogen atoms are spaced farther apart as opposed to the (110) lattice plane, thus, reducing the magnitude of the interaction between the Hydrogen atoms. The band gap for either plane is relatively close. (6.8eV for the (110) and 6.9 for the (111)) In the case of armchair CNTs and zigzag CNTs, there is practically no difference in the (111) and (110) lattice planes for armchair nanotubes; but there is a preference for the (111) lattice plane in zigzag CNTs because these nanotubes are most affected by the H-H interactions, with the repulsive forces being greatest at smaller tube diameters. BNNTs are slightly more complex structures and lattice plane preference is dependent on nanotubes diameter. The BNNTs prefer the (110) lattice plane at a diameter of 1.4 nm and above. The energies between zigzag and armchair BNNTs is relatively the same and becomes closer at larger nanotubes diameters, 4.8 nm diameter yields a 2.2 kJ mol^{-1} per BNH_2 unit [95]. The preference for the (110) lattice plane is due to the partial ionic component of the B-N bond. This polar bond causes the Hydrogen atoms to be charged, positive when attached to Nitrogen and negative when attached to Boron. When the BNNT is in the (110) lattice plane, the electrostatic forces are mainly attractive and take place between the different charged Hydrogen atoms. In the (111)

lattice plane, there is a lack of electrostatic attractive forces and since the repulsion force is stronger between BH Hydrogen atoms than NH Hydrogen atoms the plane begins to bend. Also, the armchair BNNTs are preferred due to the H-H interactions. The relative H-H distance is greatest between BH atoms, which have a 14% increased larger bond length with respect to the NH atoms. This makes the zigzag (110) BNNTs destabilized due to the shorter distance between the nearest BH and NH hydrogen atoms inside the tubes. Thus, the larger the diameter, the longer the H-H distance making the energetic difference between zigzag and armchair nanotubes the greatest at smaller diameters [95]. The Møller–Plesset perturbation theory and DFT have shown to be powerful tools in determining relative energies for the BNNT and CNT structures. Also, this computational technique is a useful tool for determining bonding or adsorption mechanics and preferences for these types of structures.

The electronic structure of BNNT has been studied using a tight binding method and Density Functional Theory (DFT). The first study of the electronic structure was studied by Rubio et al using a Slater-Koster tight-binding scheme [96]. They found BNNT material to be semiconducting with a band gap larger than 2.0 eV for most tubes. They correlate the band gap with the diameter of the tube; larger diameter tubes have larger band gaps with a saturation value corresponding to the band gap of a hexagonal BN [96]. This was a significant step in predicting the band gap of BNNTs and understanding the electronic structure but it was evident there was a lack in the total energy calculations because of the tight binding method. It was then approached using

DFT with a local-density functional, local density approximation (LDA) [97]. They found that it was energetically more favorable to fold a hexagonal BN sheet into a BNNT then a graphite sheet into a CNT. DFT also established BNNTs are a large band gap semiconductor or rather insulating material. A 4 eV band gap was predicted but it is well known that LDA usually underestimates the band gap. DFT methods using other exchange functionals, such as, the general gradient approximation (GGA) and the hybrid functional B3LYP predicted a saturation of the band gap at 5 eV [98, 99]. Multi-walled BNNTs are slightly different because large curvature that causes hybridization between the π and σ states of the inner and outer tubes. This leads to a localization of the top valence and bottom conduction bands with directly correlates to a narrower band gap than the inner tubes [100, 101]. It is due to the fact that the inner tubes downward π shifts are larger than the outer tube. There is also a distribution of accumulated charge corresponding to that of the near-free-electron states of the BNNTs due to the hybridization between the near-free-electron states and the π states [101]. Also, DFT and tight binding formalism were used to predict the Young's Modulus of BNNTs. Hernandez et al used a non-orthogonal tight-binding formalism to predict the Young's Modulus of CNTs, boron nitride nanotubes doped with carbon and BNNTs. DFT coupled with the LDA exchange functional were used to verify the results of the model. It was predicted that the Young's Modulus for BNNTs was slightly lower than CNTs, 700-900 GPa [102].

Density Functional Theory

During the past century physicists have been working diligently to describe many particle systems. Currently, it is possible to achieve analytical solutions of the Schrodinger equation for simple systems. Also, it is possible to get numerically exact solutions for a small number of atoms and molecules [103]. Small systems are not indicative of the reality of chemical reactions or interactions between electrons in solids. Researchers have had to use simplified computational schemes in an attempt to predict the behavior of larger systems. It has been impossible to create one model that will describe all systems accurately. Recently, calculations of the electronic structure of atoms, solids and molecules has demonstrated relatively better accuracy at predicting the physical and chemical properties of a many particle system without the use of excessive computational power [103]. One of the most powerful quantum chemistry techniques to date is Density Functional Theory (DFT). The approximations and improvements to this computational technique continue to grow. DFT was first formalized in 1964 by Hohenberg and Kohn when they were able to relate the ground state properties, specifically the energy of a system, to the density distribution of electrons. Before, many approximation techniques, such as, Hartree-Fock and Configuration Interaction were used commonly and used as the foundation for DFT. DFT, with specific approximations, can be transformed to act and predict the properties of a system as would Hartree-Fock, but it is key to understand that the approximations of DFT have given rise to a technique that has the capability of predicting the properties of larger systems with less computational power. However, DFT in some cases is not as accurate as some of the

more expensive techniques, such as, couple cluster theory. Its computational cost scales with the cube of the number of atoms (N^3), where other similar computational techniques scale from N^4 and greater. DFT can predict a variety of molecular properties, such as, chemical structures, bond lengths, vibrational frequencies, enthalpies of reactions, atomization energies, ionization energies, magnetic properties, reaction paths, etc. The approximations and parameters within DFT can be tailored to model specific scenarios or to predict specific properties of a system. Like all approximation techniques, the initial parameters or functions used within the computation will impact the results negatively or positively. This technique is useful and employed for simulations in the nanoscale because of the length regime that it is capable of modeling. Thus, it is important to understand the algorithms, functions, parameters and assumptions made within DFT.

Formal Derivation

The goal of approximation techniques in solid state physics and quantum chemistry is to solve the time-independent, non-relativistic Schrodinger equation [103]. We look at the Hamiltonian of a system with infinite number of atoms. It takes the form [103]:

$$\hat{H}\psi_i(\vec{x}_1, \vec{x}_2, \ldots\ldots \vec{x}_N \vec{R}_1, \vec{R}_2, \ldots\ldots \vec{R}_M) = E_i\psi_i(\vec{x}_1, \vec{x}_2, \ldots\ldots \vec{x}_{N,} \vec{R}_1, \vec{R}_2, \ldots\ldots \vec{R}_M)$$

This is the Hamiltonian for a system consisting of N electrons and M Nuclei. The Hamiltonian can further be written to describe three components: kinetic energy of nuclei and electrons, attractive interaction between nuclei and electrons and repulsive potential between electron-electron interaction and nucleus-nucleus interaction:

$$\hat{H} = -\frac{1}{2}\sum_{i=1}^{N}\nabla_i^2 - \frac{1}{2}\sum_{A=1}^{M}\frac{1}{M_A}\nabla_A^2 - \sum_{i=1}^{N}\sum_{A=1}^{M}\frac{Z_A}{r_{iA}} + \sum_{i=1}^{N}\sum_{j>i}^{N}\frac{1}{r_{ij}} + \sum_{A=1}^{M}\sum_{B>A}^{M}\frac{Z_A Z_B}{R_{AB}}$$

The first two terms represent the kinetic energy of the system and the last three represent the attractive and repulsive terms of the Hamiltonian. The A and B represent the values that run over the nuclei M and i and j run over the electrons N. Then we make a first approximation to simplify the Hamiltonian known as the Born-Oppenheimer approximation. The Born-Oppenheimer approximation states that the nuclei move slower than the electrons [103, 104]. This means that the electrons are moving in a stationary field of nuclei. Then, the kinetic energy of the nuclei is approximated to be zero and the potential energy becomes a constant [103, 104]. The new form of the Hamiltonian is as shown for the electrons:

$$\hat{H}_{elec} = -\frac{1}{2}\sum_{i=1}^{N}\nabla_i^2 - \sum_{i=1}^{N}\sum_{A=1}^{M}\frac{Z_A}{r_{iA}} + \sum_{i=1}^{N}\sum_{j>i}^{N}\frac{1}{r_{ij}} = \hat{T} + \hat{V}_{Ne} + \hat{V}_{ee}$$

Now, we can state that the solution to the Schrodinger equation with the new Hamiltonian operator will be the electron wave function and the electron energy

$$\hat{H}_{elec}\psi_{elec} = E_{elec}\psi_{elec}$$

The total energy will be a combination of the electron energy and the constant nuclear repulsion:

$$E_{tot} = E_{elec} + E_{nuc}; \qquad E_{nuc} = \sum_{A=1}^{M} \sum_{B>A}^{M} \frac{Z_A Z_B}{R_{AB}}$$

Now, we move on to bridge the electron energy with the expectation value of the energy and calculating the ground state energy E_0. If a system is in a state ψ then the expectation value of the energy is:

$$E[\psi] = \frac{<\psi|\hat{H}|\psi>}{<\psi|\psi>}$$

$$<\psi|H|\psi> = \int \psi^* \hat{H} \psi d\vec{x}$$

We can then find the ground state of the system by applying the variational principle, which states that the energy computed from a guessed ψ is an upper bound to the true ground-state energy E_0 [103, 104]. Thus, a full minimization of the functional $E[\psi]$ with respect to all allowed N electrons wave functions will give the true ground state and the true ground state energy E_0 which takes the form:

$$E_0 = min_{\psi \to N} E[\psi] = min_{\psi \to N} <\psi|\hat{T} + \hat{V}_{Ne} + \hat{V}_{ee}|\psi>$$

Also, the variational principle contains a procedure to determine the ground-state wave function and the ground state energy for a system with a given nuclear potential V_{ext} and N number of electrons. It can also be used to determine other properties of interest, but what is important is that we have determined that the ground state energy is a functional

of the nuclear potential and the number of electrons. The electron density is defined as the integral over the spin coordinates of all electrons and over all but one of the spatial variables:

$$p(\vec{r}) = N \int \ldots \int |\psi(\vec{x}_1, \vec{x}_2, \ldots . x_N)|^2 ds_1 d\vec{x}_2 \ldots . d\vec{x}_N$$

The electron density is a non-negative function of only three spatial variables. It is a probability of finding an electron in a specific volume element. Thus, it is a function that vanishes at infinity and integrates to the total number of electrons. Also, electron density is an observable and can be measured experimentally by such methods as x-ray diffraction. The electron density is the fundamental core of DFT and it was derived that the energy could be given completely in terms of electron density by the Thomas-Fermi model [103]. The Thomas-Fermi model was considered the first form of DFT and was established in 1927 [103]. It is based on the uniform electron gas in which it was proposed that the kinetic energy took the form of the functional:

$$T_{TF}[p(\vec{r})] = \frac{3}{10}(3\pi^2)^{2/3} \int p^{5/3}(\vec{r}) d\vec{r}$$

The total energy of the atom can then be calculated by adding the kinetic energy functional with the classical expression for the nuclear-nuclear potential and the electron-electron potential:

$$E_{TF}[p(\vec{r})] = \frac{3}{10}(3\pi^2)^{2/3} \int p^{5/3}(\vec{r})d\vec{r} - Z\int \frac{p(\vec{r})}{r}dr + \frac{1}{2}\int\int \frac{p(\vec{r}_1)p(\vec{r}_2)}{r_{12}}d\vec{r}_1 d\vec{r}_2$$

It was by the Thomas-Fermi model that the energy of a system can be completely written in terms of electron density. The variational principle was used to determine the correct density in the equation of the total energy. Hohenberg and Kohn took the model one step further and introduced the Hohenberg-Kohn Theorem. The theorem states that the external potential is a unique functional of the electron density and demonstrates that the electron density determines the Hamiltonian operator [55, 103, 104]. If one has the Hamiltonian operator they can calculate all the properties of a system. Thus, by calculating the electron density can determine the Hamiltonian and therefore determine the properties of the system. It can be shown that there cannot be two different external potentials that give the same electron density for the ground state. This confirms that the electron density determines the number of electrons and external potential. Also, it was concluded that the ground state energy is a functional of the number of electrons and external potential by a procedure within the variational principle. Thus, if one knew the electron density of the system they could determine all the properties of the ground state and express the energy in terms of electron density:

$$E[p] = T[p] + E_{Ne}[p] + E_{ee}[p]$$

The nucleus-electron interaction is straightforward and can be represented simply by coulombs law:

$$E_{Ne}[p] = \int p(\vec{r}) V_{Ne}(\vec{r}) d\vec{r}\,;\;\; V_{Ne}(\vec{r}) = \sum_{A}^{M} \frac{Z_A}{|\vec{R}_A - \vec{r}|}$$

$$E_{Ne}[p] = \sum_{A}^{M} \int \frac{Z_A p(\vec{r})}{|\vec{R}_A - \vec{r}|}$$

The new equation for the energy takes the form of:

$$E[p] = F_{HK}[p] + \sum_{A}^{M} \int \frac{Z_A p(\vec{r})}{|\vec{R}_A - \vec{r}|}$$

$$F_{HK}[p] = T[p] + E_{ee}[p]$$

The functional F_{HK} is the most important functional for DFT. If it was known the Schrödinger equation could be solved exactly and since it is a universal functional it could be applied to any system regardless the size or complexity. For example, it could be applied to a hydrogen atom as well as being applied to larger systems, such as, polymers or DNA [55, 103, 104]. The F_{HK} demonstrates the strength and usefulness of DFT. Unfortunately, it is extremely difficult to solve this functional exactly and hence portions of the functional must be approximated. It is possible however to extract the classical portions of the E_{ee} which takes the form of J[p]:

$$J[p] = \frac{1}{2} \int \int \frac{p(\vec{r}) p(\vec{r}')}{|\vec{r} - \vec{r}'|} d\vec{r} d\vec{r}'$$

$$E_{ee} = \frac{1}{2}\int\int \frac{p(\vec{r})p(\vec{r}')}{|\vec{r}-\vec{r}'|} d\vec{r}d\vec{r}' + E_{ncl} = J[p] + E_{ncl}$$

In the new equation for the electron-electron repulsive term E_{ncl} represents the non-classical contribution, which pertains to the self-interaction correction, exchange and Coulomb correlation. The two major challenges to DFT are the explicit forms of the functional T[p] and E_{ncl}. A key factor to discovering the ground state energy and ground state wave function is that we must have the ground state electron density. How can it be confirmed that a certain density is the ground state density? Hohenberg- and Kohn came up with a second theory that states that F_{HK}[p] functional will express the ground state energy of a system and delivers the lowest energy if and only if the input density is the true ground state density. Again, this is a reference to the variational principle:

$$E_0 \leq E[\tilde{p}] = T[\tilde{p}] + E_{Ne}[\tilde{p}] + E_{ee}[\tilde{p}]$$

Thus, if an electron density is associated with an external potential, V_{ext} and satisfies the necessary boundary conditions:$\tilde{p}(\vec{r}) \geq 0$ and $\int \tilde{p}(\vec{r})d\vec{r} = N$, the energy obtained will represent the upper bound of the true ground state energy. It will only be the true ground state energy if the electron density is that of the true ground state. Now it is possible to express the ground state energy as:

$$E_0 = min_{p\to N}(F_{HK}[p] + \int p(\vec{r})V_{Ne}(\vec{r})d\vec{r})$$

The complete form of the universal function, F_{HK}, is still unknown. The major challenges lay within the kinetic energy and the non-classical term of the electron-electron repulsive term. Kohn and Sham proposed an idea in 1965 that suggested calculating the exact kinetic energy of a non-interacting reference system with the same density as the original interacting one. The kinetic energy of the non-interacting reference system takes the form:

$$T_s = -\frac{1}{2}\sum_{i}^{N} < \psi_i|\nabla^2|\psi_i >$$

The reference density takes the form:

$$p_s(\vec{r}) = \sum_{i}^{N}\sum_{s} |\psi_i(r,s)|^2 = p(\vec{r})$$

Where ψ_i represents the orbitals of the non-interacting system [55]. Kohn and Sham knew that T_S was not equal to the true kinetic energy of the system and introduced a separation in the universal functional.

$$F[p] = T_S[p] + J[p] + E_{XC}[p]$$

E_{XC} is defined as the exchange-correlation energy and is defined as:

$$E_{XC}[p] \equiv (T[p] - T_S[p]) + (E_{ee} - J[p])$$

Thus, it is the unknown components of the kinetic energy and electron-electron repulsive term. It can also be defined as, the missing exchange energy from anti-symmetry and the correction factor for assuming that the electrons were non-interacting or the correlation energy. The total energy takes the new form:

$$E[p] = T_S[p] + J[p] + E_{XC}[p] + E_{Ne}[p]$$

We can expand the total energy by substituting the known functional in terms of electron density.

$$E[p] = T_S[p] + \frac{1}{2}\int\int \frac{p(\vec{r}_1)p(\vec{r}_2)}{r_{12}} d\vec{r}_1 d\vec{r}_2 + E_{XC} + \int V_{Ne} p(\vec{r}) d\vec{r}$$

To apply the variational principle and minimize energy in terms of orbitals, we must first translate the total energy into orbitals ψ_i.

$$E[p] = -\frac{1}{2}\sum_i^N < \psi_i|\nabla^2|\psi_i > + \frac{1}{2}\sum_i^N\sum_j^N \int\int |\psi_i(\vec{r}_1)|^2 \frac{1}{2r_1} \left|\psi_j(\vec{r}_2)\right|^2 d\vec{r}_1 d\vec{r}_2 +$$

$$+E_{XC}[p] - \sum_i^N \int \sum_A^M \frac{Z_A}{r_{1A}} |\psi_i(\vec{r}_1)|^2 \, d\vec{r}_1$$

As can be seen by the total energy equation, the only term that does not have an explicit form is the exchange-correlation energy. This is no surprise as it is still unclear how to solve the unknown portions pertaining exchange energy and correlation energy. However, it is still possible to continue and apply the variational principle and pursue the

orbitals that will minimize the energy expression. These new set of equations are what are known as the Kohn-Sham equations [55, 103, 104].

$$\hat{h}_{KS}\psi_i = \epsilon_i\psi_i$$

$\hat{h}_{KS}$ is the Kohn-Sham operator, that when applied to the orbitals ψ_i will give the energy of the orbitals ε_i of the system. $\hat{h}_{KS}$ is a combination of the kinetic energy and the effective potential:

$$\hat{h}_{KS} = -\frac{1}{2}\nabla^2 + V_{eff}$$

The effective potential is an expression of three components: the electron-electron repulsive potential, the exchange-correlation potential and the nucleus-electron attraction potential.

$$V_{eff}(\vec{r}) = V_{ee} + V_{XC} + V_{Ne} = \int \frac{p(\vec{r}_2)}{r_{12}} + V_{XC}(\vec{r}_1) - \sum_A^M \frac{Z_A}{r_{1A}}$$

$$\hat{h}_{KS} = -\frac{1}{2}\nabla^2 + \left[\int \frac{p(\vec{r}_2)}{r_{12}} + V_{XC}(\vec{r}_1) - \sum_A^M \frac{Z_A}{r_{1A}}\right]$$

Applying the Kohn-Sham operator to the orbitals will give the minimized orbital to obtain the ground state energy of the system.

$$\left(-\frac{1}{2}\nabla^2 + \left[\int \frac{p(\vec{r}_2)}{r_{12}} + V_{XC}(\vec{r}_1) - \sum_A^M \frac{Z_A}{r_{1A}}\right]\right)\psi_i = \epsilon_i \psi_i$$

Also, it is important to note that the exchange-correlation energy is the partial derivative of the exchange-correlation potential [55, 103, 104].

$$V_{XC} = \frac{\partial E_{XC}[p]}{\partial p}$$

Once, the proper contributions are substituted into the effective potential, it is substituted into the one-particle equations above. Then it will be possible to determine the orbitals, which in turn will give the ability of determining the ground state electron density and ground state energy. Of course, just one factor remains and that is producing an approximation method to solve for the exchange-correlation functional. An approximation is needed because it is still unknown how to solve this functional exactly, but, if it were possible then one could solve for the exact energy of the system.

Exchange-Correlation Functionals

Next, we must understand the different exchange-correlation functionals to fully understand the mechanics behind DFT. It is important to note that there is no direct hierarchy when selecting the exchange-correlation functional. In general, selecting an exchange-correlation functional depends strictly on the atoms or system attempting to be modeled. One cannot simply use a higher or more complicated exchange-correlation functional and expect better results. As was stated before, this is why it is important to

understand the system being modeled and all parameters associated with the system and the different exchange-correlation functionals. The exchange-correlation functionals are what distinguish what DFT model from another.

The first and basis of all exchange-correlation functionals is known as Local Density Approximation (LDA). It is based on the concept that the electron density behaves as a uniform electron gas. This is a system in which the electrons move on a positive background and the total ensemble is neutral [103]. LDA is centered on being able to write the exchange-correlation functional in this form:

$$E_{XC}^{LDA}[p] = \int p(\vec{r})\epsilon_{XC}\big(p(\vec{r})\big)d\vec{r}$$

In this expression of the exchange-correlation functional, $\epsilon_{XC}(p(r))$ is the energy of a uniform electron gas with density p and is multiplied by the probability that there is an electron at position r. It is possible to further split the energy into its two distinct parts, exchange and correlation.

$$\epsilon_{XC}\big(p(\vec{r})\big) = \epsilon_X\big(p(r)\big) + \epsilon_C(p(\vec{r}))$$

The exchange portion has already been derived in the 1920's by Bloch and Dirac and takes the form:

$$\epsilon_x = -\frac{3}{4}\left(\frac{3p(\vec{r})}{\pi}\right)^{1/3}$$

There are many approximations for the correlation energy of a uniform electron gas that that can be employed in LDA, such as the Vosko, Wilk and Nusair (VWN) derivation. LDA's exchange energy is typically within ten percent, but the smaller correlation energy is typically overestimated by up to a factor of 2. It has been historically good at giving bond lengths of solids and molecules within two percent of experimental values. LDA typically fails in cases of heavy fermions where electron-electron interaction effects are extremely important [103]. It is the least computationally intensive of all the approximations but also considered to be the least accurate in most cases.

The next exchange-correlation functional with greater accuracy after LDA is the generalized gradient approximation (GGA). This was also a huge step in making DFT one of the most used and reliable forms of modeling systems. Instead of just evaluating an electron density at a point, it adds the information for the electron density gradient [105]. This allows for the functional to address the non-homogeneity of the electron density. The form of the GGA exchange-correlation energy is as follows:

$$E_{XC}^{GEA}[p_\alpha, p_\beta] = \int f(p_\alpha, p_\beta, \nabla p_\alpha, \nabla \rho_\beta) d\vec{r}$$

This is the general form and there are many different GGAs, such as, Perdew Wang 91 (PW91), Becke 88 (B88), and Lee Yang Parr (LYP). The different forms of GGA follow the same principle as detailed in the general equation, but have slight differences in handling the exchange or the correlation energy of the system. GGA has made DFT a

significant contributor to quantum chemistry because it has reduced the LDA errors of atomization energies of a set of molecules by a factor of 3.

The other forms of the exchange-correlation functional are called hybrid functionals. Hybrid functionals are exchange-correlation functionals that utilize a portion of the exact exchange from Hartree-Fock Theory. One of the most common hybrid functionals is called Becke, 3-parameter, Lee-Yang-Parr (B3LYP). We incorporate Hartree-Fock exchange by first starting with the expression of the Hamiltonian with a perturbation strength λ [103].

$$H_\gamma = T + V_{ext}(\gamma) + \gamma V_{ee}$$

If λ is equal to one, it transforms into the Hamiltonian for the interacting system and the external potential is the nuclear-electron attraction potential. That will yield the same Hamiltonian as was derived before for DFT. In the case λ is equal to zero, you get the non-interacting limit and we again use the Kohn-Sham approximation for the kinetic energy of the system. In the case of the kinetic energy a single Slater determinant of the Kohn-Sham orbitals, ψ_i, will solve the Schrödinger equation exactly. However, normally a single Slater determinant of the Kohn-Sham orbital will not solve the Schrödinger equation exactly, but hypothetically, in the limit as λ=0, it will. This mathematical limit will never exist because in reality the electrons and the nucleus do interact, but if we perform a slight modification and say that the limit must be 0<λ<1. Then we can adjust the external potential so that the same electron density is obtained for either limit. This is

an attempt to cross smoothly between the two limits of interest, the interacting λ=1 and the non-interacting λ=0. A formal way of connecting the non-interacting and interacting case has been established. Next, by utilizing the adiabatic connection formula it allows a formal way of writing the exchange-correlation energy as [103, 106]:

$$E_{XC} = \int_0^1 < \psi_\lambda | V_{XC}(\lambda) | \psi_\lambda > d\,\lambda$$

It is not possible to solve directly so another approximation is made. We assume that if λ is linear we can approximate that the exchange-correlation energy will take the form:

$$E_{XC} \approx \frac{1}{2} < \psi_0 | V_{XC}(0) | \psi_0 > + \frac{1}{2} < \psi_1 | V_{XC}(1) | \psi_1 >$$

The first portion is the non-interacting limit, thus ψ_0 is a Slater determinant and we can use the Hartree-Fock equations for the exchange energy. In the case of the interacting limit, it is still unknown and some type of approximation method such as Local Spin Density approximation (LSDA) must be used. It is mandatory to use the LSDA approximation as there are many hybrid functionals that contain other approximation techniques. The importance here is that the new exchange-correlation functional will be a mix of the Hartree-Fock exchange and one of the DFT approximations, such as, GGA or LDA. For example, the hybrid functional with LSDA approximation will take the form:

$$E_{XC} = \frac{1}{2} E_X^{HF} + \frac{1}{2} (E_X^{LSDA} + E_C^{LSDA})$$

This is a relatively simple hybrid functional, but there are other hybrid functionals that encompass the true hybrid meaning, such as, the most famous and widely used hybrid functional B3LYP.

$$E_{XC} = (1-a)E_X^{LSDA} + aE_X^{HF} + b\Delta E_X^{B88} + (1-c)E_C^{LSDA} + c\Delta E_C^{GGA}$$

As can be seen in the equation the approximation of the exchange-correlation energy has many terms that come from various approximations, such as, LSDA, GGA, and B88 but it also contains a portion of the non-interacting exchange which is solved by the Hartree-Fock Equations.

CHAPTER II

PREDICTING THE YOUNG'S MODULUS OF THE BORON NITRIDE NANOTUBE USING COMPUTATIONAL TECHNIQUES

Introduction to Property Prediction of BNNTs

The first logical step of understanding the interaction between the Epon 862/W resin system and BNNT is to create a model capable of simulating and predicting the properties of the BNNT. There are many MD methods used today to simulate polymers, but simulating nanotubes is a challenging task. Material Studios by Accelrys was used because it provides convenient tools for building systems with nanotubes and adds a variety of simulation methods varying from quantum chemistry to classical mechanics. The property of interest is the Young's Modulus of the BNNT. The focus was centered on the Young's Modulus because the hope is that the addition of BNNTs with superior mechanical properties, such as, Young's Modulus will enhance the Young's Modulus of the Epon 862/W resin system.

Simulation Details

In Materials Studios 6.0 Accelrys, a vast library of tools and force fields that can be applied in various computational models, the CASTEP module, which is based upon Density Functional Theory, was the best choice for the BNNT system because of its demonstrated success in simulating Boron Nitride systems and the length scale of the

system[102]. Two types of nanotubes were used in the simulation, (6,6) and (8,8) each with a length of 24.6 Å. These are armchair nanotubes with diameters of 8.14 angstrom for the (6,6) and 10.85 angstrom for the (8,8). The simulation process consists of five steps:

1. Construction of a BNNT and a Periodic Box,
2. Energy Minimization
3. Geometry optimization
4. Molecular Dynamics (MD)
5. Calculation of Elastic Constants for analysis of Mechanical Properties

For the construction of the BNNT's in Material Studio, the periodic box was built using three lattice parameters labeled A, B, and C, which are perpendicular to each other. A and B are the magnitude of the x and y vectors respectively of the box, x being the horizontal distance and y being the vertical distance. These values were determined using the theoretical value of ~2.28g/cm^3 which gave both A and B the value of 9.45 Å and the depth value for C, or the z coordinate length, of 24.6 Å [12]. After the box and nanotube were constructed, the system was ready for Energy Minimization and then the Geometry Optimization step. Geometry Optimization begins by dividing the nanotube into segmented units as shown in Figure 1. Each unit in Figure 1 consists of 12 boron and 12 nitrogen atoms. The reasoning behind why CASTEP divides the 24.6 Å long nanotubes into ten identical cells is to aid in calculation speed. Since, CASTEP uses quantum mechanics as well as Molecular Dynamics to model the various systems, it aids

in calculation speed if one can divide the system into identical cells and add the effects of each cell to approximate the behavior of the entire system.

The geometry optimized system (i.e. bond lengths and angles are set to give the lowest energy configuration for the system) is then simulated using MD parameters (i.e. temperature, pressure, stress and strain) to obtain the values such as, density, volume, number of atoms, and charge distribution, that are needed to describe the mechanical properties of the system. Table 1 contains a list of the parameters used in the MD simulation. Once the MD simulation is completed, CASTEP is used to calculate the elastic constants of the BNNT system and the mechanical properties such as Young's modulus and Poisson's ratio. The lattice parameters for the boxed system were 9.45 Å in the x and y plane and 24.6 Å for the depth or 2.46 Å per identical unit cell. An issue arose after the geometry optimization of the 9.45 Å periodic box, the BNNT structure became distorted as shown in Figure 2. A technique called linear extrapolation was performed to correct the distortion. Increased lattice parameters were used resulting in structures that were not distorted, depicted in Figure 3. A set of four runs were compiled to get sufficient data to describe the modulus at the theoretical density. The lattice parameters are shown in Table 2 and were based upon Kelkar et al [107].

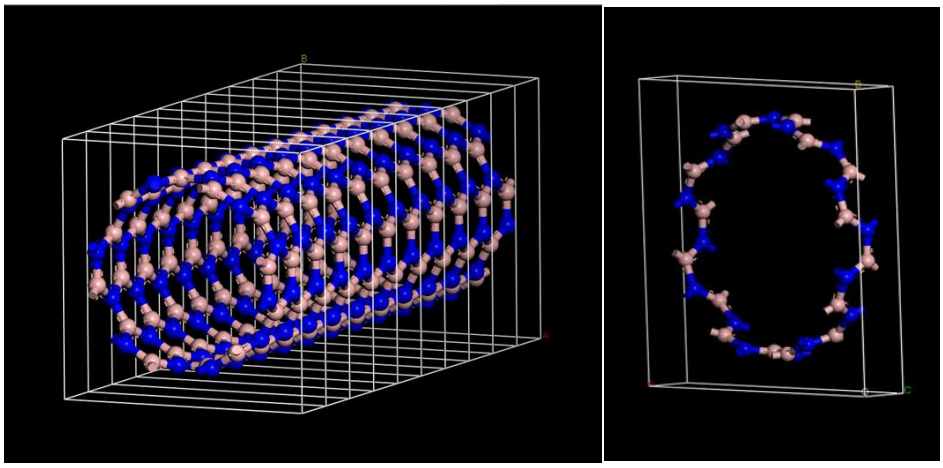

(a) (b)

Figure 1. (a) 6,6 Boron Nitride Nanotube Divided into 10 Unit Cells after Geometry Optimization, (b) Single Unit Cell of BNNT.

Table 1. Settings for MD Simulation Using CASTEP Module in Material Studios 6.0.

Setting	Simulation Parameters
Barostat	Andersen
MDTemperature	298.0K
Thermostat	Nose
FixCenterOfMass	No
LangevinConstant	0.1
NoseRatio	1
NumSteps	50000
Ensemble	NVT
TimeStep	1.0 fs

Table 2. Parameters for MD Simulation for (6,6) & (8,8) BNNT's.

(6,6) BNNT				
Run #	1	2	3	4
Diameter of BNNT (Å)	8.14	8.14	8.14	8.14
Lattice size (A=B, C)	11.483, 24.595	12.631, 24.595	13.894, 24.595	15.283, 24.595
Volume (Å^3)	3243.092	3923.955	4747.918	5744.68
Density (g/cm^3)	1.520	1.26	1.04	0.858
(8,8) BNNT				
Run #	1	2	3	4
Diameter of BNNT (Å)	10.85	10.85	10.85	10.85
Lattice size (A=B, C)	14.134, 24.595	15.283, 24.595	16.000, 24.595	16.970, 24.595
Volume (Å^3)	4919.626	5744.685	6296.351	7082.925
Density (g/cm^3)	1.34	1.148	1.047	0.931

As shown in Table 2, as lattice parameters were increased, the density of the system decreased. The simulations performed using the parameters in Table 2 are shown in Figure 3.

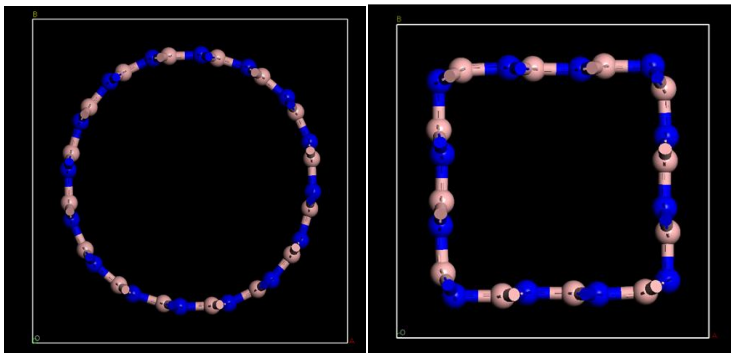

(a) (b)

Figure 2. 6,6 BNNT after Geometry Optimization, (a) Undistorted (b) Distorted.

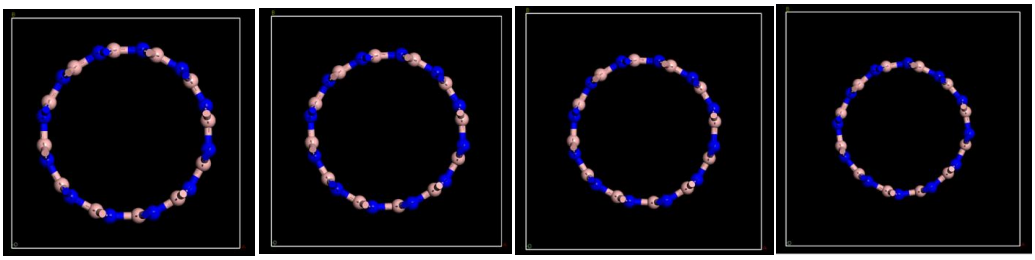

(a) (b) (c) (d)

Figure 3. Depicting the Increased Lattice Size Parameters from a-d of (6,6) BNNT, (a) 11.483 Å , (b) 12.631 Å, (c) 13.894 Å, (d)15.283 Å.

Results

Each simulation was repeated three times per set of lattice parameters. Each data point represents the mean value for the Young's Modulus at each density. The data was then analyzed using a linear regression method and a linear trend line fitted to the data to extrapolate the value of the Young's modulus at the theoretical density of ~2.28 g/cm^3, as seen in Figure 4 for the (6,6) BNNT and Figure 5 for the (8,8) BNNT. P values and 95 %

confidence intervals were computed using MedCalc statistical software to give validity and significance to the trend at the lower densities, which gave confidence in the extrapolated values at the theoretical density (~2.28 g/cm^3). The extrapolated value of the (6,6) BNNT is 830.41GPa at the density of ~2.28 g/cm^3 and the extrapolated value for the (8,8) is 776.21 GPa.

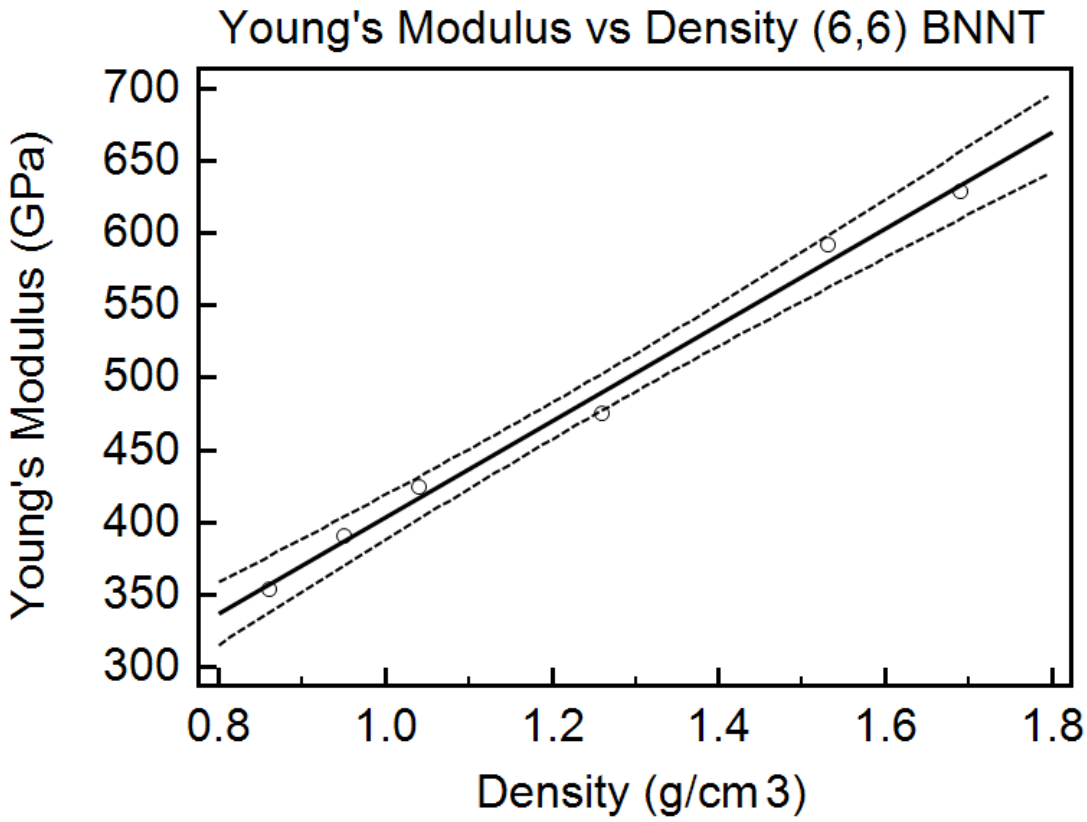

Figure 4. Young's Modulus vs. Density for (6,6) BNNT, Young's Modulus at a Density of 2.3 g/cm3 = 830.39 GPa (Dashed line represents 95% confidence interval).

Table 3. Regression Analysis Table for (6,6) BNNT.

Dependent Y	Young's Modulus				
Independent X	Density				
Sample size	6				
Coefficient of determination R^2	0.9920				
Residual standard deviation	11.1477				
y = 70.8471 + 333.1333 x					
Parameter	Coefficient	Std. Error	95% CI	t	P
Intercept	70.8471	18.8629	18.4754 to 123.2188	3.7559	0.0198
Slope	333.1333	14.9841	291.5307 to 374.7360	22.2324	<0.0001
Source	DF	Sum of Squares	Mean Square		
Regression	1	61424.3740	61424.3740		
Residual	4	497.0826	124.2706		
F-ratio	494.2791				
Significance level	P<0.001				

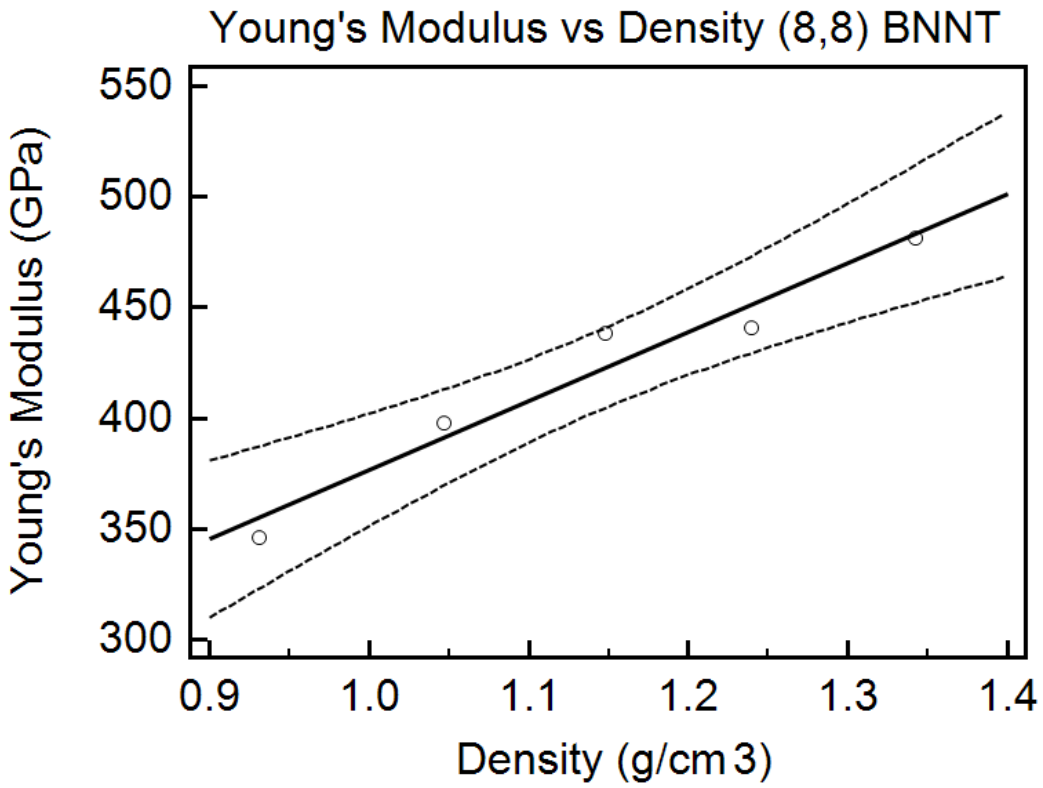

Figure 5. Young's Modulus vs. Density for (8,8) BNNT, Young's Modulus at the Density of 2.3 g/cm3 = 776.22 GPA (Dashed line represents 95% confidence interval).

Table 4. Regression Analysis Table for (8,8) BNNT.

Dependent Y	Young's Modulus				
Independent X	Density				
Sample size	6				
Coefficient of determination R^2	0.9539				
Residual standard deviation	12.7030				
y = 64.8451 + 312.0004 x					
Parameter	Coefficient	Std. Error	95% CI	t	P
Intercept	64.8451	45.5359	-80.0705 to 209.7607	1.4240	0.2496
Slope	312.0004	39.5831	186.0293 to 437.9715	7.8822	0.0043
Source	DF	Sum of Squares	Mean Square		
Regression	1	10025.4068	10025.4068		
Residual	3	484.0972	161.3657		
F-ratio	62.1285				
Significance level	P=0.004				

Discussion

By modifying the lattice parameters and using the extrapolation technique we were able to predict the Young's Modulus values of BNNT [92]. P values are below 0.05 which gives good significance in the linear trend. Also, the 95 percent confidence interval establishes good linearity with all data points as well as at the extrapolated point of ~2.28 g/cm^3. The simulation combines the strength of Density Functional Theory and incorporates our modifications to the unit cell in order to make precise predictions of the experimental Young's modulus for BNNT's. Also, our predicted values come within one percent of the predicted theoretical value of 870 GPa as described by Hernandez et al [102]. This MD simulation supports the use of Materials Studios 6.0 Accelerys as a viable and useful tool for property prediction of materials that are yet to be characterized.

Conclusion

The major role of this computational simulation was to establish a modeling method and system to predict the properties of an unknown system. It was established that Material Studios 6.0 Accelerys contains the tools and approximation methods to predict the properties of the BNNT within 1% of other commonly accepted techniques in the field. Also, we established that DFT is a viable method for performing the necessary simulations to predict the properties of the system. However, there is an issue with computational time that may affect simulations parameters when simulating larger systems, such as, the epoxy resin. Still, this model has given a better understanding of all the parameters necessary within our system and can be fine tuned to accommodate for optimal computational time and resources.

CHAPTER III

STUDYING THE EFFECTS OF HYDROGENATION ON THE YOUNG'S MODULUS OF BNNTS

Introduction to Hydrogenated BNNTs

A part of the radiation shielding strategy is to add hydrogen to the system for particle fragmenting and to help slow down high energy neutrons to increase the efficiency of neutron absorption by B^{10}. The goals of the this computational simulation are to understand the loading mechanisms of hydrogen on to BNNTs, to identify the most stable forms of hydrogenated BNNTs and to understand the effects of hydrogen on the mechanical properties of BNNTs. This investigation will use similar techniques to those employed to obtain the mechanical properties and to identify the stable states of hydrogenated BNNTs.

There are two methods of incorporating hydrogen into the BNNT structure. The first method is physisorption of the hydrogen atoms onto the surface of the BNNT via Van der Waals forces. Chemisorption is the second method, in which hydrogen is chemically bonded to the Boron and Nitrogen atoms via covalent or hydrogen bonds. Experimental studies have been conducted to understand the adsorption mechanism of Hydrogen onto BNNTs and have shown that an average of ~2.6% by weight of Hydrogen can be adsorbed onto BNNTs without any post processing.

Also, it has been demonstrated that an uptake of ~4.2% by weight of hydrogen can be adsorbed if BNNTs contain defects and that different defects can influence the preferred adsorption site of the hydrogen onto the BNNTs surface. Desorption studies have shown that the majority of hydrogen adsorbed onto BNNTs is chemisorbed [108, 109]. Also, hydrogen prefers to adsorb over Nitrogen atoms as opposed to Boron atoms and diameter or curvature of the BNNT influences the adsorption of the hydrogen onto the BNNT [110, 111]. NASA has demonstrated that BNNTs with a 5% by weight of hydrogen is optimally the best radiation shielding nanofiller. All of these insights were taken into consideration when building and understanding the influence of hydrogenation on the mechanical properties of the BNNTs.

Simulation Details

Materials Studios 6.0 by Accelrys was used to perform the Molecular Dynamics (MD) Simulation. A universal force field was used to perform the dynamics on the hydrogenated BNNTs, inside the CASTEP module which uses Density Functional Theory (DFT) to calculate the various parameters of the system. The simulation process consists of six steps:

1. Construction of a BNNT and a Periodic Box,
2. Loading of the BNNT with hydrogen
3. Energy Minimization
4. Geometry optimization

5. Calculation of Elastic Constants

6. Calculation of Mechanical Properties

Again, the construction of the BNNT and its periodic box was performed using a construction tool within the Materials Studios 6.0 Accelrys software. Once the construction of the BNNT and periodic box has been completed, we begin to load the BNNT with hydrogen. A fully hydrogenated BNNT structure, resulting in a 8% by weight of hydrogen. This is not a feasible percentage of hydrogenation but was chosen because it would be a limit bounding case or represent the extreme effect that BNNTs would experience after hydrogenation. Also, it would define the bounds of the effects of hydrogenation of BNNTs. Thus, the extreme case or limit bounding case would still give insight into whether or not hydrogenation will play a role in the viability of BNNTs as a structural and radiation shielding additive. Four different fully hydrogenated BNNT configurations were examined: 1.) Hydrogen chemically bonded externally to boron and nitrogen, 2.) Hydrogen chemically bonded to boron externally and nitrogen internally, 3.) Hydrogen chemically bonded internally to boron and nitrogen and 4.) Hydrogen chemically bonded internally to nitrogen and externally to boron. The two structures with the lowest energy and a stable structure were the externally hydrogenated BNNT (HBNNT) and the externally hydrogenated boron and internally hydrogenated nitrogen HBNNT. These structures were also confirmed to be the most stable in terms of energy by Tanskanen et al [95]. Also, two different size nanotubes were simulated, (6,6) and (8,8) armchair nanotubes.

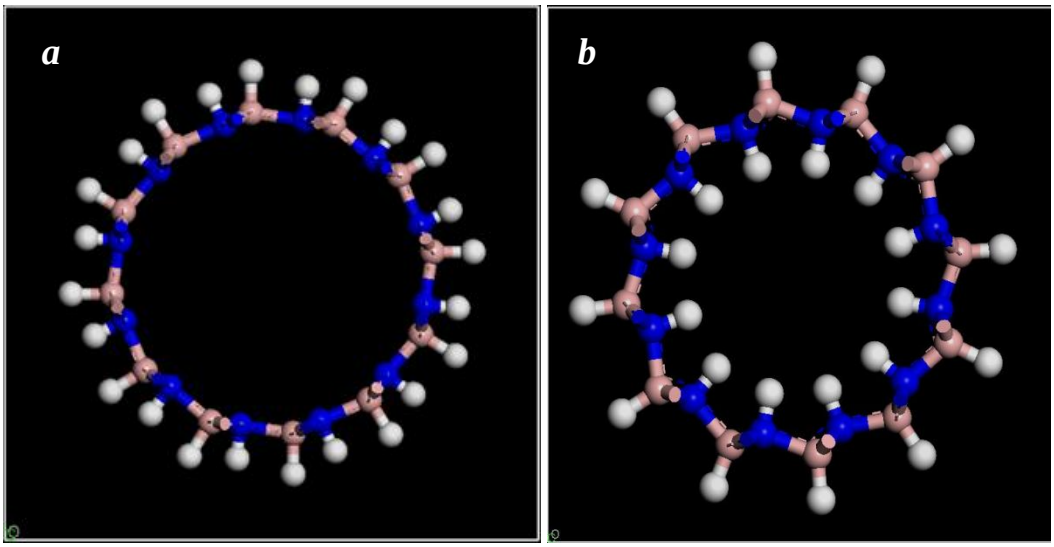

Figure 6. a. HBNNT with Hydrogen Externally Bonded, b. HBNNT with Hydrogen Externally Bonded on Boron and Internally Bonded on Nitrogen.

Next, geometry optimization is performed on the HBNNTs using DFT, and the hybridized functional (Becke, 3-Parameter, Lee Yang (B3LYP)). The B3LYP hybridized functional was chosen to perform the geometry optimization because it had shown good success in optimizing hydrogenated structures [95]. Again, the linear extrapolation was utilized to overcome the distorted structure of the hydrogenated BNNTs at the lattice parameters that yielded the theoretical density, ~2.62 g/cm^3. Thus, four larger periodic boxes were constructed to lower the overall density of the system and a linear regression method was used to extrapolate the Young's Modulus to the theoretical density of the BNNTs [107]. Lastly, the elastic constants are calculated using DFT with a GGA approximation and the Perdew Wang 91 (PW91) exchange-correlation functional set

[112]. Then, the Material Studios software analyzes the elastic constant and calculates the Young's modulus for the HBNNT systems.

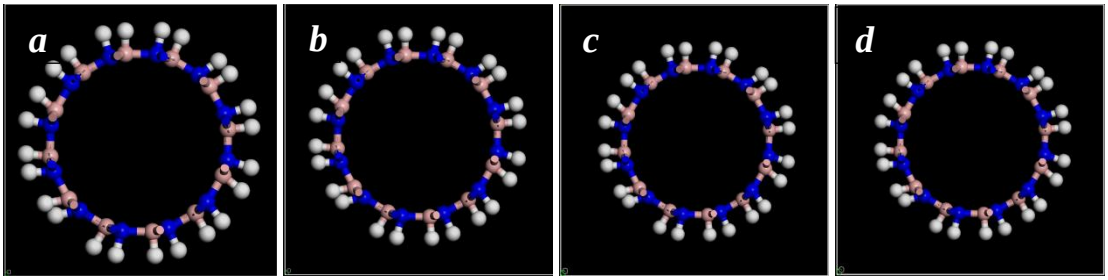

Figure 7. Depicting the Increased Lattice Size Parameters of (6,6) BNNT, (a) 12.3 Å , (b) 13.5 Å, (c) 14.8 Å, (d) 16.2 Å.

Lattice parameters were derived by increasing the lattice parameters of the previous theoretical density correct system until geometry optimization did not cause distortion within the structure. Then the three remaining boxes were constructed by the previous lattice parameters plus ten percent, which was chosen to give a good range between data points. This is depicted in the table below.

Table 5. Physical Characteristics of the Unit Cells Used for (6,6) BNNTs with Hydrogen.

(6,6) BNNT with Hydrogen				
Run #	1	2	3	4
Diameter of BNNT (Å)	8.14	8.14	8.14	8.14
Lattice size (A=B, C)	12.3, 24.595	13.5,24.595	14.8, 24.595	16.2, 24.595
Density (g/cm^3)	1.383	1.148	0.955	0.797
(8,8) BNNT with Hydrogen				
Run #	1	2	3	4
Diameter of BNNT (Å)	10.85	10.85	10.85	10.85
Lattice size (A=B, C)	15.5, 24.595	17.0,24.595	18.6, 24.595	20.5, 24.595
Density (g/cm^3)	1.525	1.329	1.190	1.103

Results

The Young's Modulus for BNNT and the two configurations of HBNNTs were determined using the extrapolation technique (figures 3 and 4). Table 2 shows predicted values of E where theoretical density of 2.28 g/cm^3 and 2.62 g/cm^3 were used for BNNT and HBNNT, respectively. In case of (6,6) nanotubes, addition of Hydrogen to the structure of tube resulted in 11.6 percent decrease in Young's modulus (for both

configurations) while for (8,8) nanotubes a smaller decrease is observed with 10 percent for the external Hydrogen configuration and 7 percent for Hydrogen on the external side of B and the internal side of N configuration.

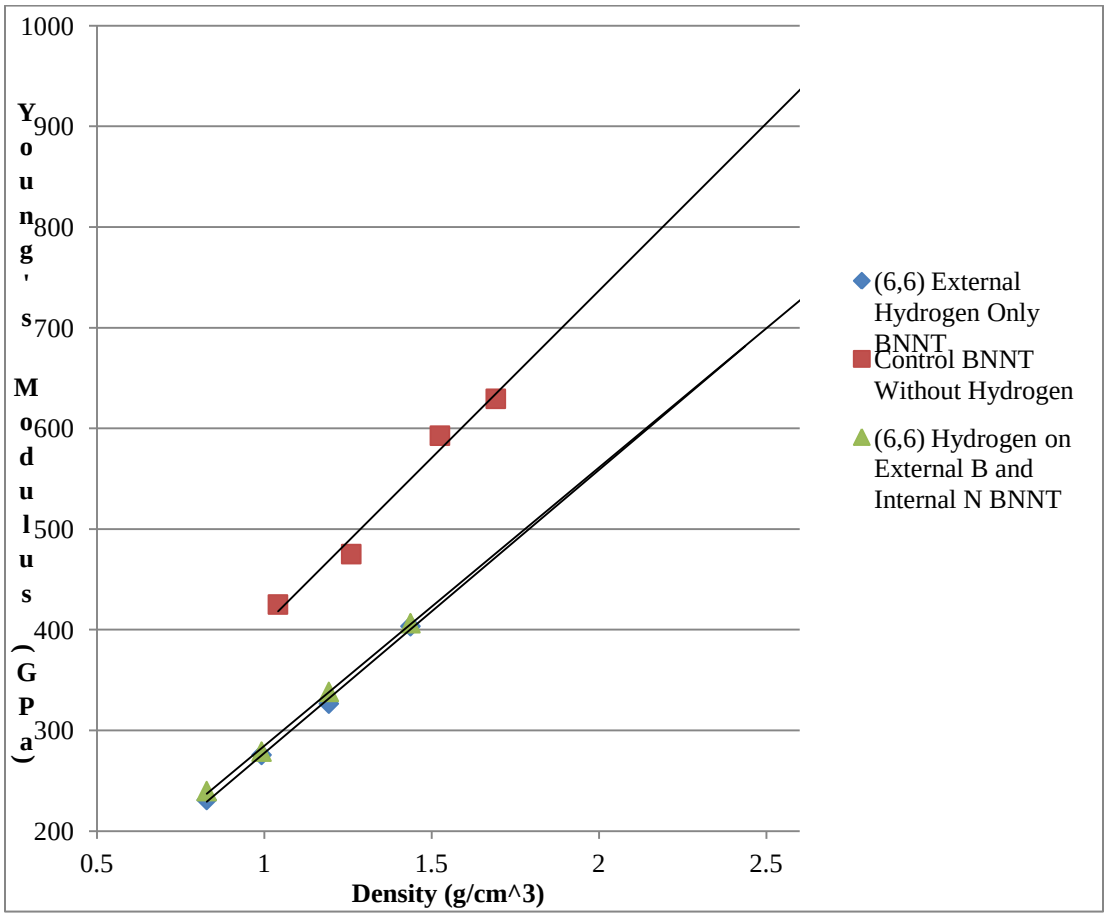

Figure 8. Young's Modulus vs. Density for (6,6) BNNT w and w/o Hydrogen.

Therefore, it is expected that by introducing Hydrogen to the structure of nanotubes, the Young`s modulus value will decrease by the average of 8.5 percent.

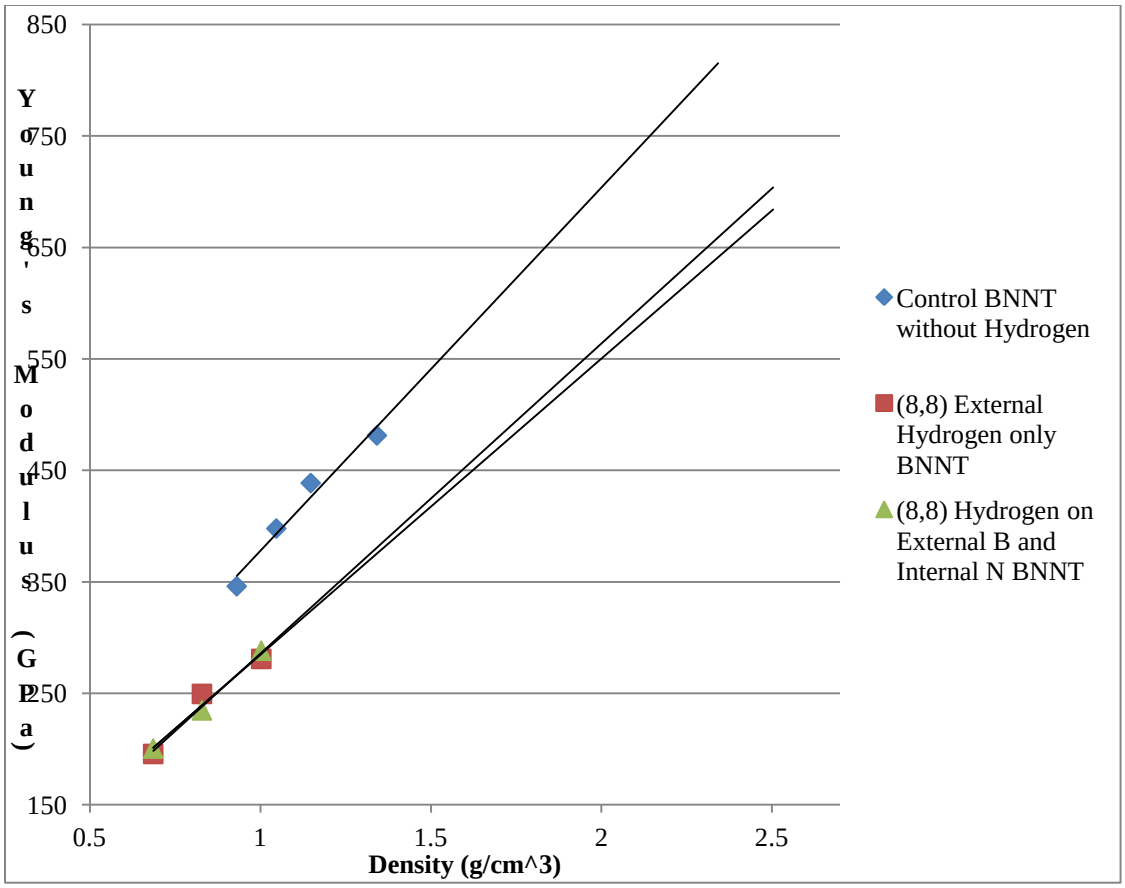

Figure 9. Young's Modulus vs. Density for (8,8) BNNT w and w/o Hydrogen.

Table 6. Depicts Difference in Young's Modulus between Hydrogenated and Non-Hydrogenated BNNTs.

Predicted Young`s modulus for (6,6) and (8,8)BNNTs and HBNNTs		
BNNTs Type	**6,6**	**8,8**
External Hydrogen Only	733	715
Hydrogen on External B and Internal N	732	736
No Hydrogen	830	795

Discussion

Using the extrapolation technique with the Material Studios software has shown that it is possible to predict Young's Modulus for BNNTs [13]. Results show an 11 % decrease in the Young's Modulus for the (6,6) HBNNTs and an 8.5 % decrease for the (8,8) HBNNTs . Even though further investigation is needed, addition of Hydrogen on only external sites has been demonstrated to have less effect on Young`s modulus of nanotubes with larger diameter. It is well known that the diameter plays an important role in the bonding of the hydrogen to the BNNT and therefore would be reasonable to believe that diameter would have an influence on the overall structural behavior of the nanotube. The relationship between tube diameter and the effect of introducing Hydrogen on Young`s modulus may be explained through atomic interactions and spacing between Hydrogen and B and N atoms. For smaller diameter tubes, e.g.(6,6) with 0.814 nm diameter, the distances between atoms is much less and thus positions of the additional hydrogen atoms can have a greater influence on the structure and mechanical properties of the BNNTs. On the other hand, the larger (8,8) Nanotubes (diameter of 1.085 nm) show a dependence on the configuration of the hydrogen which again can be due to the inter atomic distance between the atoms when it is bonded inside or outside the tube. Also, the increased distance could have been the reason why the Young's Modulus was effected less in the (8,8) BNNT. However, further investigation would be required to understand the true cause behind the effect of hydrogenation on the Young's Modulus of the BNNTs and the diameter of the tubes.

Although, based on presented results, addition of Hydrogen reduces the elastic modulus of BNNTs and degrades mechanical properties; HBNNTs still offer a unique and interesting combination of strength and shielding capability. Researchers have long tried to improve the mechanical strength of carbon composite by adding Carbon Nanotubes, but the results are not as promising as was expected. Addition of Carbon nanotubes into composites has introduced new challenges such as dispersion of nanotubes throughout the composite, nanotube agglomeration, interface interaction between nanotube and matrix, a limit on the maximum percentage of Carbon nanotubes that can be incorporated into the composite and many others. Therefore, HBNNTs can be interesting candidates for space application, considering that they possess a combination of properties including improved radiation shielding properties, high Young`s modulus (=> 700 GPa comparing to 150 GPa for carbon fiber) and light weight. Once fabrication challenges are solved and good quality composites are made using HBNNTs, addition of Boron Nitride nanotubes are expected to increase the mechanical strength of carbon fiber nanocomposite while improving chemical and thermal stability [6,10,14]. This would still result in an enhancement of the mechanical properties of the conventionally accepted and used carbon fiber composites.

Conclusion

Studying a boundary case has shown the extreme effects of hydrogen on the Young's Modulus of the BNNTs. Even at this unrealistic boundary, BNNTs appear to be an acceptable additive to carbon fiber-based nanocomposites. Also, since this configuration of HBNNTs is a non-realistic case, realistic HBNNTs would be

hydrogenated to a much lower percentage, resulting in a greater Young's Modulus for the nanomaterial. This greater Young's Modulus solidifies and reassures researchers that BNNTs can improve the Young's Modulus and radiation shielding capabilities of the current and commonly used carbon fiber composites for aerospace applications. In conclusion, hydrogenated BNNTs are theoretically predicted to be a viable choice in radiation shielding nanocomposites.

CHAPTER IV

PREDICTING THE YOUNG'S MODULUS AND GLASS TRANSITION TEMPERATURE OF EPON 862/W RESIN SYSTEM

Introduction to the Epon862/W Resin System

Epon 862/W resin system is a thermoset resin, which means that after curing it at elevated temperatures, usually above 200 Fahrenheit, it will irreversibly solidify. The solidification process is caused by cross linking of the Epon 862 and "W" curing agent. This resin system is strong because of its high cross linking density. Optimal cross linking occurs when the curing agent is mixed with the Epon 862 at a ratio of 100 grams to 26.4 grams of "W". These ratios have already been determined and tested by the manufacturer and provided on the materials data sheet. Figure 10 and 11 show the molecular structure of Epon 862 and the curing agent "W".

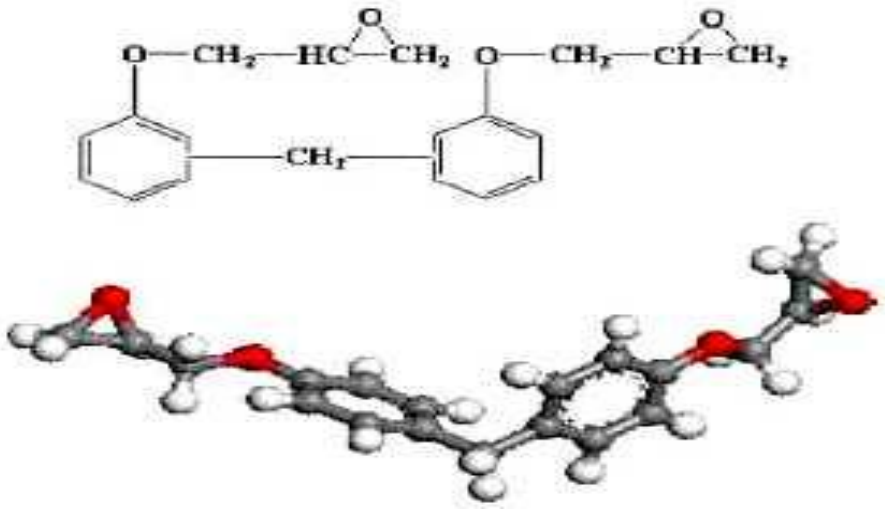

Figure 10. Diglycidyl Ether of Bisphenol F (EPON 862)

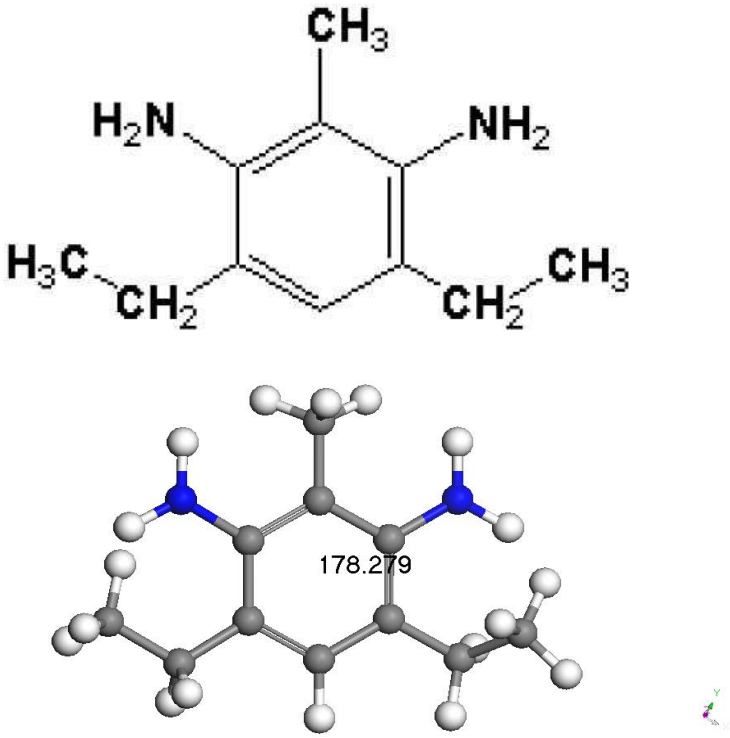

Figure 11. Diethylmethylbenzenediamine(DETDA) "W".

Cross linking occurs between the nitrogen on the "W" curing agent and the epoxide group on the Epon 862 as shown in Figure 3 [113]. Curing temperature also plays a role in the mechanical and thermal properties of the resin. An optimal curing cycle was developed to give the optimal mechanical and thermal properties.

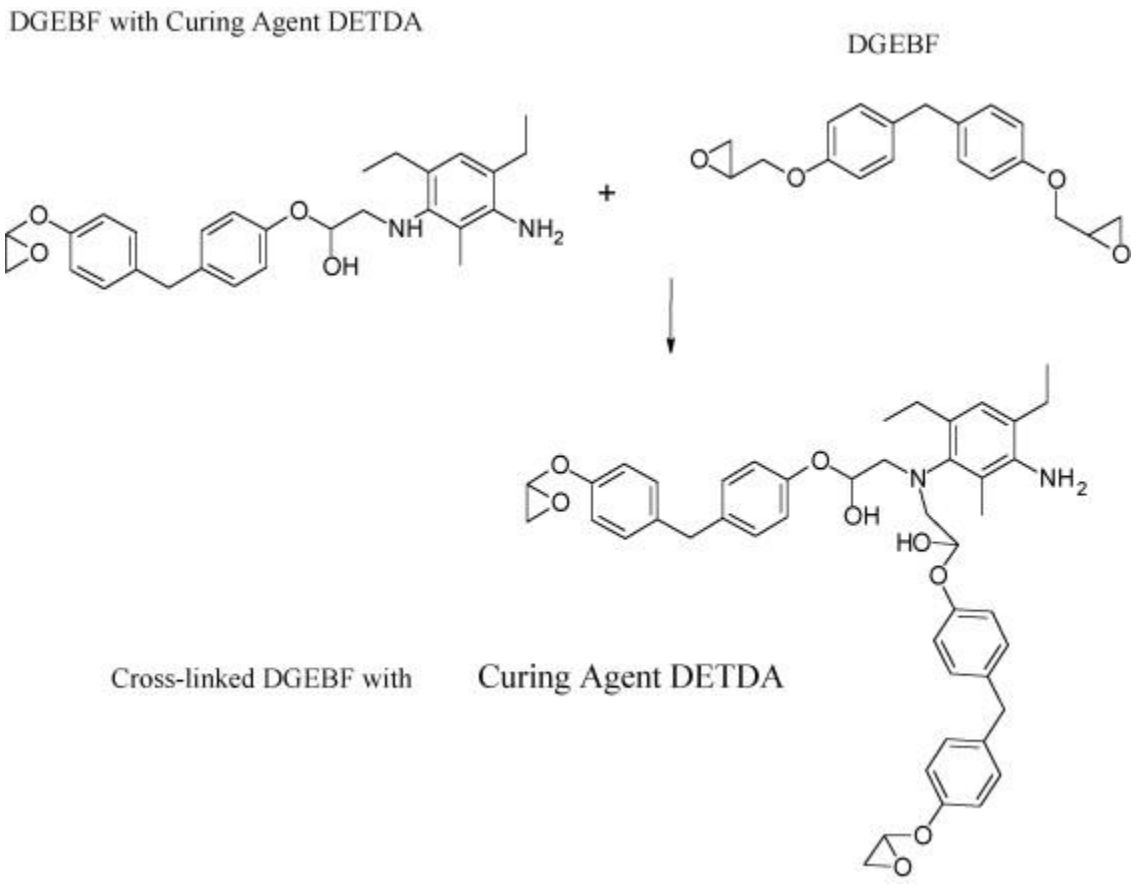

Figure 12. Demonstrating the Cross Linking Mechanism of Epon 862 with Curing Agent "W".

Fully cured Epon 862/W resin system at the optimal conditions contains a 2 to 1 ratio of Epon 862 to "W" curing agent. This results in a unit cell of 8 Epon 862 molecules cross

linked with 4 “W” curing agent molecules (Figure 4). For simulation purposes this will be the unit cell utilized in the computational studies. All complete cells will be packed to obtain the density of the cured Epon862/W resin system of 1.2 g/cm^3.

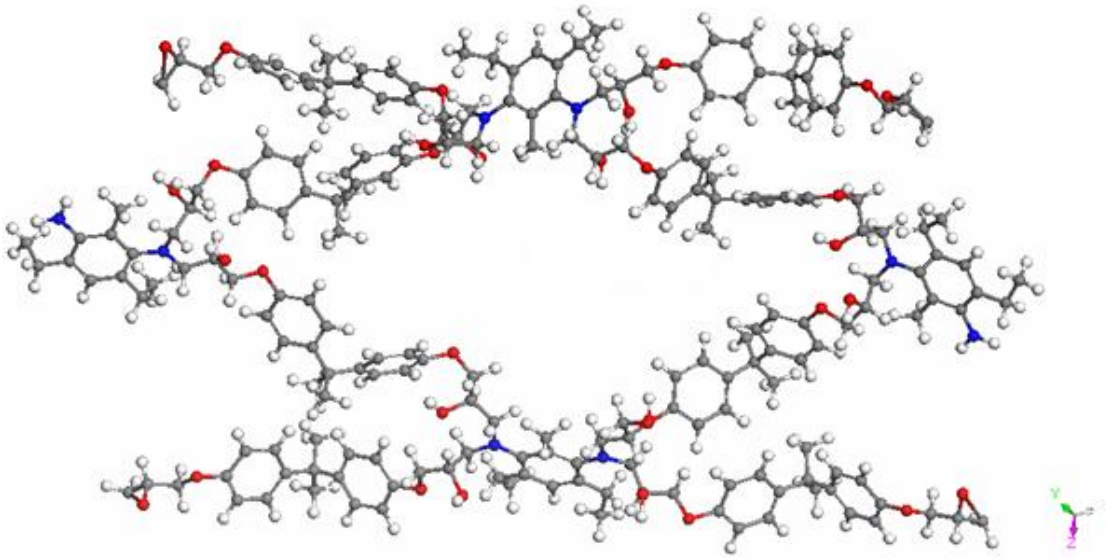

Figure 13. 2:1 Epon862/W Resin System Unit Cell.

Typical experimental values of the Young’s Modulus for the Epon 862/W cured resin system is between 2.48 GPa and 3.79 GPa depending on curing cycle and ratios. Simulation methods predict slightly higher values for the Young’s modulus, 4.847 GPa to 4.9 GPa [114]. The goal is to adjust the current BNNT model to obtain the Tg and Young’s Modulus of the Epon 862/W resin system with good consistency.

Simulation Details

One of the biggest challenges with developing computational models is to choose a technique that is efficient and accurate. As the system has grown from a single

nanotube to a hydrogenated nanotube, DFT has been the primary core of the model. Unfortunately, with the size of the Epon862/W Resin system, a hybrid model was adopted. Early, when the BNNTs were hydrogenated, a hybrid model consisting of B3LYP and GGA (PW91) was used to predict the mechanical properties of the system. The core was still a majority of DFT techniques, but the dynamics were performed with classical mechanics methods and the Universal Force Field. Results, were consistent with what was to be expected when the BNNTs were hydrogenated. The new Epon 862/W resin system is a much larger system and quantum chemistry techniques will take years to perform the calculations on these systems. Thus, we move to more classical approaches and use the Forcite Module with the Universal Force field to perform many of the tasks previously performed by DFT. The systems are constructed using the Amorphous tool in Materials Studio 6.0 Accelrys. The periodic box is constructed and packed with the quadcell structure, Epon 862 and "W" curing agent until a density of 1.2 g/cm^3 is achieved which represents the experimental density values for the Epon 862/W resin system.

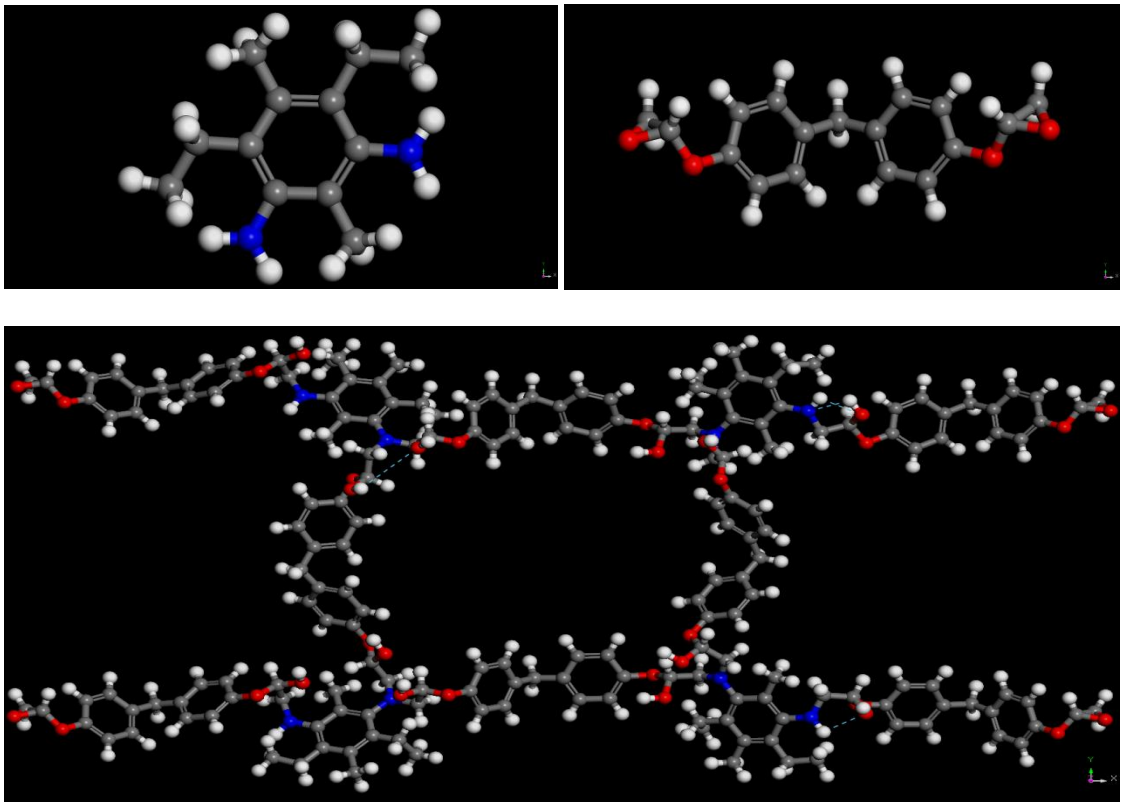

Figure 14. Depiction of Elements Used by Amorphous Tool to Pack Unit Cell to 1.2 g/cm^3.

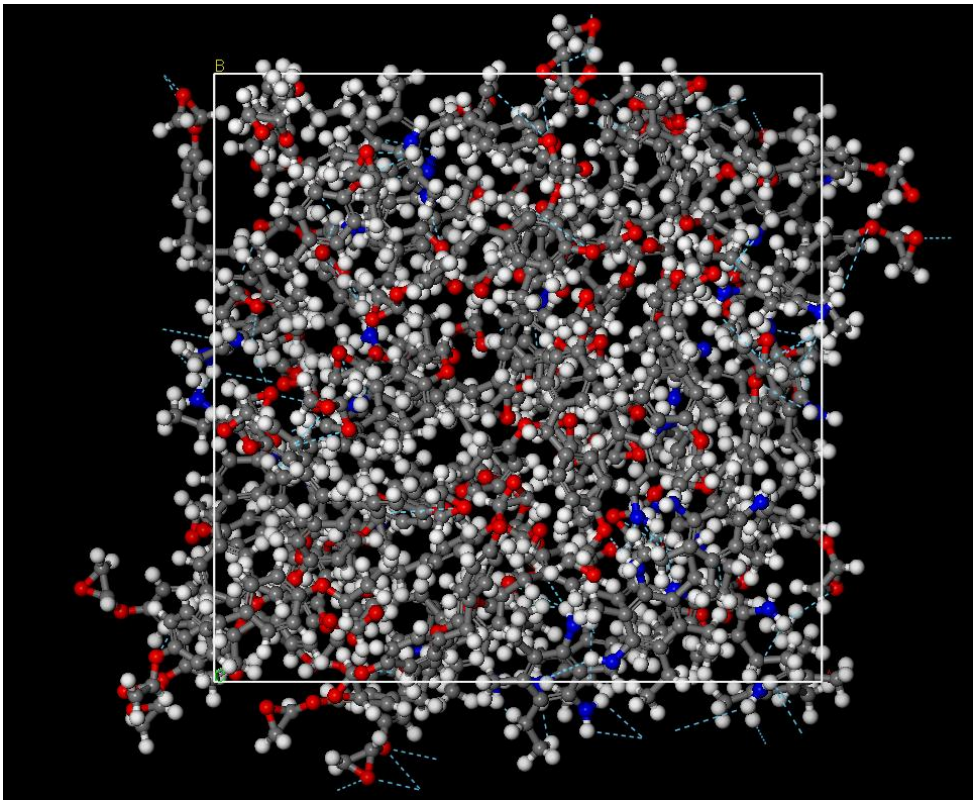

Figure 15. Unit Cell after Amorphous Tool has Packed Periodic Box to a Density of 1.2 g/cm3 with Epon 862/W Resin Components.

The periodic box was constructed with lattice parameters: 30Å by 30Å by 24.6Å and kept constant throughout all Epon 862/W resin system simulations. These lattice parameters were chosen to give a realistic number of atoms to the system and still accommodate the BNNT at a future date. Many different configurations were packed to accommodate for randomization due to cross linking and orientation (Figure 16).

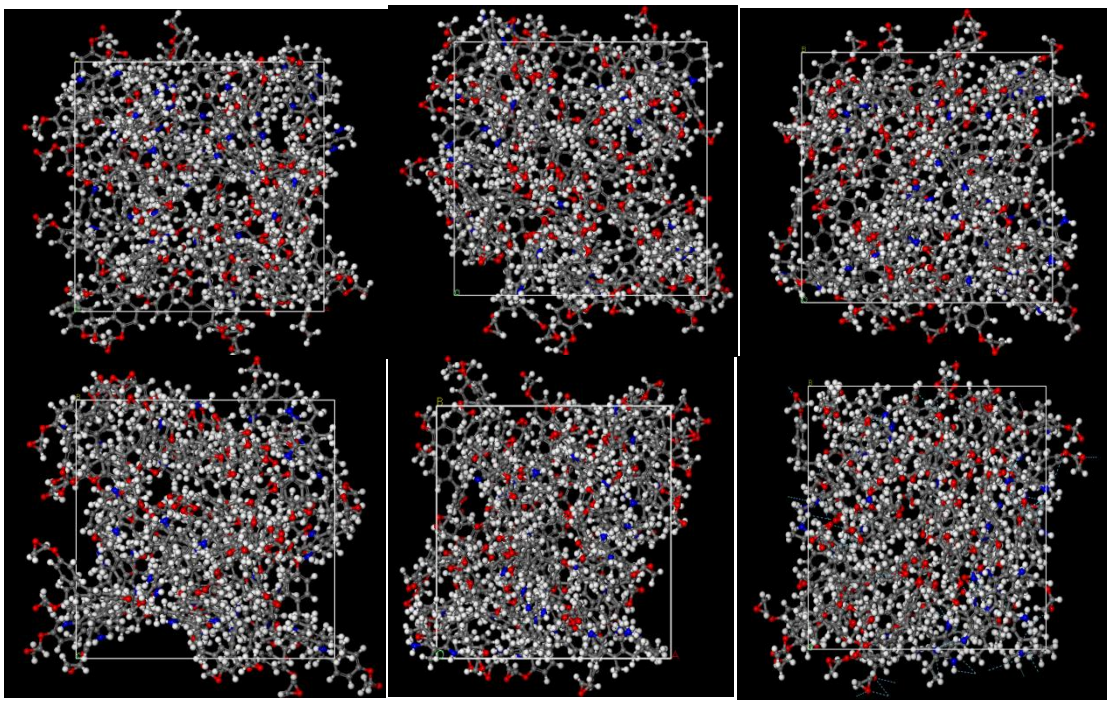

Figure 16. Different Packing Configurations but all with a Density of 1.2 g/cm^3.

The method of simulation is similar to that previously used to simulate the BNNTs and HBNNTs. The five simulation steps are as follows:

1. Energy Minimization
2. Geometry Optimization
3. Constant number of atoms, volume and temperature (NVT) Molecular Dynamics (MD) Simulation
4. Constant number of atoms, pressure and temperature (NPT) MD Simulation
5. Calculation of Mechanical Properties

Energy minimization was done using the Universal Force Field. There were various options to perform the geometry optimization in the Forcite module, but the steepest descent method gave the best results when optimizing this particular system. Next, was the NVT MD simulation to equilibrate the Epon 862/W resin system. The Anderssen method was use to maintain the temperature of the system, which was, allowed to equilibrate for 50 picoseconds (ps) with 1 femtosecond (fs) time steps at a temperature of 298K (Table 7).

Table 7. List of Parameters for NVT Simulation.

Setting	**Simulation Parameters**
Thermostat	Andersen
MDTemperature	298.0K
FixCenterOfMass	No
NumSteps	50000
Ensemble	NVT
TimeStep	1.0 fs

After NVT equilibration was NPT equilibration, similar parameters were chosen for the NPT; including 50 ps run with 1 fs time steps at room temperature. The thermostat was consistent with the NVT equilibration, Andersen method, and the barostat was the Berenendsen method (Table 8). After the equilibration step, the elastic constants were calculated using the hybrid method that utilizes the Universal force field. After the elastic constants were calculated, analysis was performed to extract the Young's Modulus of the system.

Table 8. List of Parameters for NPT Simulation.

Setting	Simulation Parameters
Thermostat	Andersen
BaroStat	Berendsen
MDTemperature	298.0K
FixCenterOfMass	No
NumSteps	50000
Ensemble	NPT
TimeStep	1.0 fs

Results

The density and Young's Modulus were calculated as the average value of the six systems. Six iterations were taken to construct the average value of the properties for each individual system of the Epon 862/W resin system. No extrapolation techniques were needed to determine the values of the glass transition temperature or Young's Modulus. The average value of the Young's Modulus was calculated to be 11.92 GPa. The glass transition temperature of the resin system was determined by annealing the resin from 298 Kelvin and increasing the temperature by 5 Kelvin until reaching a final temperature of 500 Kelvin. An increment of 5 Kelvin was chosen due to the slight variation in temperature produced by the Berendesen thermostat, which maintains the temperature for the system. The Berendesen thermostat produces a standard deviation of plus or minus 2-3 degrees giving a possible accuracy within 5-6 Kelvin. This process was again repeated six cycles and the densities at each temperature were averages of the six iterations. The figure below depicts change in density as the resin is heated to its

glass transition temperature and up to 500 Kelvin. It is shown below that the greatest decrease in density occurs between 396K and 416K. The midpoints between these two values give us a glass transition temperature of 406K or 133 degrees Celsius.

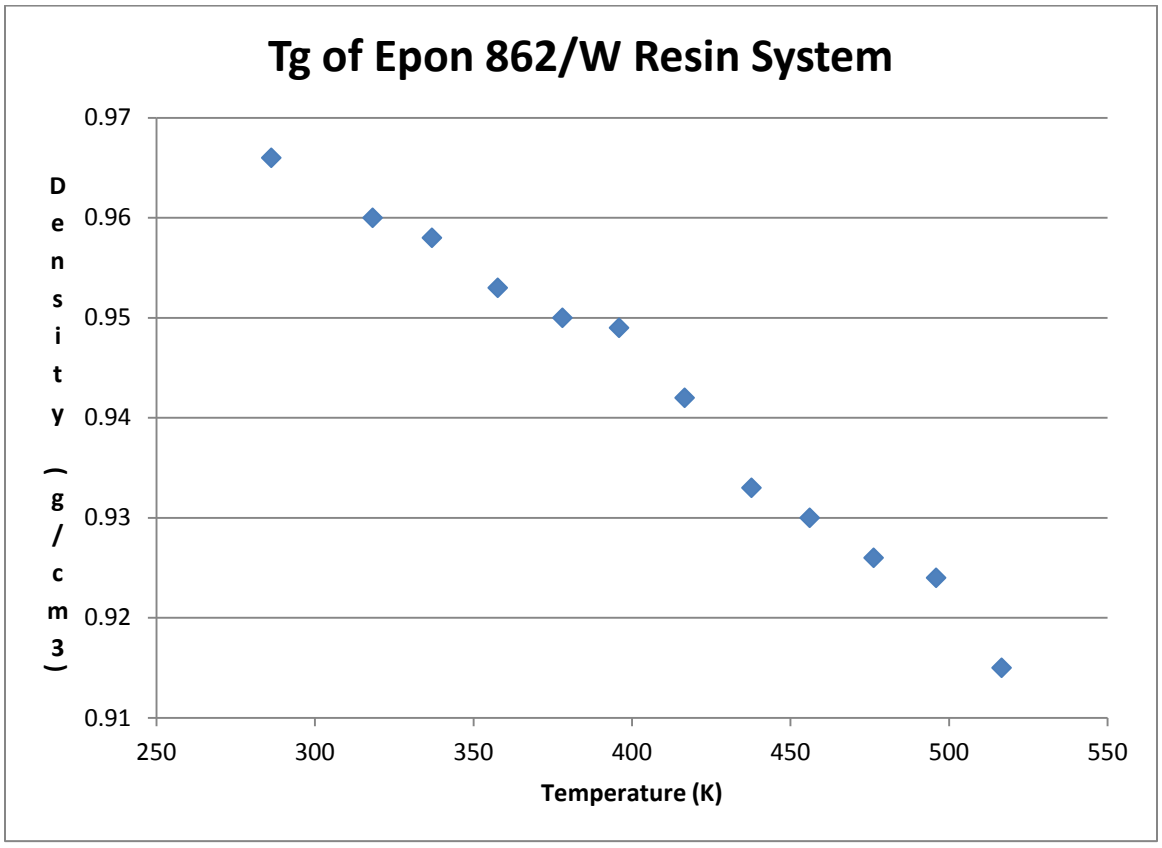

Figure 17. Depicting the Predicted Tg for the Epon 862/W Resin System.

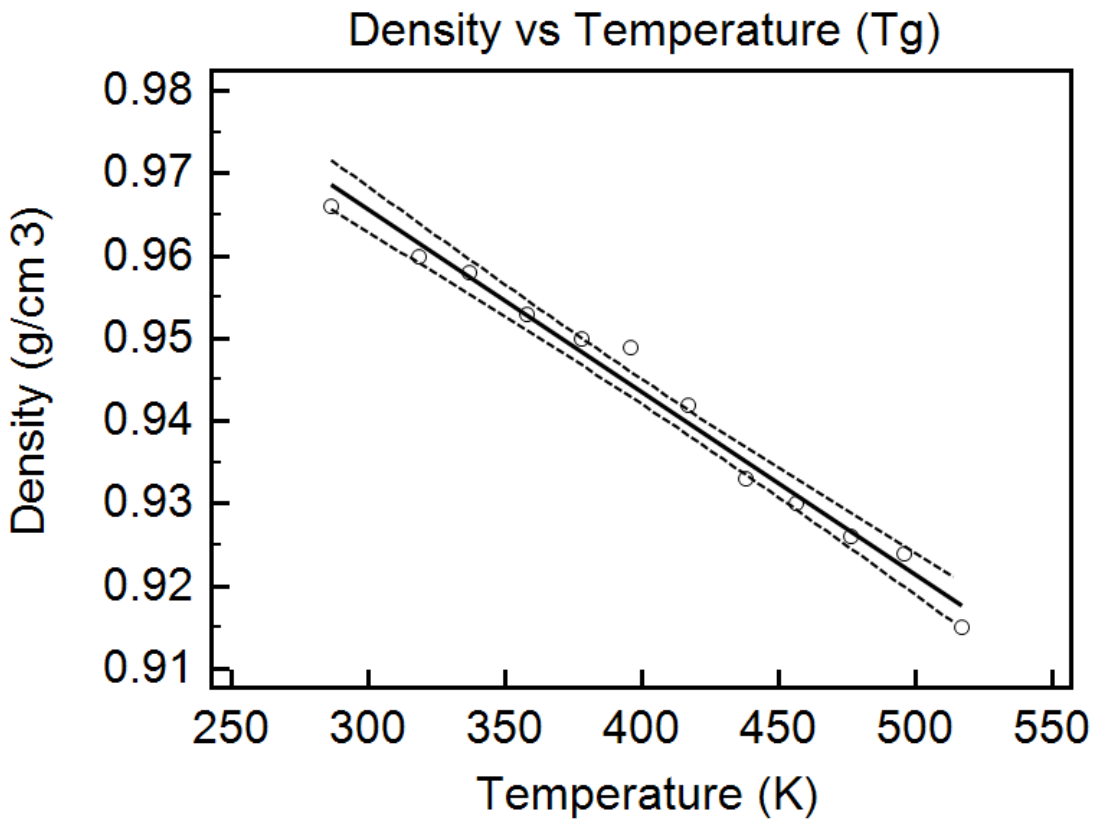

Figure 18. Graph of Resin Tg with 95% Confidence Interval.

Table 9. Regression Analysis for Glass Transition Temperature of Epoxy Resin System.

Sample size					12
Coefficient of determination R^2					0.9811
Residual standard deviation					10.5416
y = 4595.6946 + -4446.8318 x					
Parameter	Coefficient	Std. Error	95% CI	t	P
Intercept	4595.6946	183.7091	4186.3651 to 5005.0241	25.0161	<0.0001
Slope	-4446.8318	194.9591	-4881.2277 to -4012.4359	-22.8091	<0.0001
Source		DF	Sum of Squares	Mean Square	
Regression		1	57813.4993	57813.4993	
Residual		10	1111.2576	111.1258	
F-ratio				520.2529	
Significance level				P<0.001	

Discussion

A Young's Modulus of ~12 GPa for just resin is about 3 times higher than what is commonly seen in experiment. Many factors, such as, cross linking density, processing method, curing cycle, ratio of Epon to curing agent, and defects in the polymer chain can contribute to the fact that the computational system is higher than the experimental values. Computational methods generally simulate perfect cross linking, no defects and perfect ratios of Epon 862 to "W" curing agent. Thus, a ~12 GPa Young's Modulus for this system is not uncommon to be seen in computational simulations. Also, it is important to note that the focus of this study is to study the interfacial interaction between the resin and the BNNT and to study effect of BNNTs on the Young's Modulus and glass transition temperature of the resin system. The purpose of simulating the resin was to

first develop a viable method of simulating the system and to establish the control or base line for the system. If the simulations where BNNTs are incorporated into the system result in an increase in Young's Modulus or glass transition temperature of the system, it can be concluded that it was due to the addition of the BNNTs.

The model was able to predict the glass transition temperature of the system as well as the Young's Modulus. Similar factors that affect the Young's Modulus of a system can also affect the glass transition temperature of a system. The general experimental values for glass transition temperature of this resin system range between 125 to 130 degrees Celsius. The 95% confidence interval also verified that the Tg occurred between 396 K and 416 K by establishing the data points which fell outside the trend or the greatest change in density (figure 18). The percentage change in density and the 95% confidence interval established by the computational model predicts a slightly higher value for the glass transition temperature, 133 degrees Celsius, which is due to reasons similar to the reasons for the elevated value for the Young's Modulus. However, it is slightly closer to the experimental values, which would indicate that defects do not affect the glass transition temperature as much as they would the Young's Modulus. Defects will change the strength of the bonding in the polymer but might introduce other forms of bonding that could help to maintain some of the thermal properties of the polymer. This would have to be studied further with experimental and computational kinematics, introducing known defects that will bring the system closer to reality so that it would be possible to understand the interaction and bonding of real systems. As long

as the systems are built the same way when incorporating BNNTs it is possible to study the effects of nanotubes because a base line or control has been established for the Epon 862/W resin system.

Conclusions

The Amorphous Module was used to create a resin system with the desired density of 1.2 g/cm^3. Once the resin system and periodic box are established, a hybrid modeling system was developed that utilized the Universal force field and the Forcite Module to perform the calculations to determine the Young's Modulus and glass transition temperature of the system. The Young's Modulus and glass transition temperature were higher than what is commonly seen in experiment, but this inaccuracy is due to the fact that in computational model systems are generally considered at the theoretical limits due to the lack of imperfections in the system. However, the control system has now been established and can be used in comparison with the BNNT infused systems. The next step is to incorporate resin systems with BNNTs and study the interfacial interactions between the two materials.

CHAPTER V

COMPUTATIONAL MODELING OF THE INTERACTION BETWEEN THE EPON 862/W RESIN SYSTEM AND BORON NITRIDE NANOTUBES

Introduction to the Interaction between Epon862 Resin System and BNNTs

There are many methods for composite fabrication, such as, Vacuum Assisted Resin Transfer Molding (VARTM), Autoclave and the fiberglass spray lay-up process. All fabrication processes are unique with specific parameters and equipment to be utilized in each. Optimization of each process occurs frequently in the industry as new technology is developed or more modern styles of the process are developed. The materials used in composites can sometimes cause need for optimization as not each material will behave the same with each fabrication method. As three phase composites are becoming a wave of the future, techniques and methods to incorporate these various materials are being developed. Two of the greatest challenges are dispersion of the nanofiller and creating good interfacial connectivity between the matrix and nanofiller. Carbon nanotubes were and still are one of the most promising nanofillers to be used in the enhancement or alteration of composite materials. It was demonstrated that dispersion and good interfacial interaction was a process that needed optimization not only for the CNTs but the matrix as well [24]. Functionalization is a common technique used to enhance the interfacial connectivity of nanofillers, but again the right functional

group must be optimized to create the best effect of the nanofiller on the composite. Even though BNNTs are similar in structure to CNTs, the electronic properties are quite different. BNNTs have an asymmetric charge distribution which covers the structure in local dipoles or charge areas depending on the atom. It is a possibility that BNNTs might interface better with highly hydrogenated polymers, such as, the Epon 862/W resin system and require little to no functionalization to alter or enhance the properties of composites. The goal is to study the effects of BNNTs on the mechanical properties of the Epon 862/W resin system and their interfacial interaction.

Simulation Details

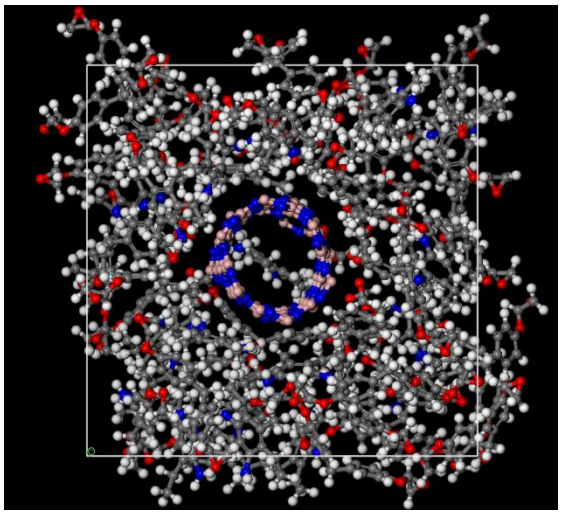

Figure 19. 4 Ring (6,6) BNNT with Epon 862/W Resin System.

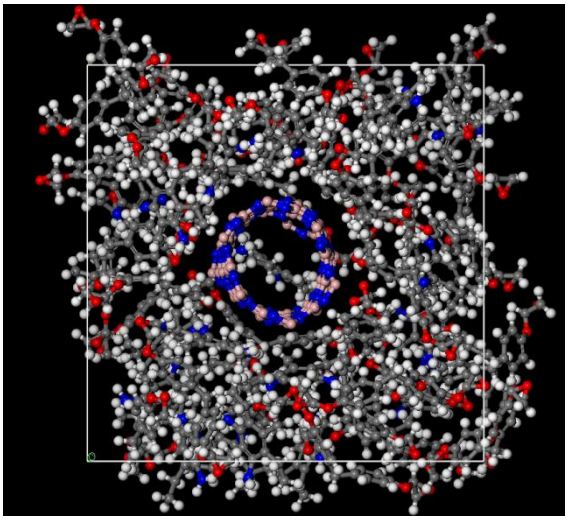

Figure 20. 7 Ring (6,6) BNNT with Epon 862/W Resin System.

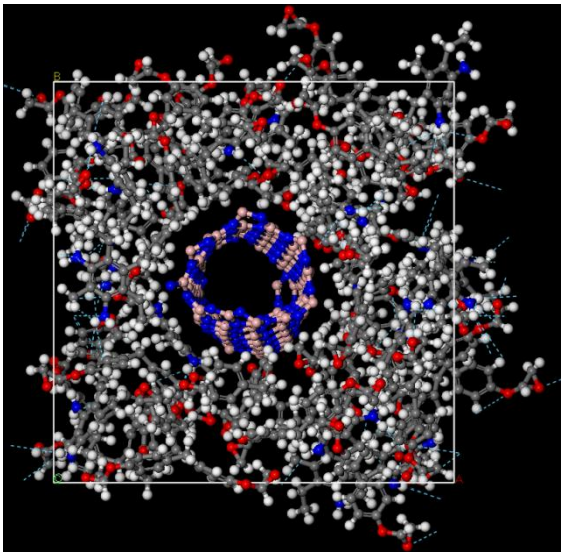

Figure 21. 10 Ring (6,6) BNNT with Epon 862/W Resin System.

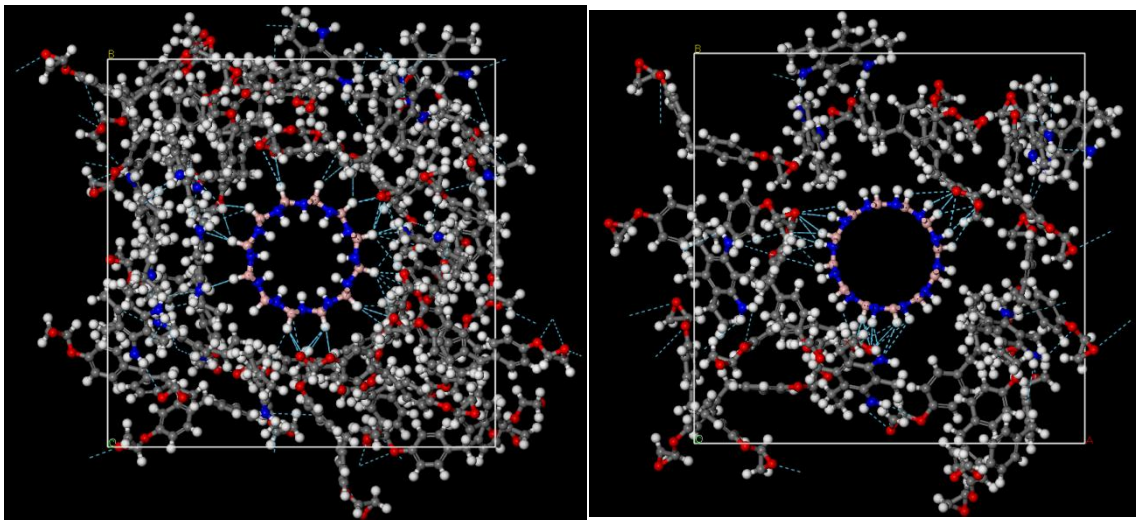

Figure 22. Left: 4 Ring (6,6) HBNNT(External Boron and Internal Nitrogen) with Epon 862/W Resin System, Right: 4 Ring (6,6) HBNNT (Externally Bonded) with Epon 862/W Resin System.

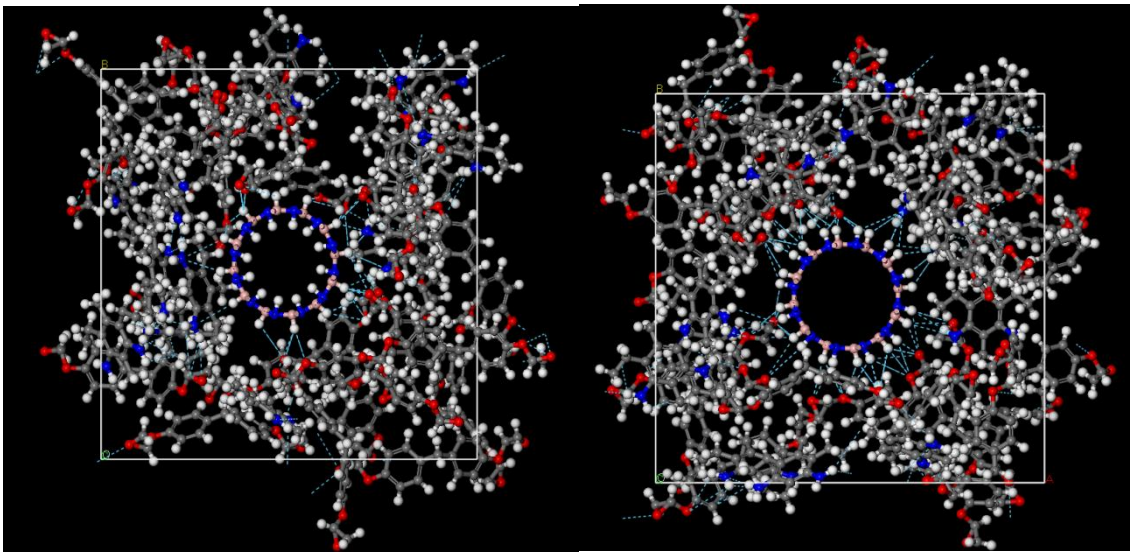

Figure 23. Left: 7 Ring (6,6) HBNNT(External Boron and Internal Nitrogen) with Epon 862/W Resin System, Right: 7 Ring (6,6) HBNNT (Externally Bonded) with Epon 862/W Resin System.

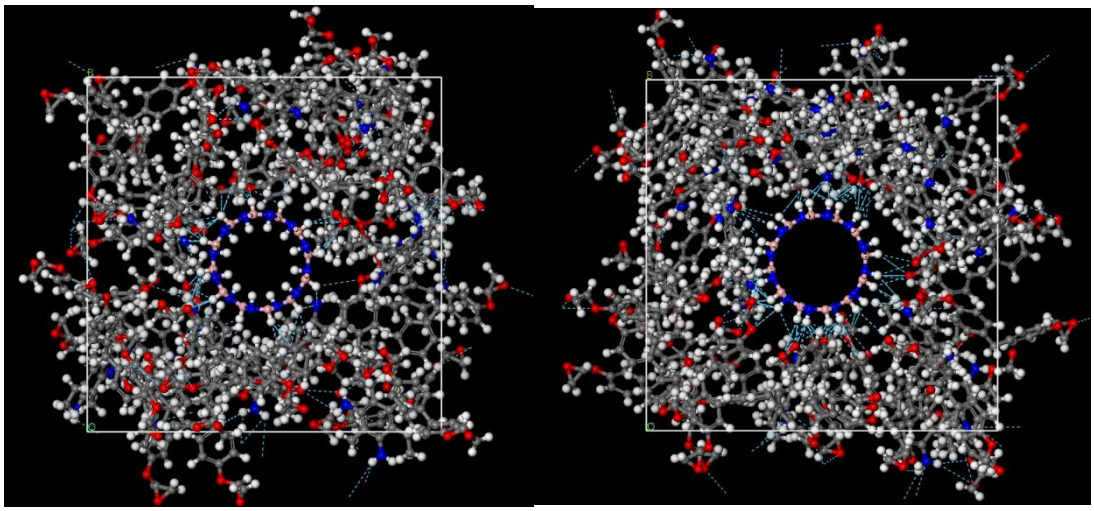

Figure 24. Left: 7 Ring (6,6) HBNNT(External Boron and Internal Nitrogen) with Epon 862/W Resin System, Right: 7 Ring (6,6) HBNNT (Externally Bonded) with Epon 862/W Resin System.

Results

The goal of the simulation was to establish a model to predict the mechanical properties of the system at a specific concentration of BNNTs. We studied the Epon 862/W resin system with (6,6) BNNT, Epon 862/W with externally hydrogenated BNNT and Epon 862/W internally and externally hydrogenated BNNT. Stability of the BNNT was limited to a minimum length of three rings. A structure of less than three rings would result in the BNNT being warped and distorted by the Epon 862/W resin system. It was not feasible to achieve a volume of resin that would be consistent with experimental constraintsand thus a higher percentage of BNNT was simulated to test the prediction capability of the model. Since, percentages of BNNT are above realistic values, simulation predictions were compared to the theoretical values generated by the

rule of mixtures. The rule of mixtures is divided between an upper limit, which assumes parallel orientation to the load being experienced by the material. The lower limit is assuming orientation is perpendicular to the axis of the load, which would result in the lowest possible modulus. The goal is for the model to predict within the upper and lower limit of the rule of mixtures. It is also important that the P-value must be within the 95% confidence limit to establish a good trend that can later be used in order to continue to build larger models and to apply the same techniques until realistic percentages of BNNT are achieved.

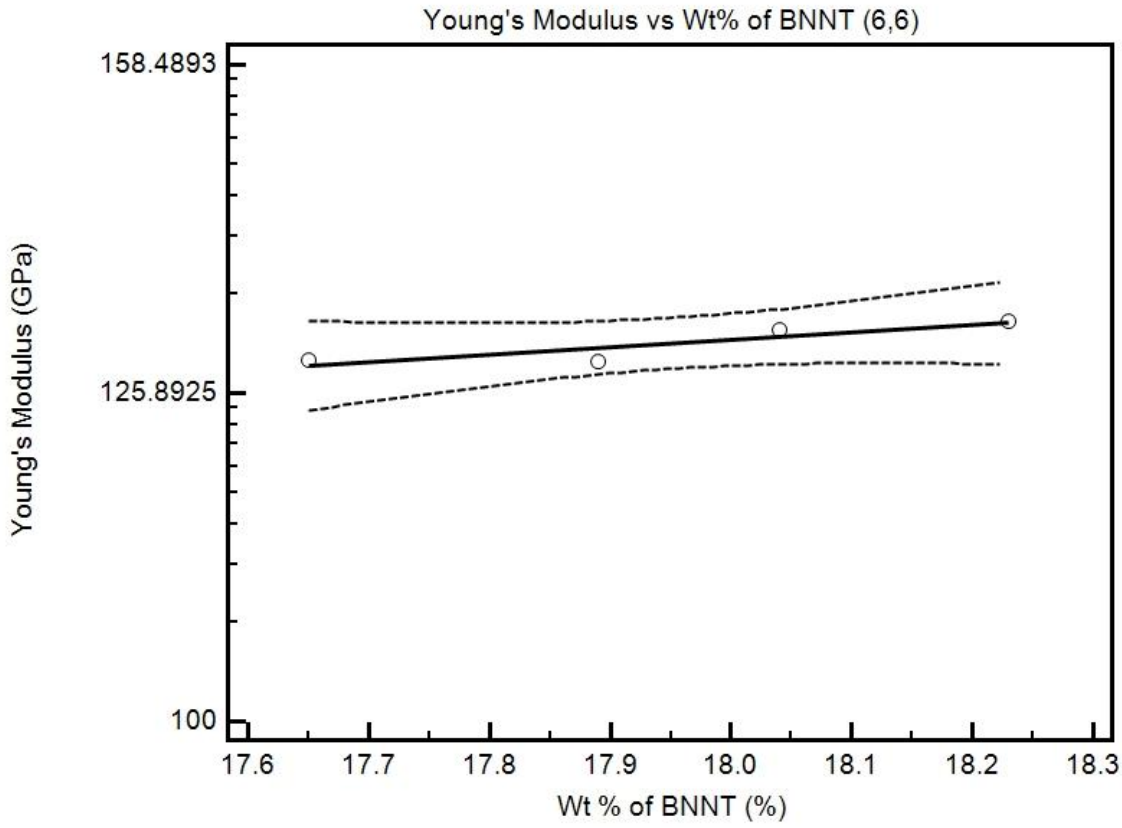

Figure 25. Predicting the Young's Modulus of Infused Epon 862/W Resin with 6,6 BNNT (Dashed line represents 95% confidence interval).

Table 10. Regression Analysis of Young's Modulus for (6,6) BNNT Infused Resin System.

Sample size					4
Coefficient of determination R^2					0.9620
Residual standard deviation					0.3204
y = 18.2256 + 5.3695 x					
Parameter	Coefficient	Std. Error	95% CI	t	P
Intercept	18.2256	13.5564	-40.1030 to 76.5542	1.3444	0.3110
Slope	5.3695	0.7551	2.1207 to 8.6183	7.1112	0.0192
Source	DF	Sum of Squares		Mean Square	
Regression	1	5.1918		5.1918	
Residual	2	0.2053		0.1027	
F-ratio				50.5694	
Significance level				P=0.019	

The upper bound of the rule of mixtures takes the form:

$$E_c = E_n f + E_m(1 - f)$$

E_c, E_n and E_m represent the Young's Modulus for the composite, nanofillers and matrix. The Young's Modulus of the nanomaterials is then multiplied by the volume fraction of nanomaterials, f. Similarly, the lower bound of the rule of mixtures for the Young's modulus takes the form:

$$E_c = \frac{E_n E_m}{E_m f + E_n(1 - f)}$$

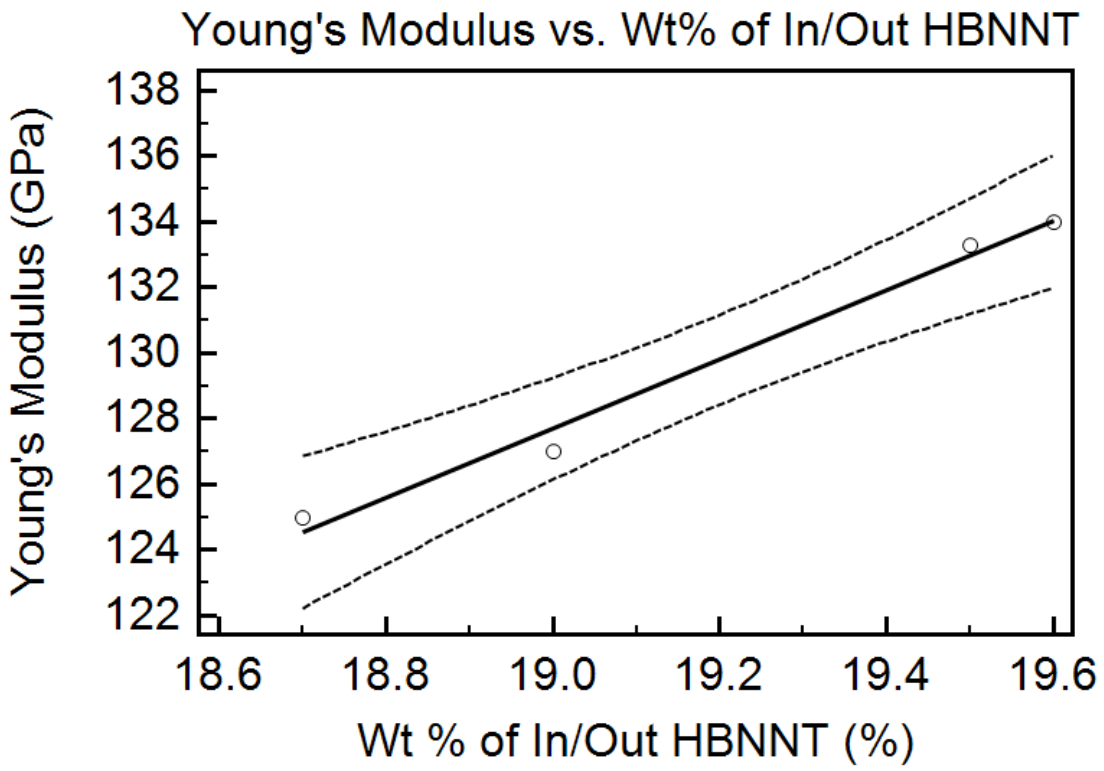

Figure 26. Predicting the Young's Modulus of Infused Epon 862/W Resin with (6,6) Internally and Externally Hydrogenated BNNT (Dashed line represents 95% confidence interval).

Table 11. Regression Analysis of Young's Modulus for (6,6) Internally and Externally HBNNT Infused Resin System.

Sample size					4
Coefficient of determination R^2					0.9867
Residual standard deviation					0.6359
y = -72.4351 + 10.5343 x					
Parameter	Coefficient	Std. Error	95% CI	t	P
Intercept	-72.4351	16.6174	-143.9338 to -0.9364	-4.3590	0.0488
Slope	10.5343	0.8653	6.8111 to 14.2575	12.1738	0.0067
Source	DF		Sum of Squares		Mean Square
Regression	1		59.9248		59.9248
Residual	2		0.8087		0.4043
F-ratio					148.2008
Significance level					P=0.007

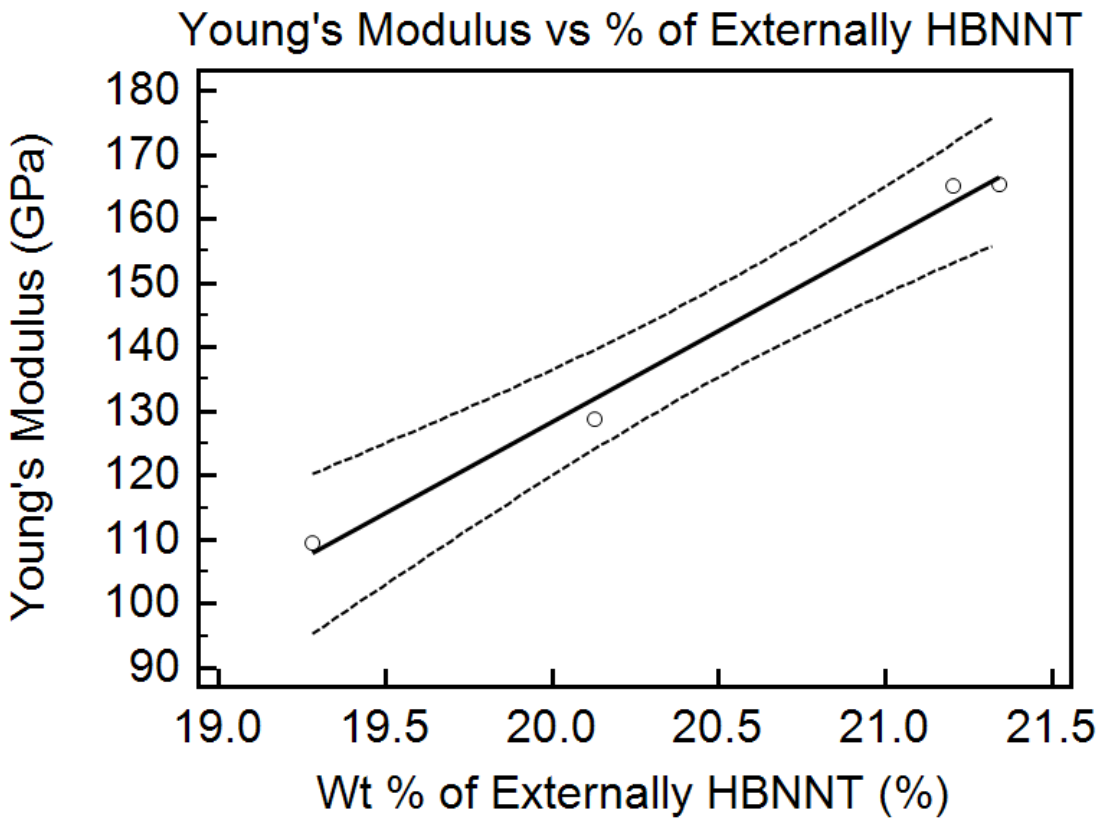

Figure 27. Predicting the Young's Modulus of Infused Epon 862/W Resin with (6,6) Externally Hydrogenated BNNT.

Table 12. Regression Analysis of Young's Modulus for (6,6) Internally and Externally HBNNT Infused Resin System.

Sample size					4
Coefficient of determination R^2					0.9905
Residual standard deviation					3.3137
y = -440.5930 + 28.4481 x					
Parameter	Coefficient	Std. Error	95% CI	t	P
Intercept	-440.5930	40.4486	-614.6294 to -266.5566	-10.8927	0.0083
Slope	28.4481	1.9727	19.9602 to 36.9359	14.4209	0.0048
Source	DF	Sum of Squares		Mean Square	
Regression	1	2283.5867		2283.5867	
Residual	2	21.9616		10.9808	
F-ratio				207.9620	
Significance level				P=0.005	

Table 13. Theoretical and Predicted Young's Modulus for 20% BNNT

20% BNNT	Plain Tube	Internally and Externally Hydrogenated	Externally Hydrogenated
Rule of Mixture Upper Bound	175.5	157.7	147.6
Rule of Mixture Lower Bound	14.8	14.8	14.8
Model Prediction	125.6	138.3	128.4

Table 14. Theoretical and Predicted Young's Modulus for 21% BNNT.

21% BNNT	Plain Tube	Internally and Externally Hydrogenated	Externally Hydrogenated
Rule of Mixture Upper Bound	216.4	164.9	154.9
Rule of Mixture Lower Bound	15.8	15.0	15.0
Model Prediction	131.0	148.8	130.7

Table 15. Theoretical and Predicted Young's Modulus for 22% BNNT.

22% BNNT	Plain Tube	Internally and Externally Hydrogenated	Externally Hydrogenated
Rule of Mixture Upper Bound	191.9	172.1	162.2
Rule of Mixture Lower Bound	15.2	15.2	15.2
Model Prediction	136.4	159.3	153.8

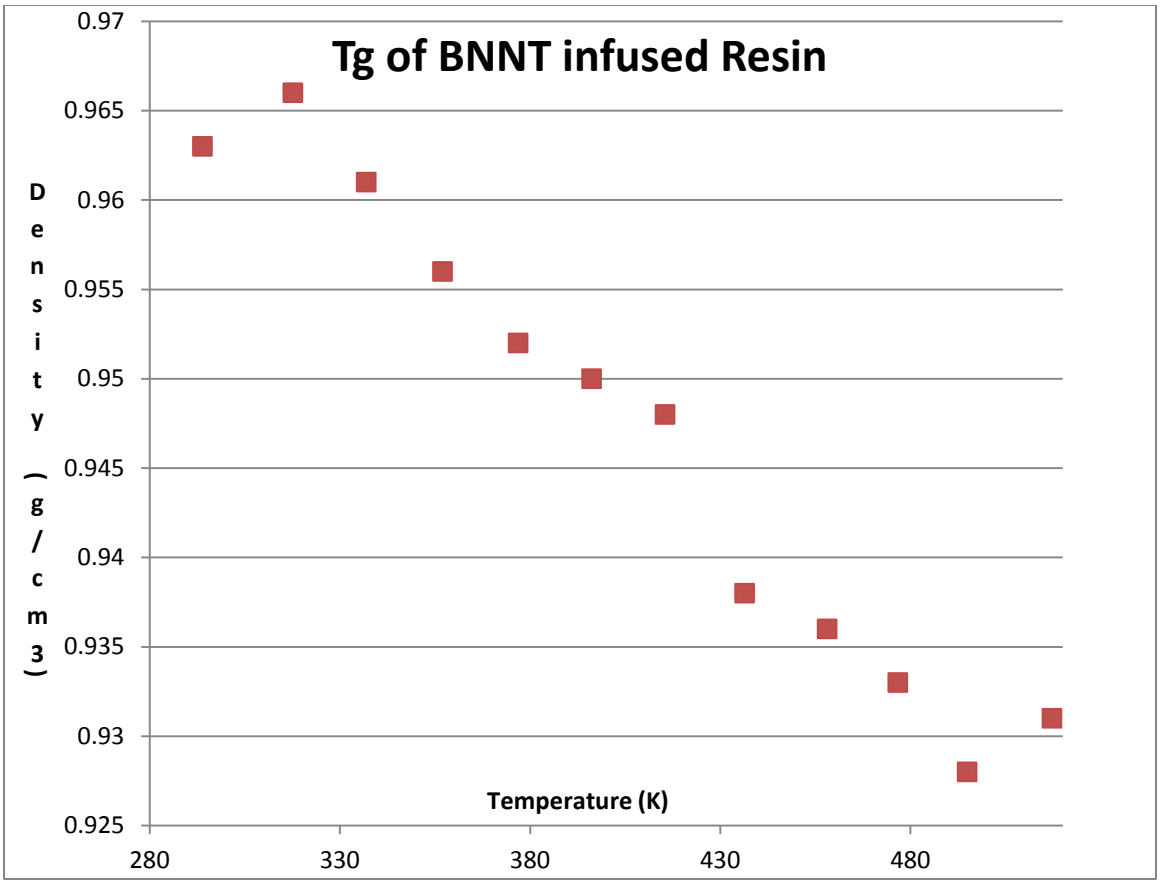

Figure 28. Depicting the Sudden Drop in Density that Indicates the Glass Transition Temperature of BNNT Infused Epon 862/W Resin.

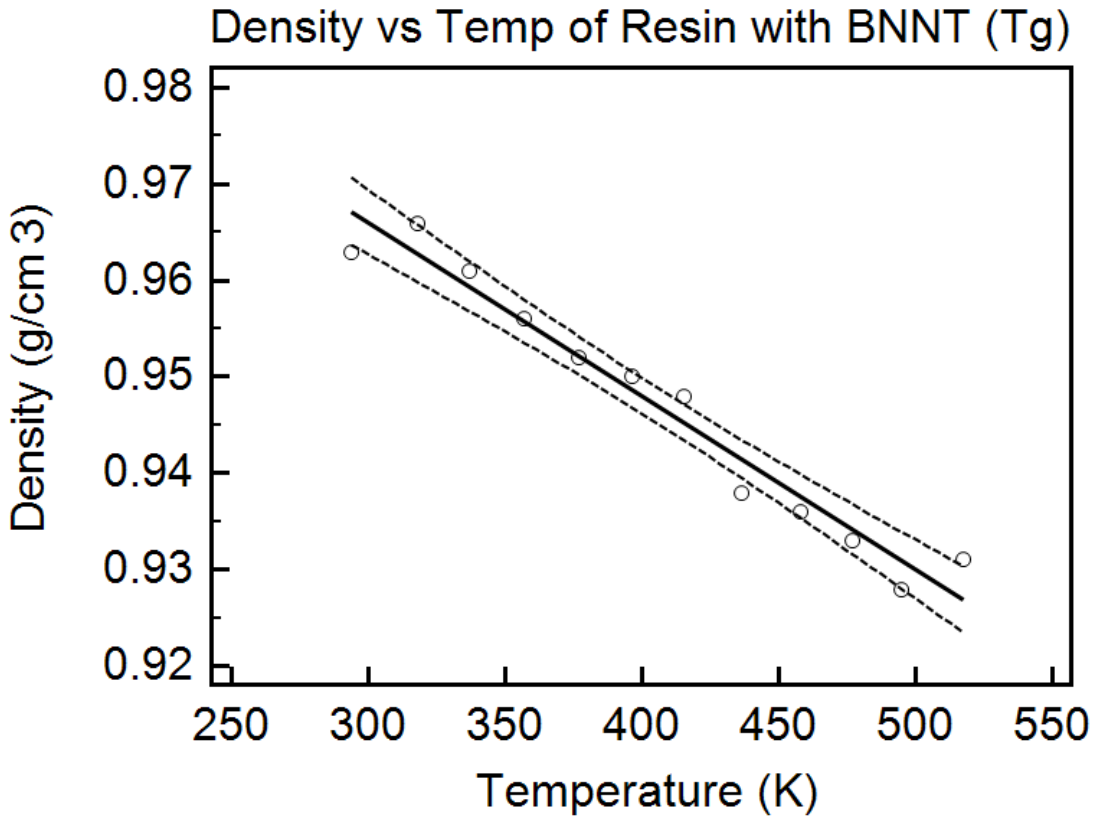

Figure 29. Graph of Resin with BNNT, Tg, (Dashed line represents 95% confidence interval).

Table 16. Regression Analysis of Glass Transistion Temperature of BNNT Infused Resin System.

Sample size					12
Coefficient of determination R^2					0.9587
Residual standard deviation					0.002832
y = 1.0200 + -0.0001801 x					
Parameter	Coefficient	Std. Error	95% CI	t	P
Intercept	1.0200	0.004871	1.0092 to 1.0309	209.4267	<0.0001
Slope	-0.0001801	0.00001181	-0.0002064 to -0.0001537	-15.2421	<0.0001
Source	DF	Sum of Squares	Mean Square		
Regression	1	0.001863	0.001863		
Residual	10	0.00008021	0.000008021		
F-ratio			232.3223		
Significance level			P<0.001		

The glass transition temperature was predicted between the 415 K and 436 K. Taking the midpoint, the glass transition temperature is predicted to be 426 K or 153 degrees Celsius. This is an improvement to the resin system without BNNTs, indicating bonding and an enhancement in the thermal properties of the two phase resin system.

Discussion

Due to computational computing constraints elevated percentages of BNNT were infused into the resin. It was established that a minimum of three rings were necessary to maintain the structure of the BNNT. When attempting to establish values used in the experiment it was quickly learned that more computational power and memory was needed. However, elevated percentages were feasible resulting in predicted values of the

higher percentages of BNNT infused resin systems. Figures 25, 26 and 27 express the trend of the varying percentages of BNNT incorporated into the Epon 862/W resin system. Percentages varied between 20 to 22% respectively and computationally predicted values were within in the theoretical limits described by the rule of mixtures, which was important in establishing confidence in the computational model. The computational model does not predict the theoretical upper limit, which indicates that the varying cells were effective in capturing some of the random cross linking, orientation, ratio of Epon to W and defects that would be seen in experimental values. However, the computational values are closer to the upper limits and more varying cells would be required to capture all of the conditions found in the experimental results. This is consistent with what is seen in the values of the Young's Modulus for the Epon 862/W resin system without BNNTs. Also, the Young's Modulus of the new BNNT infused resin systems are much larger, 125 GPa to 160 GPa depending on percentage of BNNT and type of BNNT, than that of the resin which indicates a clear increase in the mechanical properties of the resin. Interaction of the BNNT with the Epon 862/W resin system plays an important role in the effect that the BNNTs will have with the resin system. Hydrogen bonding was suggested between the alcohol groups, produced after the cross linking between the W and Epon 862, and the negatively charged nitrogen's produced by the asymmetric charged distribution between boron and nitrogen. This gives BNNTs an advantage to CNTs because no functionalization is required in order to create good interfacial connectivity between the nanotube and the Epon 862/W resin system.

However, functionalized BNNTs could improve the effect the BNNTs have on the mechanical properties of the resin system.

The glass transition temperature of the material was predicted by the computational model to improve by adding BNNTs. The predicted Tg for the resin system with 20% or more of BNNT was ~153 degrees Celsius. Tg can only be influenced if there is some form of bonding that occurs between the epoxy resin system and nanofiller. As was seen with the Young's Modulus, the computational model suggests that it is hydrogen bonding that occurs between the alcohol groups and the negatively charged nitrogen on the BNNTs. The Tg of the BNNT infused resin matrix was also verified using the 95% confidence interval which identified the points at which the density changed the greatest indicating the Tg of the material.

Conclusions

The computational simulation was able to predict the Young's Modulus and glass transition temperature of the BNNT infused resin systems with high percentages of BNNTs. Further computational power and memory will be required to simulate the resin systems with lower percentages of BNNTs in order to achieve realistic experimental values. However, the predicted computational values fell within the theoretical limits if it was feasible to achieve such percentages of BNNTs within the epoxy resin system. Also, the variation in cells which accounted for the change in orientations, ratios of Epon 862 to W and cross linking densities allowed for the model to achieve values that were slightly lower than the upper theoretical limit. Thus, with further variation in the cells it

would become feasible to achieve realistic experimental values within the model that could be used to optimized composite fabrication and nanofiller incorporation. It was suggested that hydrogen bonding was occurring between the BNNTs and Epon 862/W resin system, resulting in improvement in the mechanical and thermal properties of the resin system after the addition of BNNTs.

CHAPTER VI

FABRICATION AND ANALYSIS OF TWO PHASE COMPOSITES COMPOSED OF EPON862/W RESIN SYSTEM AND BORON NITRIDE NANOTUBES

Materials and Fabrication Process

The Epoxy resin Epon 862 and hardener DETDA were purchased from Miller Stephenson Chemical Company Inc. Boron Nitride Nanotubes were purchased from Nanotech Labs. Scanning electron microscope and Helium Ion Microscope images were coated with a 5 nm layer of gold palladium to aid in the imaging. Nanotube morphology consisted of multi-walled tubes with various lengths, 1 micron to 4 micron, and diameters, 60-100nm (Figure 30 & 32). The material was 70% pure and still had traces of the catalyst elements. Boron Nitride Nanoparticles were purchased from US Research Nanomaterials, Inc.

Two phase nanocomposites were fabricated using an open mold setup. To maintain viscosities suitable for the HVARTM fabrication method, three weight percentages of nano-fillers were examined, 0.015%, 0.0825% and 0.15%. For quality purposes, a control sample was created for each nanocomposite to take in account environmental factors in the laboratory. The panels were fabricated on a glass substrate with an open mold made of wood. The mold was protected with peel ply which was heat gunned to fit the mold. All control panels were hand-mixed and fabricated using the

HVARTM method. For nanocomposite fabrication, a combination of magnetic stirring and sonication was needed to homogenously disperse the nanomaterial without degrading the properties of the resin matrix (Figure 31). The mixing process began with one hour of magnetic stirring of the nanomaterial within the Epon 862. Then the Epon mixed with nanomaterial was sonicated for fifteen minutes, followed by adding the curing agent while the mixture was sonicated for another fifteen minutes. Figure 32 represents TEM images before and after the dispersion method, demonstrating good separation of the nanomaterial from large agglomerations.

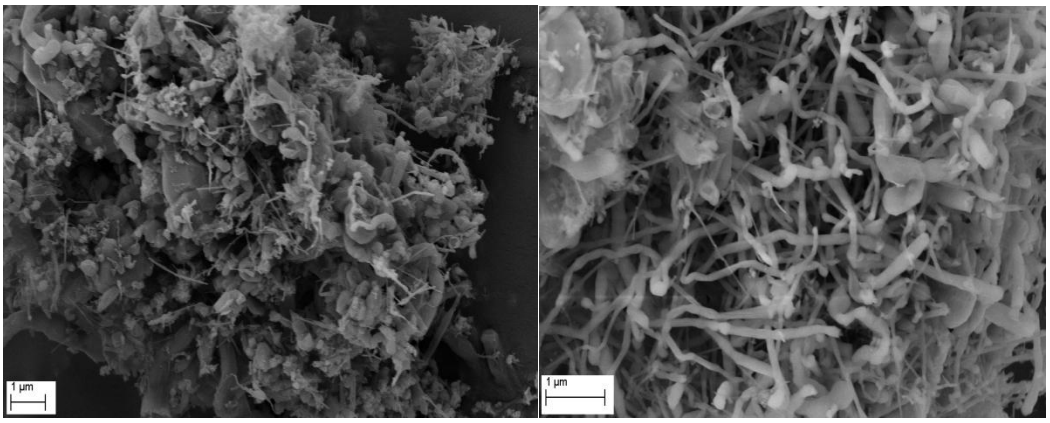

Figure 30. BNNT Raw Material Fabricated by Nanotech Labs

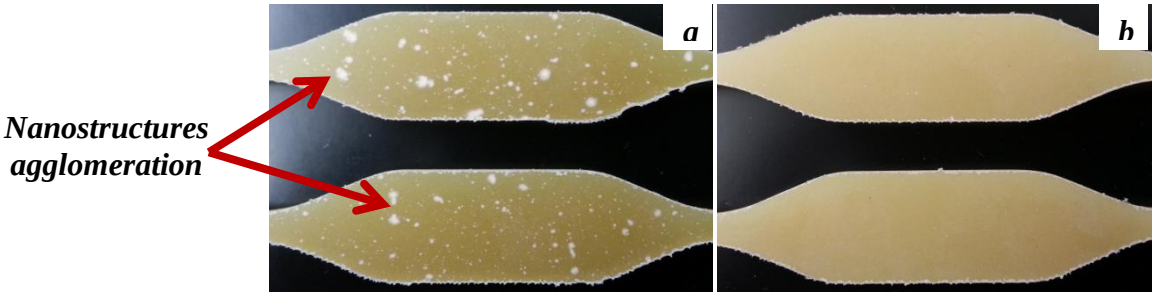

Figure 31. Nanostructures Dispersion in Composite Panels Using Different Mixing Process; a) Only Sonication, b) Combination of Magnet Stirring and Sonication.

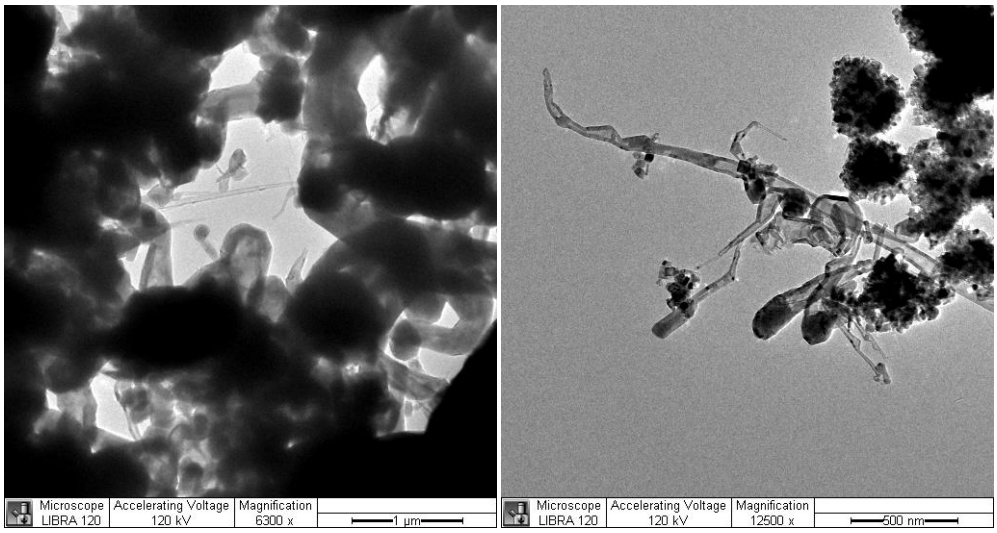

Figure 32. Left -TEM Image of BNNT Raw Material Before Sonication, Right – TEM Image of BNNT Raw Material after Sonication

Once the nanostructures were dispersed in the resin and satisfactory homogeneity is achieved using both magnet stirring and sonication, the resin was degassed at 70 °C and vacuum of 25 to 30 inHg for no more than 20 minutes. The degassed resin was cured at 250 °F for 2 hr and post-cured at 350 °F for another 2 hr. This particular curing process

was used based on previous attempts in which our research team has optimized the curing process of Epoxy 862 in order to obtain higher tensile strength [115].

Property Evaluation: Tg, Tensile Strength and Young's Modulus

After the panels were completely cured, they were taken to a water jet cutting machine and cut to the specific ASTM standard D638. A maximum of six specimens were cut from each panel and used to test the tensile strength and glass transition temperature (Tg) of the two phase composites. The specimens were loaded on an Instron test frame 3384 and tested with the strain rate of 0.05 in/min to obtain tensile strength (Figure 2).

The thermal properties were studied using a Perkin Elmer Differential Scanning Calorimeter 6000 to obtain the glass transition temperature. The heating rate of the DSC was set at 10 °C/min from 30 °C to 400 °C for the first samples and to 250 °C afterward (up to six samples were tested for each panel).

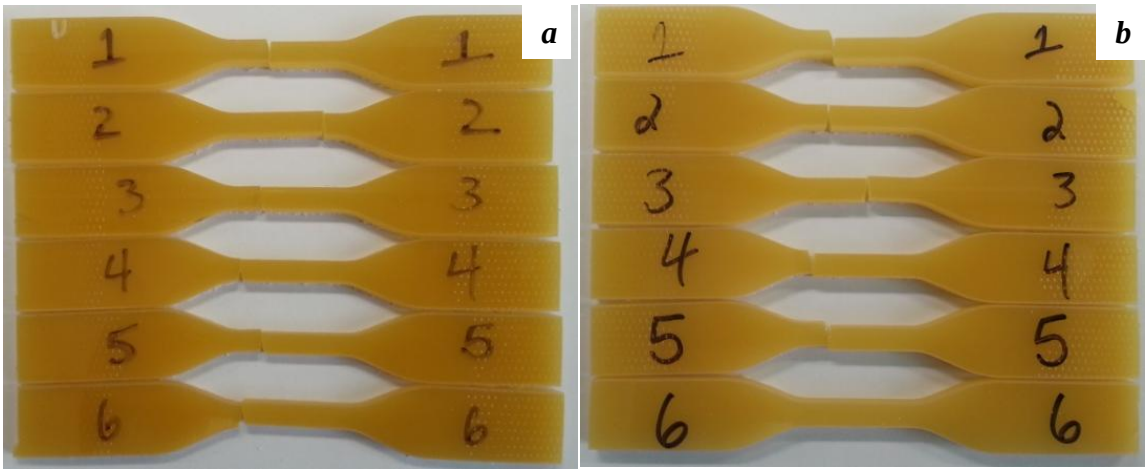

Figure 33. Tensile Test Dog Bone Samples; a) Resin Mixed with BNNTs, b) Resin Mixed with BNPs.

Results

Tensile strength and Young's Modulus for each percentage of nanofiller was taken as an average over the six specimens tested. Figure 34 and 35 shows the tensile strength of six composite panels loaded with nanostructures and compares them with their own control sample result. Figure 36 demonstrates the Young's Modulus of the BNNT infused resin compared with the control resin. Each loaded composite had a separate control in order to account for any changes in the laboratory`s environmental condition which has an influence on the degree of cure for the resin and ultimately its tensile strength and Young's Modulus. No significant differences in tensile strength or Young's Modulus were detected when BNNTs were added to the Epoxy 862 resin system, but BNP samples show more variation in tensile strength (strength is increased in

the 0.015 % and 0.0825% BNP cases while it decreased in the case of 0.15 % BNPs) when compared to control samples.

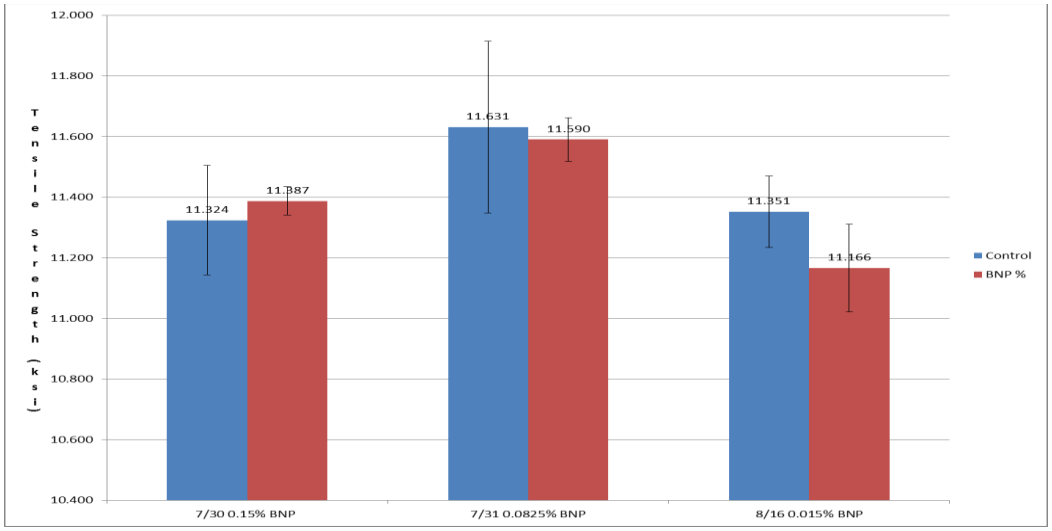

Figure 34. Tensile Strength of Infused Resin with BNPs

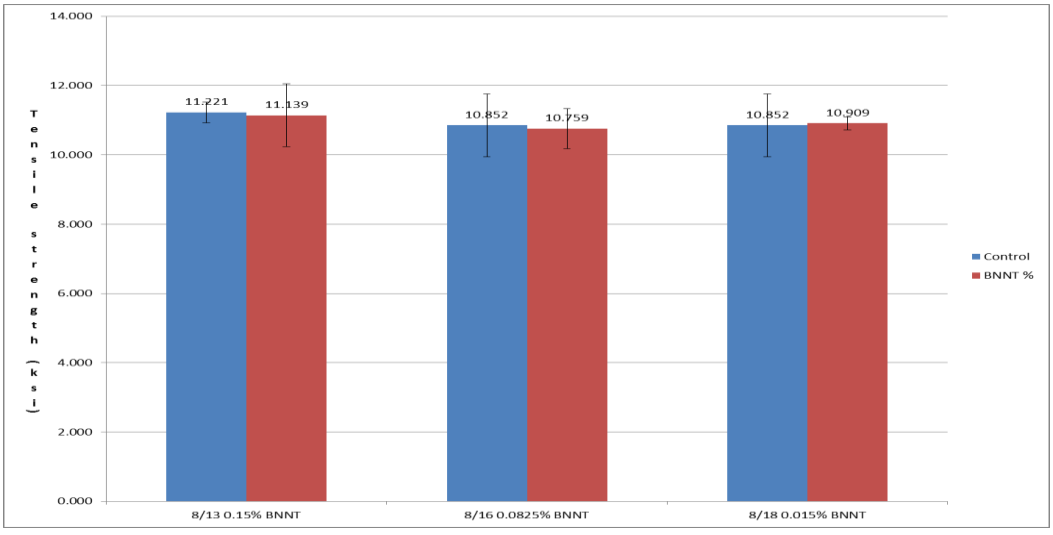

Figure 35. Tensile Strength of BNNT Infused Resin.

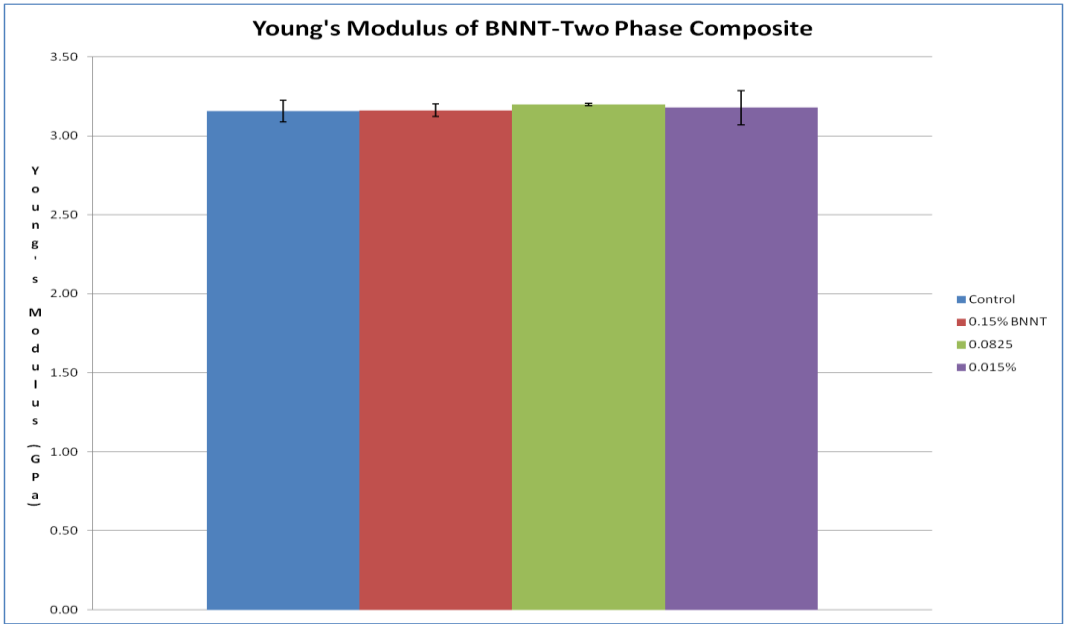

Figure 36. Young's Modulus of BNNT + Epon 862/W Resin System vs. Control Sample.

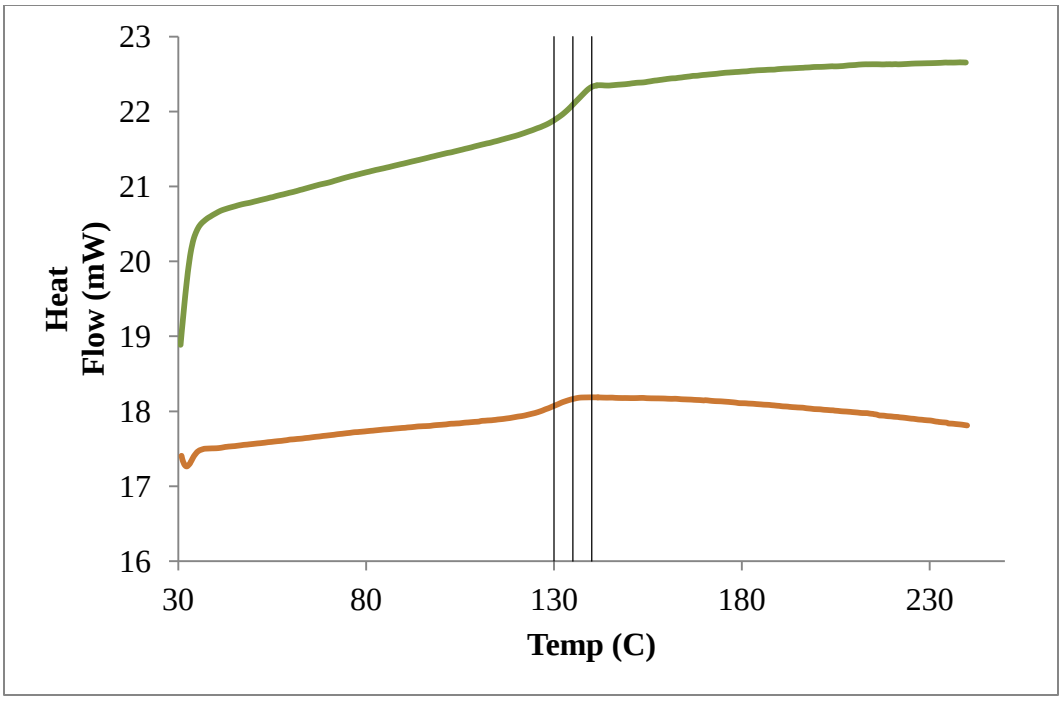

Figure 37. DSC Graph for 0.15 % BNNT (Green) and Control (Orange) Samples (Black Lines Represent Temperature at 130, 135 and 140 °C).

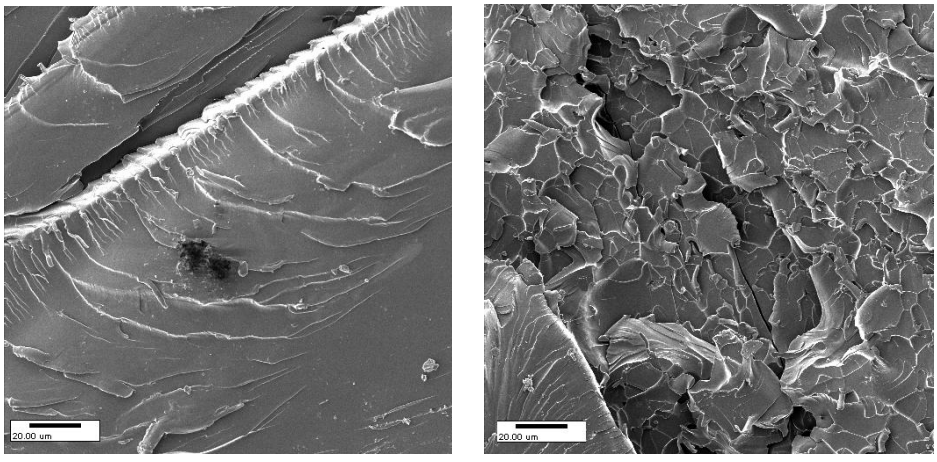

Figure 38. Left – Cross Section of Resin with BNNT after Tensile Test, Right – Cross Section of Resin after Tensile Test

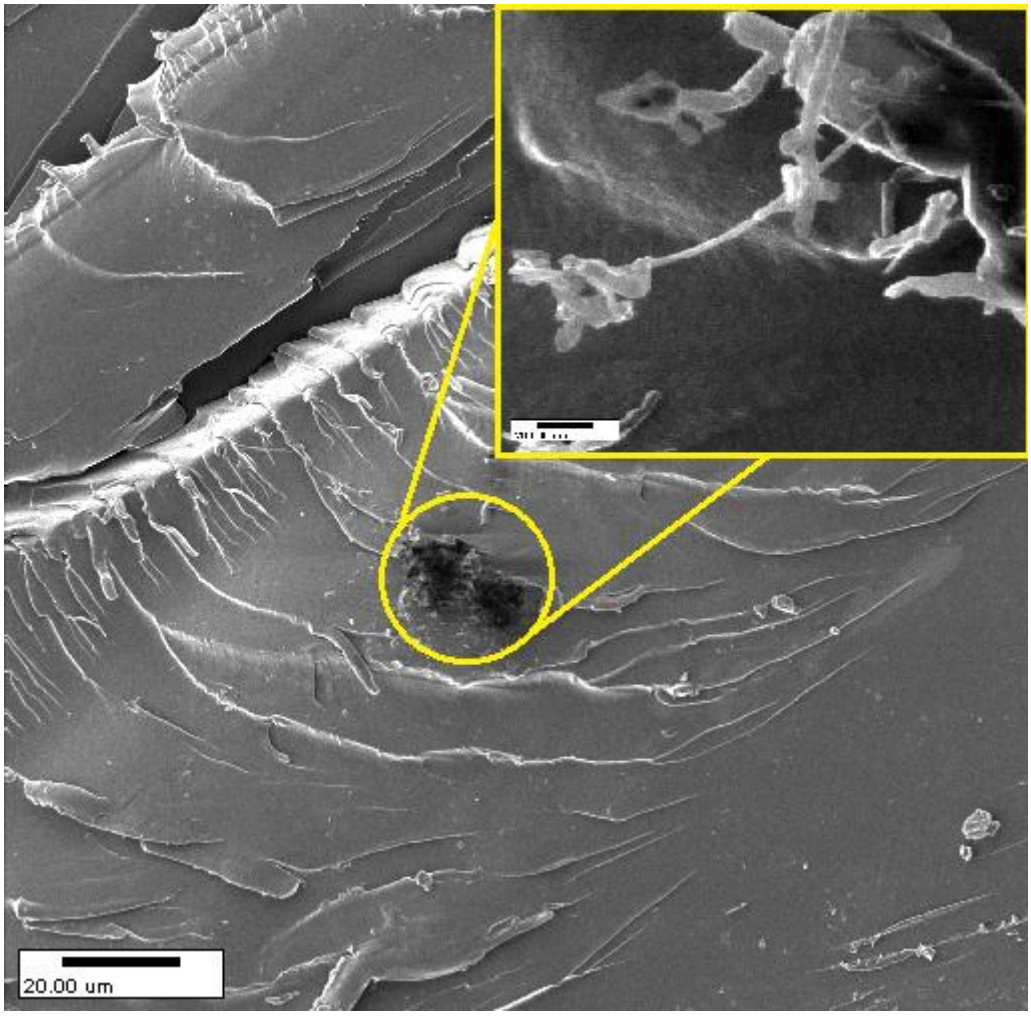

Figure 39. BNNT's Found in Cross Section Crack of BNNT Infused Resin System

Figure 38 depicts the cross sectional break of the Epon 862/W resin specimens with and without BNNT's. Figure 39 demonstrates that a small amount of BNNTs were found on the cross sectional break of the BNNT infused resin specimens verifying that the nanomaterial was dispersed into small agglomerates throughout the composite.

Discussion

Although the graph suggests that lower percentages of BNPs might have a better chance of improving the tensile strength of the Epoxy 862 resin system, but considering the data range and their overlap, these results show no conclusive trends. It needs to be noted that the large deviation in tensile strength of BNP composite panels shown in this graph is due to the large magnification and scaling used. The data obtained from tensile strength tests have a minimum Coefficient of Variation (COV in percentage) of 0.41 % and maximum of 2.44 % which is far below the 5 % accepted value.

Based on this study and NASA's previous finding, it seems Boron Nitride nanostructures are able to bring better radiation shielding capability to the resin with minimum side effects since no degradation in tensile strength or Young's Modulus of composite panels was observed [116, 117]. This result confirms our initial expectation that adding BNPs to the polymeric matrix would not improve the tensile strength due to the fact that the BNPs are not structural materials. In case of BNNTs, the lack of enhancement to the tensile strength or Young's Modulus may be due to the 70% purity of the BNNT material used in the experiment. Even though there was no improvement to the tensile strength or Young's Modulus, these results have helped build our understanding of the BNNT - polymer interface. It appears that the resin matrix can be successfully used to build composites with BNNT additives without functionalizing the BNNTs to enhance bonding. The BNNT case is considerably different from the case of CNTs, where functionalization is required to create a good interfacial bond between the matrix and nano-filler. Without functionalization, CNTs degrade the material's tensile

strength and Young's Modulus by acting as defects within the resin matrix. It is hypothesized that since BNNTs have an asymmetric charge distribution because of the difference in electronegativity of the boron and nitrogen atoms, there are local areas of negative charge over the nitrogen atoms and local areas of positive charge over the boron atoms. The local negative charge on the nitrogen atoms allows for hydrogen bonding to occur between the nanotubes and the alcohol groups on the resin after cross linking. The hydrogen bonding establishes good interfacial interaction between the BNNT and resin matrix.

Another indicator of hydrogen bonding is the effect of BNNTs on the Tg of the two phase composites. The polymer material with BNNT added consistently demonstrated a 3 degree Celsius improvement in Tg when compared to the controls (Figure 37). The Tg cannot be altered by materials with higher thermal properties unless there is bonding that occurs between the two materials. Further investigation on the effect of BNPs on the resin showed that their effect on the Tg of the composite was inconclusive. It is hypothesized that the data was inconsistent due to the size distribution of the BNP material used in fabricating the nano-infused resins. Interaction between the matrix and BNPs could be significantly altered if size of the particles were to increase. Larger particle size would be expected to degrade the ability of the BNPs to effectively interact and bond.

Conclusions

Successful integration of BNNTs and BNPs in Epoxy 862/"W" resin matrix was demonstrated. There was no degradation to the tensile strength or Young's Modulus of the two phase nanocomposites. It was expected in the case of BNPs due to the fact that BNP's are not a structural material. It is suspected that the BNNT infused nanocomposites did not demonstrate improvement in the tensile strength or Young's Modulus because of the 70% purity of BNNT material. Thus, with higher purity BNNT material or by adding functional groups, one might expect to see an enhancement in the mechanical properties of the nanocomposites. Also, seeing no degradation in the mechanical properties of the BNNT or BNP nanocomposite without functionalizing the nanomaterials prior to infusing indicates that there is good interfacial interaction occurring between the nano-fillers and resin matrix. It is suspected that this behavior is due to hydrogen bonding caused by asymmetric charge distribution on the surface of the nanofillers. Data obtained for the Tg of the BNNT infused resin demonstrated a consistent three degree Celsius improvement for each sample. This study demonstrates that Boron Nitride additives offer suitable interfacial connectivity with Epoxy resin, thus eliminating one of the primary challenges with incorporating nano-fillers into composites. Also, functionalization may provide an opportunity for potential improvement of the mechanical and thermal properties of BNNT and BNP infused nanocomposites. Further investigation is required to understand the inconsistent Tg data for the BNP infused resins.

REFERENCES

[1] C. C. F. Sheila A. Thibeault, "Radiation Shielding Materials Containing Hydrogen, Boron, and Nitrogen: Systematic Computational and Eperimental Study," *NIAC*, pp. 1-29, 2012.

[2] L. W. Townsend, "Optical model analyses of heavy ion fragmentation in hydrogen targets," *Physical Review C*, vol. 49, pp. 3158-3161, 06/01/ 1994.

[3] R. Andrews and M. C. Weisenberger, "Carbon nanotube polymer composites," *Current Opinion in Solid State and Materials Science*, vol. 8, pp. 31-37, 1// 2004.

[4] J. N. Coleman, U. Khan, W. J. Blau, and Y. K. Gun'ko, "Small but strong: A review of the mechanical properties of carbon nanotube–polymer composites," *Carbon*, vol. 44, pp. 1624-1652, 8// 2006.

[5] N. G. Sahoo, S. Rana, J. W. Cho, L. Li, and S. H. Chan, "Polymer nanocomposites based on functionalized carbon nanotubes," *Progress in Polymer Science*, vol. 35, pp. 837-867, 7// 2010.

[6] Z.-M. Li, S.-N. Li, M.-B. Yang, and R. Huang, "A novel approach to preparing carbon nanotube reinforced thermoplastic polymer composites," *Carbon*, vol. 43, pp. 2413-2416, 9// 2005.

[7] X.-L. Xie, Y.-W. Mai, and X.-P. Zhou, "Dispersion and alignment of carbon nanotubes in polymer matrix: A review," *Materials Science and Engineering: R: Reports*, vol. 49, pp. 89-112, 5/19/ 2005.

[8] Z. Spitalsky, D. Tasis, K. Papagelis, and C. Galiotis, "Carbon nanotube–polymer composites: Chemistry, processing, mechanical and electrical properties," *Progress in Polymer Science*, vol. 35, pp. 357-401, 3// 2010.

[9] J. Yu, Y. Chen, R. G. Elliman, and M. Petravic, "Isotopically Enriched 10BN Nanotubes," *Advanced Materials*, vol. 18, pp. 2157-2160, 2006.

[10] C. Sun, H. Yu, L. Xu, Q. Ma, and Y. Qian, "Recent Development of the Synthesis and Engineering Applications of One-Dimensional Boron Nitride Nanomaterials," *Journal of Nanomaterials*, vol. 2010, pp. 1-16, 2010.

[11] C. Zhi, Y. Bando, C. Tang, and D. Golberg, "Boron nitride nanotubes," *Materials Science and Engineering: R: Reports,* vol. 70, pp. 92-111, 2010.

[12] L. C. Marvin, "The Physics of Boron Nitride Nanotubes," *Physics Today,* pp. 34-38.

[13] M. Radosavljević, J. Appenzeller, V. Derycke, R. Martel, P. Avouris, A. Loiseau, *et al.*, "Electrical properties and transport in boron nitride nanotubes," *Applied Physics Letters,* vol. 82, pp. 4131-4133, 2003.

[14] M. Ishigami, S. Aloni, and A. Zettl, "Properties of Boron Nitride Nanotubes," *AIP Conference Proceedings,* vol. 696, pp. 94-99, 2003.

[15] H. M. Ghassemi, C. H. Lee, Y. K. Yap, and R. S. Yassar, "Field emission and strain engineering of electronic properties in boron nitride nanotubes," *Nanotechnology,* vol. 23, p. 105702, Mar 16 2012.

[16] J. Cumings and A. Zettl, "Field emission and current-voltage properties of boron nitride nanotubes," *Solid State Communications,* vol. 129, pp. 661-664, 2004.

[17] C. Zhi, Y. Bando, C. Tang, D. Golberg, R. Xie, and T. Sekigushi, "Phonon characteristics and cathodolumininescence of boron nitride nanotubes," *Applied Physics Letters,* vol. 86, pp. -, 2005.

[18] C.-H. Park, C. D. Spataru, and S. G. Louie, "Excitons and Many-Electron Effects in the Optical Response of Single-Walled Boron Nitride Nanotubes," *Physical Review Letters,* vol. 96, p. 126105, 03/30/ 2006.

[19] L. Wirtz, A. Marini, and A. Rubio, "Excitons in Boron Nitride Nanotubes: Dimensionality Effects," *Physical Review Letters,* vol. 96, p. 126104, 03/30/ 2006.

[20] M. Ishigami, J. D. Sau, S. Aloni, M. L. Cohen, and A. Zettl, "Observation of the Giant Stark Effect in Boron-Nitride Nanotubes," *Physical Review Letters,* vol. 94, p. 056804, 02/10/ 2005.

[21] J. S. Lauret, R. Arenal, F. Ducastelle, A. Loiseau, M. Cau, B. Attal-Tretout, *et al.*, "Optical Transitions in Single-Wall Boron Nitride Nanotubes," *Physical Review Letters,* vol. 94, p. 037405, 01/27/ 2005.

[22] Z. Gao, C. Zhi, Y. Bando, D. Golberg, and T. Serizawa, "Isolation of Individual Boron Nitride Nanotubes via Peptide Wrapping," *Journal of the American Chemical Society,* vol. 132, pp. 4976-4977, 2010/04/14 2010.

[23] Y. Chen, J. Zou, S. J. Campbell, and G. Le Caer, "Boron nitride nanotubes: Pronounced resistance to oxidation," *Applied Physics Letters,* vol. 84, pp. 2430-2432, 2004.

[24] D. Qian, E. C. Dickey, R. Andrews, and T. Rantell, "Load transfer and deformation mechanisms in carbon nanotube-polystyrene composites," *Applied Physics Letters,* vol. 76, pp. 2868-2870, 2000.

[25] T. Terao, C. Zhi, Y. Bando, M. Mitome, C. Tang, and D. Golberg, "Alignment of Boron Nitride Nanotubes in Polymeric Composite Films for Thermal Conductivity Improvement," *The Journal of Physical Chemistry C,* vol. 114, pp. 4340-4344, 2010/03/18 2010.

[26] X. Huang, C. Zhi, P. Jiang, D. Golberg, Y. Bando, and T. Tanaka, "Polyhedral Oligosilsesquioxane-Modified Boron Nitride Nanotube Based Epoxy Nanocomposites: An Ideal Dielectric Material with High Thermal Conductivity," *Advanced Functional Materials,* vol. 23, pp. 1824-1831, 2013.

[27] C. C. F. Sheila A. Thibeault, "Radiation Shielding Materials Containing Hydrogen, Boron, and Nitrogen: Systematic Computational and Experimental Study."

[28] R. Arenal, X. Blase, and A. Loiseau, "Boron-nitride and boron-carbonitride nanotubes: synthesis, characterization and theory," *Advances in Physics,* vol. 59, pp. 101-179, 2010/03/01 2010.

[29] R. J. L. Nasreen G. Chopra, K. Cherrey, Vincent H. Crespi, Marvin L. Cohen, Steven G. Louie, A. Zettl, "Boron Nitride Nanotubes," *Science,* vol. 269, pp. 966-967, 1995.

[30] A. Z. John Cumings, "Mass-production of boron nitride double-wall nanotubes and nanococoons," *Chemical Physics Letters,* vol. 316, pp. 211-216, 2000.

[31] T. S. Bartnitskaya, G. S. Oleinik, A. V. Pokropivnyi, and V. V. Pokropivnyi, "Synthesis, structure, and formation mechanism of boron nitride nanotubes," *Journal of Experimental and Theoretical Physics Letters,* vol. 69, pp. 163-168, 1999/01/01 1999.

[32] T. O. Ichihito Narita, "Synthesis of Boron Nitride Nanotubes by using YB_6 powder," *Solid State Communications,* vol. 122, pp. 465-468, 2002.

[33] K. Suenaga, "Synthesis of Nanoparticles and Nanotubes with Well-Separated Layers of Boron Nitride and Carbon," *Science,* vol. 278, pp. 653-655, 1997.

[34] D. Golberg, Y. Bando, M. Eremets, K. Takemura, K. Kurashima, and H. Yusa, "Nanotubes in boron nitride laser heated at high pressure," *Applied Physics Letters*, vol. 69, pp. 2045-2047, 1996.

[35] G. W. Zhou, Z. Zhang, Z. G. Bai, and D. P. Yu, "Catalyst effects on formation of boron nitride nano-tubules synthesized by laser ablation," *Solid State Communications*, vol. 109, pp. 555-559, 2/17/ 1999.

[36] Y. Chen, L. T. Chadderton, J. F. Gerald, and J. S. Williams, "A solid-state process for formation of boron nitride nanotubes," *Applied Physics Letters*, vol. 74, pp. 2960-2962, 1999.

[37] S. K. Singhal, A. K. Srivastava, and R. B. Mathur, "Growth of Boron Nitride Nanotubes Having Large Surface Area Using Mechanothermal Process," *World Journal of Nano Science and Engineering*, vol. 01, pp. 119-128, 2011.

[38] W.-Q. Han, W. Mickelson, J. Cumings, and A. Zettl, "Transformation of BxCyNz nanotubes to pure BN nanotubes," *Applied Physics Letters*, vol. 81, pp. 1110-1112, 2002.

[39] S. B. Mikhael Bechelany, Arnaud Brioude, David Cornu, Pierre Stadelmann, Chatherine Charcosset, Koffi Fiaty, Philippe Miele, "Synthesis of Boron Nitride Nanotubes by a Template-Assisted Polymer Thermolysis Process," *American Chemical Society*, vol. 111, pp. 13378-13384, 2007.

[40] Y. Wang, Y. Yamamoto, H. Kiyono, and S. Shimada, "Highly ordered boron nitride nanotube arrays with controllable texture from ammonia borane by template-aided vapor-phase pyrolysis," *J. Nanomaterials*, vol. 2008, pp. 1-7, 2008.

[41] Y. Qiu, J. Yu, J. Yin, C. Tan, X. Zhou, X. Bai, *et al.*, "Synthesis of continuous boron nitride nanofibers by solution coating electrospun template fibers," *Nanotechnology*, vol. 20, p. 345603, 2009.

[42] D. Golberg, Y. Bando, W. Han, K. Kurashima, and T. Sato, "Single-walled B-doped carbon, B/N-doped carbon and BN nanotubes synthesized from single-walled carbon nanotubes through a substitution reaction," *Chemical Physics Letters*, vol. 308, pp. 337-342, 7/23/ 1999.

[43] D. Golberg, Y. Bando, K. Kurashima, and T. Sato, "Ropes of BN multi-walled nanotubes," *Solid State Communications*, vol. 116, pp. 1-6, 8/22/ 2000.

[44] K. B. Shelimov and M. Moskovits, "Composite Nanostructures Based on Template-Grown Boron Nitride Nanotubules," *Chemistry of Materials,* vol. 12, pp. 250-254, 2000/01/01 1999.

[45] Y. Huang, J. Lin, C. Tang, Y. Bando, C. Zhi, T. Zhai, *et al.*, "Bulk synthesis, growth mechanism and properties of highly pure ultrafine boron nitride nanotubes with diameters of sub-10 nm," *Nanotechnology,* vol. 22, p. 145602, 2011.

[46] O. R. Lourie, C. R. Jones, B. M. Bartlett, P. C. Gibbons, R. S. Ruoff, and W. E. Buhro, "CVD Growth of Boron Nitride Nanotubes," *Chemistry of Materials,* vol. 12, pp. 1808-1810, 2000/07/01 2000.

[47] C. H. Lee, M. Xie, V. Kayastha, J. Wang, and Y. K. Yap, "Patterned Growth of Boron Nitride Nanotubes by Catalytic Chemical Vapor Deposition," *Chemistry of Materials,* vol. 22, pp. 1782-1787, 2010/03/09 2010.

[48] J. Wang, L. Zhang, G. Zhao, Y. Gu, Z. Zhang, F. Zhang, *et al.*, "Selective synthesis of boron nitride nanotubes by self-propagation high-temperature synthesis and annealing process," *Journal of Solid State Chemistry,* vol. 184, pp. 2478-2484, 9// 2011.

[49] A. Pakdel, C. Zhi, Y. Bando, T. Nakayama, and D. Golberg, "A comprehensive analysis of the CVD growth of boron nitride nanotubes," *Nanotechnology,* vol. 23, p. 215601, 2012.

[50] C. C. Tang, X. X. Ding, X. T. Huang, Z. W. Gan, S. R. Qi, W. Liu, *et al.*, "Effective growth of boron nitride nanotubes," *Chemical Physics Letters,* vol. 356, pp. 254-258, 4/22/ 2002.

[51] C. H. Lee, M. Xie, J. Wang, R. E. Cook, and Y. K. Yap, "Patterned Growth of Long and Clean Boron Nitride Nanotubes on Substrates," *MRS Online Proceedings Library,* vol. 1204, pp. null-null, 2009.

[52] M. W. Smith, K. C. Jordan, C. Park, J. W. Kim, P. T. Lillehei, R. Crooks, *et al.*, "Very long single- and few-walled boron nitride nanotubes via the pressurized vapor/condenser method," *Nanotechnology,* vol. 20, p. 505604, Dec 16 2009.

[53] M. O. Steinhauser and S. Hiermaier, "A review of computational methods in materials science: examples from shock-wave and polymer physics," *Int J Mol Sci,* vol. 10, pp. 5135-216, Dec 2009.

[54] D. R. Hartree, "The Wave Mechanics of an Atom with a Non-Coulomb Central Field. Part I. Theory and Methods," *Mathematical Proceedings of the Cambridge Philosophical Society,* vol. 24, pp. 89-110, 1928.

[55] W. Kohn and L. J. Sham, "Self-Consistent Equations Including Exchange and Correlation Effects," *Physical Review,* vol. 140, pp. A1133-A1138, 11/15/ 1965.

[56] P. Hohenberg and W. Kohn, "Inhomogeneous Electron Gas," *Physical Review,* vol. 136, pp. B864-B871, 11/09/ 1964.

[57] W. Kohn, "Density Functional and Density Matrix Method Scaling Linearly with the Number of Atoms," *Physical Review Letters,* vol. 76, pp. 3168-3171, 04/22/ 1996.

[58] R. Car and M. Parrinello, "Unified Approach for Molecular Dynamics and Density-Functional Theory," *Physical Review Letters,* vol. 55, pp. 2471-2474, 11/25/ 1985.

[59] J. C. Slater and G. F. Koster, "Simplified LCAO Method for the Periodic Potential Problem," *Physical Review,* vol. 94, pp. 1498-1524, 06/15/ 1954.

[60] P. Ballone, W. Andreoni, R. Car, and M. Parrinello, "Equilibrium Structures and Finite Temperature Properties of Silicon Microclusters from ab initio Molecular-Dynamics Calculations," *Physical Review Letters,* vol. 60, pp. 271-274, 01/25/ 1988.

[61] B. J. Alder and T. E. Wainwright, "Phase Transition for a Hard Sphere System," *The Journal of Chemical Physics,* vol. 27, pp. 1208-1209, 1957.

[62] N. Metropolis, A. W. Rosenbluth, M. N. Rosenbluth, A. H. Teller, and E. Teller, "Equation of State Calculations by Fast Computing Machines," *The Journal of Chemical Physics,* vol. 21, pp. 1087-1092, 1953.

[63] M. S. Daw and M. I. Baskes, "Embedded-atom method: Derivation and application to impurities, surfaces, and other defects in metals," *Physical Review B,* vol. 29, pp. 6443-6453, 06/15/ 1984.

[64] S. M. Foiles, M. I. Baskes, and M. S. Daw, "Embedded-atom-method functions for the fcc metals Cu, Ag, Au, Ni, Pd, Pt, and their alloys," *Physical Review B,* vol. 33, pp. 7983-7991, 06/15/ 1986.

[65] M. S. Daw, "Model of metallic cohesion: The embedded-atom method," *Physical Review B,* vol. 39, pp. 7441-7452, 04/15/ 1989.

[66] J. M. Dawson, "Particle simulation of plasmas," *Reviews of Modern Physics,* vol. 55, pp. 403-447, 04/01/ 1983.

[67] M. O. Steinhauser, "A molecular dynamics study on universal properties of polymer chains in different solvent qualities. Part I. A review of linear chain properties," *The Journal of Chemical Physics,* vol. 122, pp. -, 2005.

[68] P. J. Hoogerbrugge and J. M. V. A. Koelman, "Simulating Microscopic Hydrodynamic Phenomena with Dissipative Particle Dynamics," *EPL (Europhysics Letters),* vol. 19, p. 155, 1992.

[69] J. W. Cahn and J. E. Hilliard, "Free Energy of a Nonuniform System. I. Interfacial Free Energy," *The Journal of Chemical Physics,* vol. 28, pp. 258-267, 1958.

[70] S. Wolfram, "Undecidability and intractability in theoretical physics," *Physical Review Letters,* vol. 54, pp. 735-738, 02/25/ 1985.

[71] P. E. McHugh, R. J. Asaro, and C. F. Shih, "Computational modeling of metal matrix composite materials—I. Isothermal deformation patterns in ideal microstructures," *Acta Metallurgica et Materialia,* vol. 41, pp. 1461-1476, 5// 1993.

[72] P. E. McHugh, R. J. Asaro, and C. F. Shih, "Computational modeling of metal matrix composite materials—II. Isothermal stress-strain behavior," *Acta Metallurgica et Materialia,* vol. 41, pp. 1477-1488, 5// 1993.

[73] P. E. McHugh, R. J. Asaro, and C. F. Shih, "Computational modeling of metal matrix composite materials—IV. Thermal deformations," *Acta Metallurgica et Materialia,* vol. 41, pp. 1501-1510, 5// 1993.

[74] P. E. McHugh, R. J. Asaro, and C. F. Shih, "Computational modeling of metal matrix composite materials—III. Comparisons with phenomenological models," *Acta Metallurgica et Materialia,* vol. 41, pp. 1489-1499, 5// 1993.

[75] R. A. Gingold and J. J. Monaghan, "Kernel estimates as a basis for general particle methods in hydrodynamics," *Journal of Computational Physics,* vol. 46, pp. 429-453, 6// 1982.

[76] A. J. C. Ladd, "Short-time motion of colloidal particles: Numerical simulation via a fluctuating lattice-Boltzmann equation," *Physical Review Letters,* vol. 70, pp. 1339-1342, 03/01/ 1993.

[77] B. Devincre, "Three dimensional stress field expressions for straight dislocation segments," *Solid State Communications,* vol. 93, pp. 875-878, 3// 1995.

[78] S. J. Zhou, D. L. Preston, P. S. Lomdahl, and D. M. Beazley, "Large-Scale Molecular Dynamics Simulations of Dislocation Intersection in Copper," *Science,* vol. 279, pp. 1525-1527, March 6, 1998 1998.

[79] G. Y. Huang, Y. S. Wang, and D. Gross, "Transient dislocation emission from a crack tip under dynamic mode II loading," *Zeitschrift für angewandte Mathematik und Physik ZAMP,* vol. 53, pp. 839-854, 2002/09/01 2002.

[80] W. Cai, A. Arsenlis, C. R. Weinberger, and V. V. Bulatov, "A non-singular continuum theory of dislocations," *Journal of the Mechanics and Physics of Solids,* vol. 54, pp. 561-587, 3// 2006.

[81] J. Crank and P. Nicolson, "A practical method for numerical evaluation of solutions of partial differential equations of the heat-conduction type," *Advances in Computational Mathematics,* vol. 6, pp. 207-226, 1996/12/01 1996.

[82] D. J. Benson, "Computational methods in Lagrangian and Eulerian hydrocodes," *Computer Methods in Applied Mechanics and Engineering,* vol. 99, pp. 235-394, 9// 1992.

[83] W. K. Liu, S. Hao, T. Belytschko, S. Li, and C. T. Chang, "Multiple scale meshfree methods for damage fracture and localization," *Computational Materials Science,* vol. 16, pp. 197-205, 12// 1999.

[84] B. Akdim, R. Pachter, X. Duan, and W. W. Adams, "Comparative theoretical study of single-wall carbon and boron-nitride nanotubes," *Physical Review B,* vol. 67, p. 245404, 06/06/ 2003.

[85] P. Koskinen and V. Mäkinen, "Density-functional tight-binding for beginners," *Computational Materials Science,* vol. 47, pp. 237-253, 11// 2009.

[86] A. N. Enyashin and A. L. Ivanovskii, "Deformation mechanisms for carbon and boron nitride nanotubes," *Inorganic Materials,* vol. 42, pp. 1336-1341, Dec 2006.

[87] M. Terrones, "Carbon Nanotubes and Related Structures: New materials for the Twenty-first Century: Peter J.F. Harris, Cambridge University Press, 1999, ISBN: 0521 55446 2 (hardback). Price 50.00 GB Pounds (US $80.00)," *Carbon,* vol. 38, pp. 787-788, // 2000.

[88] R. Ma, D. Golberg, Y. Bando, and T. Sasaki, "Syntheses and properties of B-C-N and BN nanostructures," *Philos Trans A Math Phys Eng Sci,* vol. 362, pp. 2161-86, Oct 15 2004.

[89] D. Brenner, "Empirical potential for hydrocarbons for use in simulating the chemical vapor deposition of diamond films," *Physical Review B,* vol. 42, pp. 9458-9471, 1990.

[90] J. Tersoff, "New empirical approach for the structure and energy of covalent systems," *Physical Review B,* vol. 37, pp. 6991-7000, 1988.

[91] V. Verma, V. K. Jindal, and K. Dharamvir, "Elastic moduli of a boron nitride nanotube," *Nanotechnology,* vol. 18, p. 435711, 2007.

[92] A. P. Suryavanshi, M.-F. Yu, J. Wen, C. Tang, and Y. Bando, "Elastic modulus and resonance behavior of boron nitride nanotubes," *Applied Physics Letters,* vol. 84, p. 2527, 2004.

[93] J. a. P. Martin Head-Gordon, "MP2 Energy Evaluation by Direct Methods," *Chemical Physics Letters,* vol. 153, pp. 503-506, December 30, 1988 1988.

[94] C. Møller and M. S. Plesset, "Note on an Approximation Treatment for Many-Electron Systems," *Physical Review,* vol. 46, pp. 618-622, 1934.

[95] J. T. Tanskanen, M. Linnolahti, A. J. Karttunen, and T. A. Pakkanen, "Structural characteristics of hydrogenated carbon and boron nitride nanotubes: impact of H-H interactions," *Chemphyschem,* vol. 9, pp. 2390-6, Nov 10 2008.

[96] A. Rubio, J. L. Corkill, and M. L. Cohen, "Theory of graphitic boron nitride nanotubes," *Physical Review B,* vol. 49, pp. 5081-5084, 02/15/ 1994.

[97] X. Blase, A. Rubio, S. G. Louie, and M. L. Cohen, "Stability and Band Gap Constancy of Boron Nitride Nanotubes," *EPL (Europhysics Letters),* vol. 28, p. 335, 1994.

[98] Z. J.-P. Wang Yan-Li, Su Ke-He, Wang Xin, Liu Yan, Sun Xu, "A density functional theory study on parameters fitting of ultra long armchair (n, n) single walled boron nitride nanotubes," *Chin. Phys. B,* vol. 21, pp. 60301-060301, 2012-05-01 2012.

[99] G. Y. Guo, S. Ishibashi, T. Tamura, and K. Terakura, "Static dielectric response and Born effective charge of BN nanotubes from ab initio finite electric field calculations," *Physical Review B,* vol. 75, p. 245403, 06/05/ 2007.

[100] V. A. Margulis, E. E. Muryumin, and E. A. Gaiduk, "Collective electronic excitations in BN double-walled nanotubes," *Physical Review B,* vol. 78, p. 035415, 07/09/ 2008.

[101] S. Okada, S. Saito, and A. Oshiyama, "Interwall interaction and electronic structure of double-walled BN nanotubes," *Physical Review B,* vol. 65, p. 165410, 04/04/ 2002.

[102] E. Hernández, C. Goze, P. Bernier, and A. Rubio, "Elastic Properties of C and BCN Composite Nanotubes," *Physical Review Letters,* vol. 80, pp. 4502-4505, 05/18/ 1998.

[103] R. O. Jones, "The density functional formalism, its applications and prospects," *Reviews of Modern Physics,* vol. 61, pp. 689-746, 1989.

[104] P. Hohenberg, "Inhomogeneous Electron Gas," *Physical Review,* vol. 136, pp. B864-B871, 1964.

[105] J. P. Perdew, K. Burke, and M. Ernzerhof, "Generalized Gradient Approximation Made Simple [Phys. Rev. Lett. 77, 3865 (1996)]," *Physical Review Letters,* vol. 78, pp. 1396-1396, 02/17/ 1997.

[106] A. Savin, F. Colonna, and R. Pollet, "Adiabatic connection approach to density functional theory of electronic systems," *International Journal of Quantum Chemistry*, vol. 93, pp. 166-190, 2003.

[107] A. D. Kelkar, G. S. Chandekar, and R. Mohan, "Prediction of Material Properties of Single Walled Carbon Nanotube using MD Simulations," in *Nanotechnology, 2008. NANO '08. 8th IEEE Conference on*, 2008, pp. 370-373.

[108] S. H. Lim, J. Luo, W. Ji, and J. Lin, "Synthesis of boron nitride nanotubes and its hydrogen uptake," *Catalysis Today,* vol. 120, pp. 346-350, 2/28/ 2007.

[109] R. Ma, Y. Bando, H. Zhu, T. Sato, C. Xu, and D. Wu, "Hydrogen Uptake in Boron Nitride Nanotubes at Room Temperature," *Journal of the American Chemical Society,* vol. 124, pp. 7672-7673, 2002/07/01 2002.

[110] V. A. Margulis, E. E. Muryumin, and O. B. Tomilin, "ATOMIC HYDROGEN ADSORPTION ON BORON NITRIDE NANOTUBE SURFACES," in *Hydrogen Materials Science and Chemistry of Carbon Nanomaterials*, T. N. Veziroglu, S. Zaginaichenko, D. Schur, B. Baranowski, A. Shpak, V. Skorokhod, *et al.*, Eds., ed: Springer Netherlands, 2007, pp. 275-278.

[111] G. Mpourmpakis and G. E. Froudakis, "Why boron nitride nanotubes are preferable to carbon nanotubes for hydrogen storage?: An ab initio theoretical study," *Catalysis Today,* vol. 120, pp. 341-345, 2/28/ 2007.

[112] M. G. Joseph Estevez, A. D. Kelkar, "Property Predictions of Single-Walled Boron Nitride Nanotubes using Molecular Dynamics Simulaton," *AIAA,* 2012 2012.

[113] J. L. Tack, "Thermodynamic and Mechanical Properties of Epon 862 with Curing Agent DETDA by Molecular Simulation," *Thesis Texas A&M University,* p. 39, December 2006 2006.

[114] A. D. K. Francis komuves, Ram Mohan, Vinaya A. Kelkar, "Prediction of Mechanical Properties of Epon 862 (DGEBF)-W (DETDA) using MD Simulations," *AIAA,* 2010.

[115] J. E. M. Ghazizadeh, L. Zhang, and A. D. Kelkar, "Effect of Electrospun Fibers on The Mechanical and Thermal Properites of Epon 862-W Epoxy Resin System," *SAMPE,* Many 2013 2013.

[116] J. W. K. J.H. Kang, J. S. Harrison, M. W. Smith, K. Jordan, S. E. Lowther, P.T. Lillehei, S. A. Thibeault, G. Sauti, C. Park, "Boron nitride and boron nitride nanotube materials for radiation shielding," *US Patent EP2567385 A1,* 2013.

[117] C. C. F. S. A. Thibeault, G. Sauti, J.H. Kang, C. Park "Radiation shielding materials containing hydrogen, boron and nitrogen," *US Patent WO2013074134 A1,* May 23, 2013 2013.